ASM Handbook, Volume 19: Fatigue and Fracture
ASM Handbook Committee, p 771-812
DOI: 10.1361/asmhba0002406

Selecting Aluminum Alloys to Resist Failure by Fracture Mechanisms*

R.J. Bucci, ALCOA Technical Center, G. Nordmark (retired), and E.A. Starke, Jr.,
University of Virginia, Department of Materials Science and Engineering

Though virtually all design and standard specifications require the definition of tensile properties for a material, these data are only partly indicative of mechanical resistance to failure in service. Except for those situations where gross yielding or highly ductile fracture represents limiting failure conditions, tensile strength and yield strength are usually insufficient requirements for design of fracture-resistant structures. Strength by itself may not be sufficient if toughness, resistance to corrosion, stress corrosion, or fatigue are reduced too much in achieving high strength.

The achievement of durable, long-lived structural components from high-strength materials requires consideration of severe stress raisers for which possible failure mechanisms are likely to be fatigue, brittle fracture, or fracture from some combination of cyclic and static loading in corrosive environments. Good design, attention to structural details, and reliable inspection are of primary importance in controlling corrosion-fatigue and fracture. Accordingly, designers have traditionally considered the minimization of stress raisers as more important than alloy choice.

However, proper alloy selection does represent an important means of minimizing premature fracture in engineering structures. Obviously, high tensile strength is potentially detrimental in parts containing severe stress raisers for which possible failure mechanisms are likely to be fatigue, brittle fracture, or fracture in combination with corrosion, static loads, and/or cyclic loading. Likewise, selecting ductile alloys of low enough strength to ensure freedom from unstable fracture is limited by economic or technical pressures to increase structural efficiencies. Therefore, optimum alloy selection for fracture control requires careful assessment and balance of tradeoffs among the mechanical properties and corrosion behavior required for a given application.

*Adapted with permission from the article by R.J. Bucci in *Engineering Fracture Mechanics*, Vol 12, 1979, p 407-441 and from information contained in *Fatigue and Microstructure* (ASM, 1979, p 469-490) and from *Application of Fracture Mechanics for Selection of Metallic Structural Materials* (ASM, 1982, p 169-208)

In the aluminum industry, significant progress has been achieved in providing "improved" alloys with good combinations of strength, fracture toughness, and resistance to stress-corrosion cracking. Optimum selection and use of fatigue-resistant aluminum alloys also has become more of a factor for designers and materials engineers for extending fatigue life and/or structural efficiency. This emphasis on alloy development and selection is due, in part, to the greatly enhanced understanding of fatigue processes from the disciplines of strain control fatigue and fracture mechanics. The strain control approach is aimed primarily at fatigue crack initiation and early fatigue crack growth, while fracture mechanics concepts address the propagation of an existing crack to failure. This combination of knowledge from cyclic strain testing and fracture mechanics provides a basis for understanding of fatigue processes beyond the historical emphasis on crack nucleation studies from stress-controlled (stress to number of cycles, or *S-N*) fatigue testing. In this context, this article provides a brief overview on fatigue and fracture resistance of aluminum alloys.

Characteristics of Aluminum Alloy Classes

A wide variety of commercial aluminum alloys and tempers provide specific combinations of strength, toughness, corrosion resistance, weldability, and fabricability. The relatively high strength-to-weight ratios and availability in a variety of forms make aluminum alloys the best choice for many engineering applications. Like other face-centered cubic materials, aluminum alloys do not exhibit sudden ductile-to-brittle transition in fracture behavior with lowering of temperature (Ref 1, 2). Tensile test results indicate that almost all aluminum alloys are insensitive to strain rates between 10^{-5} mm/mm/sec and 1 mm/mm/sec (~10^5 MPa/sec) at room and low temperatures (Ref 2). Therefore, aluminum is an ideal material for structural applications in a wide range of operating temperatures and loading rates.

Aluminum alloys are classified in several ways, the most general according to their strengthening mechanisms. Some alloys are strengthened primarily by strain hardening (-H) while others are strengthened by solution heat treatment and precipitation aging (-T). A second commonly used system of classification is that of the Aluminum Association where the principal alloying element is indicated by the first digit of the alloy designation. Grouping of wrought aluminum alloys by strengthening method, major alloying element, and relative strength are given in Table 1. Another classification system established by the International Standards Organization (ISO) utilizes the alloying element abbreviations and the maximum indicated percent of element present (Table 2). This article utilizes the Aluminum Association system, which is described in more detail in *The Aluminum Association Standards and Data Handbook* (Ref 3) and in Volume 2 of the *ASM Handbook*.

Commercial aluminum products used in the majority of structural applications are selected from 2XXX, 5XXX, 6XXX, and 7XXX alloy groups, which offer medium-to-high strengths. Of these, 5XXX and 6XXX alloys offer medium-to-relatively high strength, good corrosion resistance, and are generally so tough that fracture toughness is rarely a design consideration. The 5XXX alloys provide good resistance to stress corrosion in marine atmospheres and good welding characteristics. Notably, this class of alloys has been widely used in low-temperature applications that satisfy the most severe requirements of liquefied fuel storage and transportation at cryogenic temperatures (Ref 2, 4, 5). Alloys of the 6XXX class, with good formability and weldability at medium strengths, see wide use in conventional structural applications. The 2XXX and 7XXX alloys generally are used in applications involving highly stressed parts. Certain alloys and tempers within these classes are promoted for their high toughness at high strength. Stress-corrosion cracking resistance of 2XXX and 7XXX

Table 1 Wrought aluminum and aluminum alloy designation system

Aluminum Association series	Type of alloy composition	Strengthening method	Range of tensile strength	
			MPa	ksi
1XXX	Al	Cold work	70-175	10-25
2XXX	Al-Cu-Mg (1-2.5% Cu)	Heat treat	170-310	25-45
2XXX	Al-Cu-Mg-Si (3-6% Cu)	Heat treat	380-520	55-75
3XXX	Al-Mn-Mg	Cold work	140-280	20-40
4XXX	Al-Si	Cold work (some heat treat)	105-350	15-50
5XXX	Al-Mg (1-2.5% Mg)	Cold work	140-280	20-40
5XXX	Al-Mg-Mn (3-6% Mg)	Cold work	280-380	40-55
6XXX	Al-Mg-Si	Heat treat	150-380	22-55
7XXX	Al-Zn-Mg	Heat treat	380-520	55-75
7XXX	Al-Zn-Mg-Cu	Heat treat	520-620	75-90
8XXX	Al-Li	Heat treat	280-560	40-80

alloys is generally not as great as in other aluminum alloy groups; however, service failures are avoided by good engineering practices and proper selection of alloy and temper or a suitable protective system. The 2XXX and 7XXX alloys see widespread use in aerospace applications. Certain 2XXX and 7XXX alloys provide good welding characteristics at high strength.

Alloys of the 1XXX class are used primarily in applications where electrical conductivity, formability, ductility, and resistance to stress corrosion are more important than strength. The 3XXX alloys, widely used in piping applications, are characterized by relatively low strengths and very good toughness, ductility, formability, brazing, and welding characteristics. The 4XXX alloys are used mainly for welding wire and brazing applications where it is desired to have a lower melting point than in the wire without producing brittleness in the weldment.

Alloy Selection Concepts. In any design plan, priority must be given to alloy properties. Optimum alloy choice involves evaluation and decision based on rating characteristics of a material that quantitatively measure resistance to failure by foreseeable failure mechanisms. In some instances, trade-off will be necessary among these material characteristics and among other factors, such as cost, fabricability, availability, expected service life, and maintainability. Relatively few generalizations can be made that will be valid for all material selection problems; individual problems must be treated separately or on the basis of closely related experience.

An important consideration to the relative ranking of importance of properties to prevent failure is the particular application and basic design strategy to which the selected alloy will be applied. It is pertinent to review basic design philosophies by which aluminum alloys are selected to resist failure by fracture mechanisms. Later discussion will treat alloy selection concepts related to the specific areas of fracture toughness, corrosion, stress-corrosion cracking (SCC), and fatigue.

Design Philosophies. In general, design philosophies for the prevention of fracture-type failures are of two basic types: safe life and damage-tolerant (or fail-safe). Neither approach is meant to be used as an extreme, nor is either approach meant to replace need for full-scale design verification tests. Many applications require a "fracture-control plan" to arrive at rational and cost-effective criteria for design, fabrication, and maintenance of reliable structures.

Safe Life Design Approach. Traditionally, component life has been expressed as the time (or number of fatigue cycles) required for a crack to be initiated and grow large enough to produce catastrophic failure. Prior to development of reliable crack detection techniques and fracture mechanics technology, little attempt was made to separate component failure into initiation and propagation stages. It was assumed that total life of a part consisted primarily of initiation of a crack, generally by fatigue or stress corrosion. Time for a minute crack to grow and produce failure was considered a minor portion of the service life. In the safe life approach, which is an outgrowth of this assumption, the designer seeks long, safe life by preventing cracks of significant size from occurring during the service life of the structure. In this approach it is the incubation period leading to development of a significant crack that is of major concern.

Small coupon-type specimens, though useful for rating materials and establishing sensitivity of various load and fabrication parameters, are not suitable for establishing the life of the part. A safe-life evaluation of a structure requires a reasonably accurate experimental simulation of the particular item of hardware. Under this procedure, accurately described loads are applied to the structure, life is determined, and a scatter factor is applied to establish the safe life of the structure. Structural "hot spots" are retrofitted as necessary. Generally, such elaborate tests prohibit evaluation of a large number of candidate materials and structural arrangements, since testing of each option may not be feasible because of economic and time constraints. Therefore, design and, consequently, material selection by this approach rely heavily on experience to eliminate need for excessive structural maintenance and retrofit.

Damage-Tolerant (Fail-Safe) Design Approach. Damage tolerance describes features of design that prohibit catastrophic loss of structural integrity. Damage tolerance evaluation of structure is intended to ensure that, should serious cracking or damage occur, the remaining structure can withstand reasonable loads without excessive structural deformation until the damage is

Table 2 ISO equivalents of wrought Aluminum Association designations

Aluminum Association international designation	ISO designation(a)
1050A	Al 99.5
1060	Al 99.6
1070A	Al 99.7
1080A	Al 99.8
1100	Al 99.0 Cu
1200	Al 99.0
1350	E-Al 99.5
...	Al 99.3
1370	E-Al 99.7
2011	Al Cu6BiPb
2014	Al Cu4SiMg
2014A	Al Cu4SiMg(A)
2017	Al Cu4MgSi
2017A	Al Cu4MgSi(A)
2024	Al Cu4Mg1
2030	Al Cu4PbMg
2117	Al Cu2.5Mg
2219	Al Cu6Mn
3003	Al Mn1Cu
3004	Al Mn1Mg1
3005	Al Mn1Mg0.5
3103	Al Mn1
3105	Al Mn0.5Mg0.5
4043	Al Si5
4043A	Al Si5(A)
4047	Al Si12
4047A	Al Si12(A)
5005	Al Mg1(B)
5050	Al Mg1.5(C)
5052	Al Mg2.5
5056	Al Mg5Cr
5056A	Al Mg5
5083	Al Mg4.5Mn0.7
5086	Al Mg4
5154	Al Mg3.5
5154A	Al Mg3.5(A)
5183	Al Mg4.5Mn0.7(A)
5251	Al Mg2
5356	Al Mg5Cr(A)
5454	Al Mg3Mn
5456	Al Mg5Mn
5554	Al Mg3Mn(A)
5754	Al Mg3
6005	Al SiMg
6005A	Al SiMg(A)
6060	Al MgSi
6061	Al Mg1SiCu
6063	Al Mg0.7Si
6063A	Al Mg0.7Si(A)
6082	Al Si1MgMn
6101	E-Al MgSi
6101A	E-Al MgSi(A)
6181	Al Si1Mg0.8
6262	Al Mg1SiPb
6351	Al Si1Mg0.5Mn
7005	Al Zn4.5Mg1.5Mn
7010	Al Zn6MgCu
7020	Al Zn4.5Mg1
7049A	Al Zn8MgCu
7050	Al Zn6CuMgZr
7075	Al Zn5.5MgCu
7178	Al Zn7MgCu
7475	Al Zn5.5MgCu(A)
...	Al Zn4Mg1.5Mn
...	Al Zn6MgCuMn

Note: The proposed ISO chemical composition standard for aluminum and its alloys references Aluminum Association equivalents as well as its own identification system. The ISO system is based on the systems that have been used by certain European countries. The main addition element is distinguished by specifying the required content (middle of range) rounded off to the nearest 0.5. If required, the secondary addition elements are distinguished by specifying the required content rounded off to the nearest 0.1, for two elements at most. (a) The chemical symbols for addition elements should be limited to four. If an alloy cannot otherwise be distinguished, a suffix in brackets is used: 6063 = Al Mg0.7Si; 6463 = Al Mg0.7Si(B); and international alloy registration, 6063A = Al Mg0.7Si(A). Note that suffixes (A), (B), and so on should not be confused with suffixes of the Aluminum Association.

detected. Consideration must be given to the probable existence of flaws (cracks) in the structure. These flaws could be initiated in service or be present as undetected initial material or fabrication defects. Given a crack-like flaw corresponding to the maximum size escaping reliable detection, life of the part is assumed to be spent propagating this flaw to the critical size that results in unstable fracture. The general design strategy is to select stress levels, configurations, and materials to provide a controlled slow rate of crack propagation with high residual strength. The designer thereby seeks to limit the rate of flaw growth so the largest flaw missed at one inspection will not cause catastrophic failure before one or more later inspections. Analysis procedures depend heavily on the use of crack growth rates and fracture toughness combined with fracture mechanics principles for prediction of crack growth life and fracture strength. Moreover, inspection is an integral part of the fracture control plan. Recognition of these principles and their implications for the safety, reliability, and durability of engineering structures has resulted in engineering standards and codes that impose requirements of fracture mechanics analyses and control of crack behavior. Perhaps the most notable of these is the Air Force structural integrity requirement (Ref 6). With this plan, use of fracture toughness and stress corrosion testing in material procurement is required to ensure that materials with properties lower than those used in design do not appear in the final structure.

Fracture Mechanics and Toughness

Fracture mechanics is concerned with catastrophic failure associated with crack-like flaws, regardless of how the flaw originated. Important parameters are crack size, local stress in the absence of the crack, yield strength, and materials fracture toughness. Use of these parameters allows prediction of the terminal flaw size in a part. The fracture mechanics approach is based on analysis of crack tip stress-strain fields. When stresses are below the yield stress, the critical stress concentration for fracture lies in the domain of linear elastic fracture mechanics and is an inherent material property K_{Ic} (plane-strain fracture toughness).

The concepts of fracture mechanics are concerned with the basic methods for predicting the load-carrying capabilities of structures and components containing cracks. The fracture mechanics approach is based on a mathematical description of the characteristic stress field that surrounds any crack in a loaded body. When the region of plastic deformation around a crack is small compared to the size of the crack (as is often true for large structures and high-strength materials), the magnitude of the stress field around the crack is commonly expressed as the stress intensity factor, K, where:

$$K = \sigma\sqrt{(a)\,Y} \qquad \text{(Eq 1)}$$

where σ = remotely applied stress, a = characteristic flaw size dimension, and Y = geometry factor, determined from linear elastic stress analysis. The stress-intensity factor, K, thus represents a single parameter that includes both the effect of the stress applied to a sample and the effect of a crack of a given size in a sample. The stress-intensity factor can have a simple relation to applied stress and crack length, or the relation can involve complex geometry factors for complex loading, various configurations of real structural components, or variations in crack shapes. In this way, linear elastic analysis of small-scale yielding can be used to define a unique factor, K, that is proportional to the local crack tip stress field outside the small crack tip plastic zone.

These concepts provide a basis for defining a critical stress-intensity factor (K_c) for the onset of crack growth, as a material property independent of specimen size and geometry for many conditions of loading and environment. For example, if a combination of σ and a were to exceed a critical value K_c, then the crack would be expected to propagate.

Tests on precracked specimens of a wide variety of materials have shown that the critical K value at the onset of crack extension approaches a constant value as specimen thickness increases. Figure 1 shows this effect in tests with 7075 aluminum alloy specimens over a range of thickness. In general, when the specimen thickness and the inplane dimensions near the crack are large enough relative to the size of the plastic zone, then the value of K at which growth begins is a constant and generally minimum value called the plane-strain fracture toughness factor, K_{Ic}, of the material. The parameter K_{Ic} is a true material property in the same sense as is the yield strength of a material. The value of K_{Ic} determined for a given material is unaffected by specimen dimensions or type of loading, provided that the specimen dimensions are large enough relative to the plastic zone to ensure plane-strain conditions around the crack tip (strain is zero in the through-thickness or z-direction).

Plane-strain fracture toughness, K_{Ic}, is also directly related to the energy required for the onset of crack propagation by the formula

$$K_{Ic} = \sqrt{\frac{EG_{Ic}}{1-\nu^2}} \qquad \text{(Eq 2)}$$

where E is the elastic modulus (in MPa or psi), ν is Poisson's ratio (dimensionless), and G_{Ic} is the critical plane-strain energy release rate for crack extension (in kJ/m^2 or in.-lb/in.^{2}). In simplified concept, G_{Ic} is the critical amount of strain energy that is released from the elastic stress field of the specimen per unit area of new cracked surface for the first small increment of crack extension. The concepts of K_{Ic} and G_{Ic} are essentially interchangeable; K_{Ic} is generally preferred because it is more easily associated with the stress or load applied to a specimen. The value of K_{Ic} is measured directly using test methods described in ASTM E-399.

In the plane-strain state, a material is at its lowest point of resistance to unstable fracture. The onset of fracture is abrupt and is most clearly

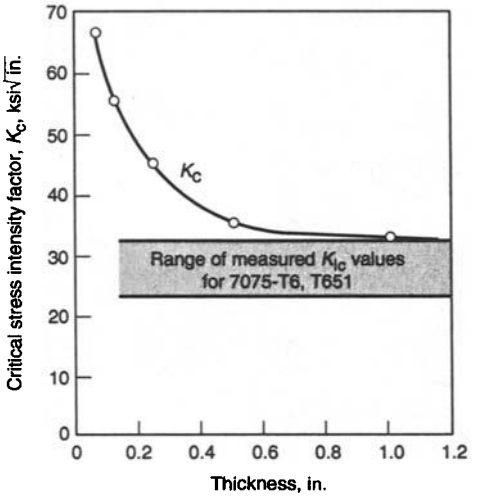

Fig. 1 Fracture toughness of 7075-T6, T651 sheet and plate from tests of fatigue-cracked center-notched specimens (transverse). Source: J.G. Kaufmann in *Review of Developments in Plane Strain Fracture Toughness Testing*, ASTM STP 463, 1970, p 7

observed in thick sections of low-ductility (high-strength) alloys, when the elastic stress state in a flawed component is highly constrained to that of plane strain. However, when stresses approach or exceed yield values, the elastic stress field surrounding the crack departs from that of plane strain (from the development of an enlarged crack tip plastic zone which generally enhances fracture toughness). With increasing load, slow stable crack extension (tearing) may accompany the increasing plastic zone size. Onset of rapid fracture occurs when increase in crack tip stress field, measured by K (increase in K due to increased nominal stress and crack length), equals or exceeds resistance to crack extension (due to an increase in plastic zone size, crack tip blunting, and change from flat to slant fracture). This behavior is most clearly seen in fracture of relatively tough thin plate and sheet alloys. Unstable fracture under these conditions cannot be described as a material property since events leading to rapid fracture are specimen configuration and size dependent. One standardized method for describing elastic-plastic fracture involves the resistance-curve or R-curve concept described in ASTM E561. Briefly, the resistance-curve concept involves measurement of the K values at which various amounts of crack growth occur in a thin-plate laboratory specimen. Then a plotted curve of K versus crack growth from the laboratory specimen can be used to predict crack-growth behavior in a structural component of the same material. Limitations of the method are that the component must have the same thickness as the laboratory specimen and that K relations must be known for both component and specimen. However, once a resistance curve is obtained for a given material and thickness, it can be used to predict the crack-growth and crack-instability behavior of other components of the same material.

***J*-Integral Method.** Another concept for use in the analysis of elastic-plastic fracture is the

Table 3 Typical room-temperature yield strength and plane-strain fracture toughness values for several high-strength aluminum alloys

Product	Alloy	Temper	Yield strength(a)		Plane-strain fracture toughness, K_{Ic}					
					L-T		T-L		S-L	
			MPa	ksi	MPa$\sqrt{m}$	ksi$\sqrt{in.}$	MPa$\sqrt{m}$	ksi$\sqrt{in.}$	MPa$\sqrt{m}$	ksi$\sqrt{in.}$
Plate	2014	T651	440	64	24	22	22	20	19	17
	2024	T351	325	47	36	33	33	30	26	24
	2024	T851	455	66	24	22	23	21	18	16
	2124	T851	440	64	32	29	25	23	24	22
	2219	T851	435	63	39	35	36	33	...	...
	7050	T73651	455	66	35	32	30	27	29	26
	7075	T651	505	73	29	26	25	23	20	18
	7075	T7651	470	68	30	27	24	22	20	18
	7075	T7351	435	63	32	29	29	26	21	19
	7475	T651	495	72	43	39	37	34	32	29
	7475	T7651	460	67	47	43	39	35	31	28
	7475	T7351	430	62	53	48	42	38	35	32
Die forgings	7050	T736	455	66	36(b)	33(b)	25(c)	23(c)	25(c)	23(c)
	7149	T73	460	67	34(b)	31(b)	24(c)	22(c)	24(c)	22(c)
	7175	T736	490	71	33(b)	30(b)	29(c)	26(c)	29(c)	26(c)
Hand forgings	2024	T852	430	62	29	26	21	19	18	16
	7050	T73652	455	66	36	33	23	21	22	20
	7075	T7352	365	53	37	34	29	26	23	21
	7079	T652	440	64	29	26	25	23	20	18
	7175	T736	470	68	37	34	30	27	26	24
Extrusions	7050	T7651x	495	72	31	28	26	24	21	19
	7050	T7351x	459	65	45	41	32	29	26	24
	7075	T651x	490	71	31	28	26	24	21	19
	7075	T7351x	435	63	35	32	29	26	22	20

(a) At 0.2% offset (longitudinal). (b) Parallel to grain flow. (c) Nonparallel to grain flow. Source: R. Bucci, *Engr. Fracture Mech.*, Vol 12, 1979, p 407-441

J-integral concept, where *J* is a nonlinear generalization of *G* (the elastic strain energy release rate). *J* can be thought of as the amount of elastic-plastic strain energy per unit area of crack growth which is applied toward extending the crack in a specimen under load. A critical value of *J*, called J_{Ic}, is the value required for the start of crack extension from a pre-existing crack. For material having a sufficiently high yield strength or for specimens of sufficient size, elastic stresses control the crack extension, and J_{Ic} is equal to G_{Ic}.

An important advantage of the J_{Ic} test method is that it can accommodate a significant amount of crack-tip blunting and general plastic deformation in the specimen. If the amount of plastic deformation is small enough, J_{Ic} will be identical to G_{Ic}, and thus J_{Ic} can be converted to an approximately equivalent measure of K_{Ic} (see Eq 2). For large amounts of plastic deformation, a size requirement limits the size of the specimen and, indirectly, the amount of plastic deformation which can be allowed. The specimen size requirement allows a significantly smaller specimen, often ten times smaller, to be tested with the J_{Ic} procedure than with the K_{Ic} procedure. So, although the J_{Ic} test is relatively time consuming due to multiple tests, it can be used over a wider range of material properties and specimen sizes than the K_{Ic} test. In addition, single-specimen J_{Ic} test procedures, such as incremental unloading methods, can reduce both testing time and the number of specimens required to obtain J_{Ic} test data. Another advantage of the J_{Ic} approach is that it makes possible the prediction of the failure load of cracked high-toughness, medium-strength alloys (with more tendency toward plastic deformation) for fracture-critical applications.

Alloy Selection for Fracture Toughness

Plane-strain fracture toughness, K_{Ic}, is particularly pertinent in materials selection because, unlike other measures of toughness, it is independent of specimen configuration. For comparison, the notch toughness of a material, which is most commonly measured by Charpy testing, does depend on the configuration of the specimen. Changes in the size of the specimen or in the root radius of the notch will affect the amount of energy absorbed in a Charpy test. The main reason for this is that the total energy required for initiation of the crack from the notch, for propagation of the crack across the specimen, and for complete fracture of the specimen is measured in a Charpy test. In contrast, a K_{Ic} test measures only the critical load required for a small extension of a pre-existing crack. Even though K_{Ic} is more difficult to measure than notch toughness, because of the requirements of a pre-existing crack and a specimen large enough for plane-strain conditions, it is a constant material property and can be more generally applied to materials selection.

In selection of structural materials, the single most important characteristic of K_{Ic} for nearly all materials is that it varies *inversely* with yield strength for a given alloy. Table 3 is a summary of plane-strain fracture toughness values for a wide variety of aluminum alloys—including 2024 and 7075, which have been used for components which do not require a high level of fracture toughness. Typical data for a lot of one high-toughness aluminum alloy (7475-T7351) are shown in Table 4.

Table 4 Typical fracture toughnesses measured on the same lot of a high-toughness 7475-T7351 aluminum alloy plate

Specified test method	Typical L-T toughness(a)	
	MPa$\sqrt{m}$	ksi$\sqrt{in.}$
ASTM E 399, K_{Ic}	55	50
ASTM E 561, *R* curve		
5% secant	45-65	40-60
25% secant	75-110	70-100
Center-cracked panel		
150 mm (6 in.) wide	130	120
Center-cracked panel		
400 mm (16 in.) wide	200	180

Note: Test sample thicknesses are those typically specified. Data are approximate and are presented to contrast different test results, not for use for design purposes. *R*-curve testing also requires tensile data for test validity checks, and these should be provided to the testing laboratory. (a) Test sample orientation code is described in ASTM E 399 (Ref 43). The first letter represents the direction of applied tensile stress: the second letter is the direction of crack growth. L, longitudinal; T, transverse; S, thickness direction

Tough aluminum alloys such as those from the 1XXX, 3XXX, 4XXX, 5XXX, and most 6XXX series do not normally exhibit elastic unstable fracture, either in test panels or in real structures. These alloys are so tough that fracture toughness is rarely a design criterion. Because of this consideration and the relative difficulty of measuring toughness in a design-oriented manner by current methods, fracture toughness information for these alloys is rather limited. Much of the data available for these alloys (Fig. 2) has been developed by extrapolation of correlations from simpler tests such as the simple tear specimen of the design shown in Fig. 3, where the resistance of a

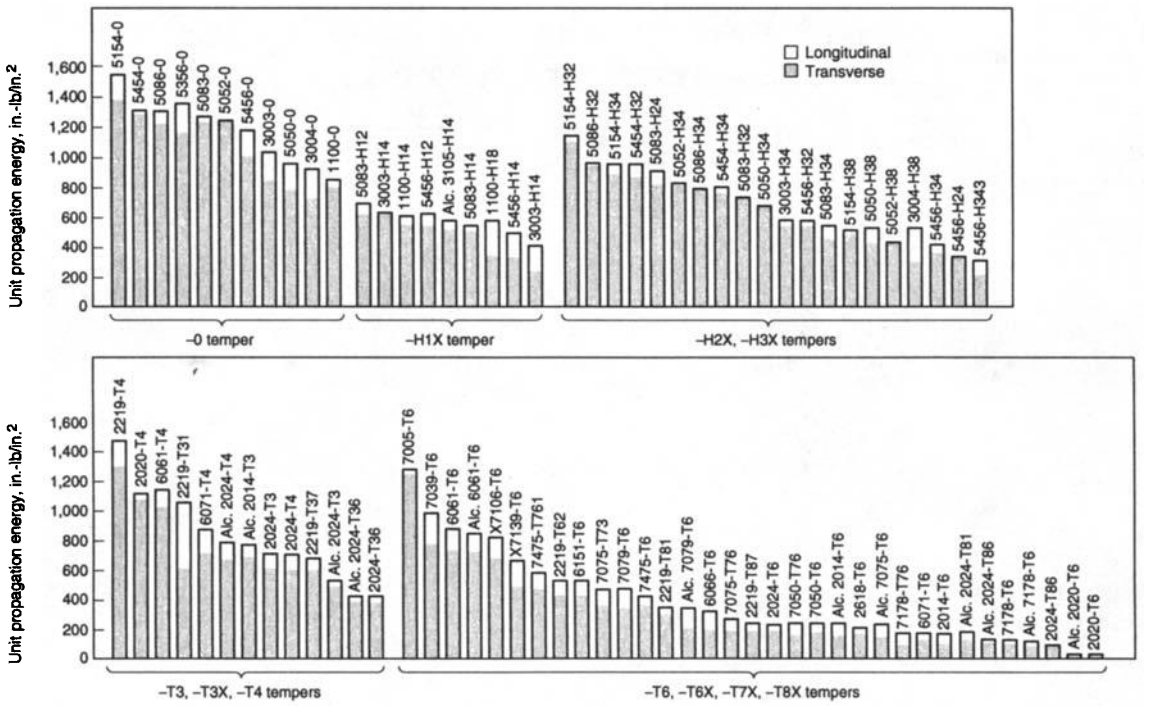

Fig. 2 Ratings of 1.6 mm (0.063 in.) aluminum sheet based on unit propagation energy (1 in. · lb/in.^{2} = 0.175 kJ/m^2)

material to crack growth in a nonuniform stress field is evaluated by measurement of appropriate areas under autographic load deformation records. A relative ranking of thin-section fracture toughness by tear tests is shown in Fig. 2 for a number of aluminum sheet alloys and tempers. Particularly, the unit propagation energy (UPE) has been found to be correlated with resistance to stable crack growth in thin sections, measured as K_{Ic} from wide-panel tests (Ref 1). These alloys are excluded from further consideration in this section.

Alloys for which fracture toughness is a meaningful design-related parameter fall into two categories:

- Controlled-toughness, high-strength alloys (i.e., those alloys developed primarily for their high fracture toughness at high strength)
- Conventional high-strength alloys, tempers, and products for which fracture toughness is a meaningful design parameter, but which are not promoted or used for fracture-critical components

The above categories are composed primarily of 2XXX and 7XXX alloys. Controlled-toughness, high-strength commercial products include 2124-T3 and T8-type sheet and plate; 2419-T6 and T8-type sheet, plate, extrusion, and forgings; 7050-T7-type plate, forgings, and extrusions; 7149-T7-type forgings; 7175-T6 and T7-type extrusions and forgings; and 7475-T6 and T7-type sheet and plate.

Recognized conventional high-strength alloys that are not produced to minimum toughness include 2014, 2024, 2219, 7075, 7079, and 7178. Typical strength and fracture toughness properties of several high-strength aluminum products are presented in Table 5. Evaluations have shown (Ref 7) that the fracture toughness of high-strength, precipitation-hardened 2XXX and 7XXX alloys is not adversely affected by high strain rate or moderate temperature reduction.

In general, fracture toughness decreases with increasing yield strength, as indicated by scatter bands of notched yield strength ratio (NYR) and UPE established for a wide variety of commercial 2XXX and 7XXX products. To develop high toughness, the microstructure must accommodate significant plastic deformation, and yet a microstructure that resists plastic deformation is needed for high strength. As indicated by Fig. 4(a) and 4(b), 7XXX alloys have the highest combination of strength and toughness of any family of aluminum alloys. In 7XXX alloys,

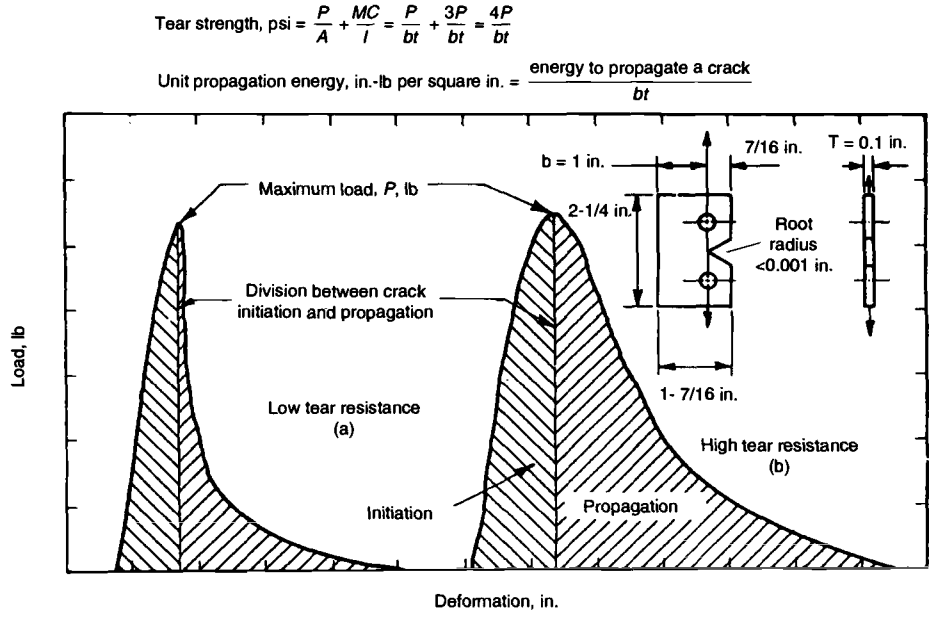

Fig. 3 Tear-test specimen and representative tear test curves

Table 5 Typical room-temperature yield strength and plane-strain fracture toughness values of several high-strength aluminum alloys

Product	Alloy	Temper	Yield strength at 0.2% offset (longitudinal)		Plane-strain fracture toughness, K_{Ic}					
					L-T		T-L		S-L	
			MPa	ksi	MPa$\sqrt{m}$	ksi$\sqrt{in.}$	MPa$\sqrt{m}$	ksi$\sqrt{in.}$	MPa$\sqrt{m}$	ksi$\sqrt{in.}$
Plate	2014	T651	440	64	24	22	22	20	19	17
	2024	T351	325	47	36	33	33	30	26	24
	2024	T851	455	66	24	22	23	21	18	16
	2124	T851	440	64	32	29	25	23	24	22
	2219	T851	435	63	39	35	36	33	...	...
	7050	T73651	455	66	35	32	30	27	29	26
	7075	T651	505	73	29	26	25	23	20	18
	7075	T7651	470	68	30	27	24	22	20	18
	7075	T7351	435	63	32	29	29	26	21	19
	7475	T651	495	72	43	39	37	34	32	29
	7475	T7651	460	67	47	43	39	35	31	28
	7475	T7351	430	62	53	48	42	38	35	32
Die forgings	7050	T736	455	66	36	33(a)	25	23(b)	25	23(b)
	7149	T73	460	67	34	31(a)	24	22(b)	24	22(b)
	7175	T736	490	71	33	30	29	26	29	26
Hand forgings	2024	T852	430	62	29	26	21	19	18	16
	7050	T73652	455	66	36	33	23	21	22	20
	7075	T7352	365	53	37	34	29	26	23	21
	7079	T652	440	64	29	26	25	23	20	18
	7175	T736	470	68	37	34	30	27	26	24
Extrusions	7050	T7651X	495	72	31	28	26	24	21	19
	7050	T7351X	459	65	45	41	32	29	26	24
	7075	T651X	490	71	31	28	26	24	21	19
	7075	T7351X	435	63	35	32	29	26	22	20

(a) Parallel to grain flow. (b) Nonparallel to grain flow

highest strength is associated with the T6 peak aged temper. Decreasing strength to acceptable levels by overaging provides a way to increase toughness (Fig. 5) as well as resistance to exfoliation, SCC, and fatigue crack growth in some 7XXX alloys. Alloys of the 2XXX class are used in both the naturally aged and artificially aged conditions. Commercial naturally aged 2XXX alloys (viz. T3- and T4-type tempers) provide good combinations of toughness and strength. Artificial aging to precipitation-hardened T8 tempers produces higher strength with some reduction in toughness, but in addition offers greater stability of mechanical properties at high temperatures and higher resistance to exfoliation and SCC.

The strength-fracture toughness interaction has been postulated to be the consequence of void link-up created by slip-induced breakdown of submicron strengthening particles, which occurs more readily at high strength levels (Ref 8). If the strengthening (matrix) precipitates are shearable they may promote strain localization which leads to premature crack nucleation and low fracture toughness. Whether or not the strengthening precipitates are sheared or looped and bypassed by dislocations depends on alloy composition and aging treatment. During aging, heterogeneous precipitation usually occurs at grain and subgrain boundaries resulting in soft, solute-denuded PFZ's in the matrix adjacent to the boundaries. The combination of these soft zones, that can localize strain, and grain boundary precipitates, that can aid in microvoid nucleation, also has an adverse effect on fracture toughness. Though this hypothesis remains unproven, it has been clearly demonstrated that the amounts, distribution, and morphology of alloy phases and second-phase particles in alloy microstructure have a large influence on toughness (Ref 9-11). Developed understanding of the interrelationships of alloy microstructure and fracture mechanisms has led to design of new commercial aluminum alloys offering optimum high strength and high toughness. Primarily, the alloy improvements have evolved through microstructural control obtained by increased purity, modified compositions, and better homogenization, fabrication, and heat treatment practices (Ref 10-15).

The balance between strength and toughness is greatly affected by a variety of processing parameters, including solution heat treatment, quenching efficiency, deformation prior to aging (for 2XXX alloys) and aging treatment. The solution heat treatment determines the amount of solute in solid solution and the vacancy content, which affects subsequent aging kinetics. Quenching affects both the microstructure and properties by determining the amount of solute that precipitates during cooling and that which is available for subsequent age hardening. It also affects the level of residual stresses which can influence manufacturing costs, fatigue and corrosion behavior. After quenching, methods to obtain a balance of properties include cold working before aging, when practical (T8 temper), and selecting aging times and temperatures to minimize grain boundary precipitates and precipitate-free zones (PFZ). The deformation prior to aging aids in the nucleation and growth of the matrix precipitates which decreases the time to reach peak strength. This, along with low-temperature aging, minimizes the amount of grain boundary precipitates

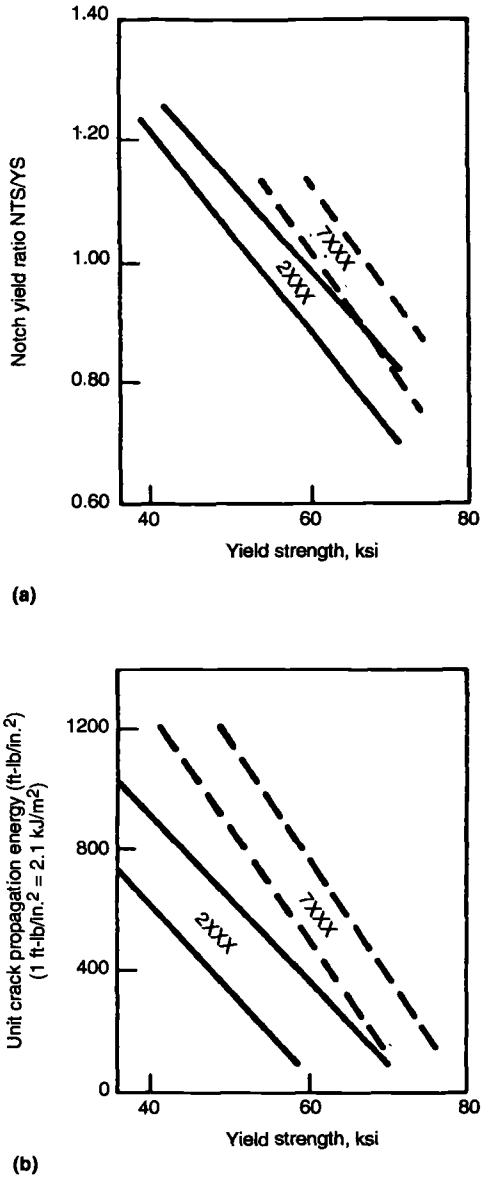

Fig. 4 Comparison of 2XXX and 7XXX commercial aluminum alloys (a) Notch toughness vs. yield strength. (b) Unit propagation energy vs. yield strength

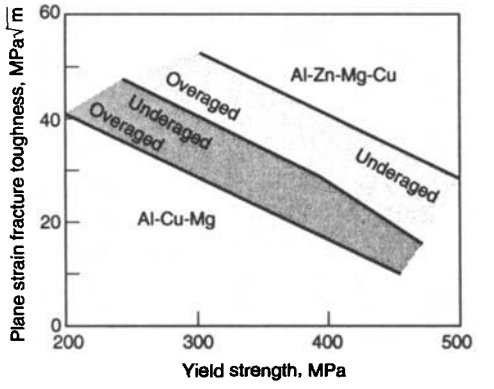

Fig. 5 Relationships of plane-strain fracture toughness to yield strength for the 2XXX and 7XXX series of aluminum alloys. Source: R. Develay, *Metals and Materials*, Vol 6, 1972, p 404

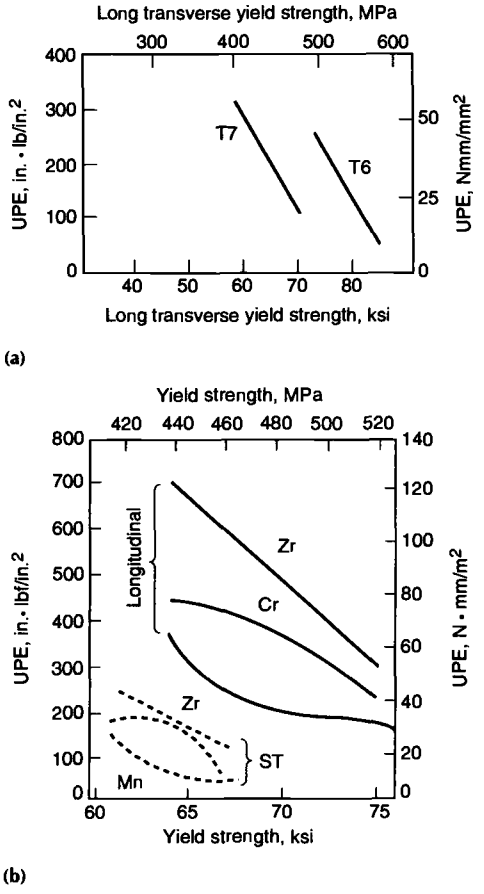

Fig. 6 Unit crack propagation energies (UPE), (a) commercial 7XXX aluminum alloy plate in peak strength and overaged tempers (Source: Ref 10) and (b) effects of dispersoid type on toughness of 75 mm (3 in.) 7075 plate (Source: J. Staley in ASTM STP 605)

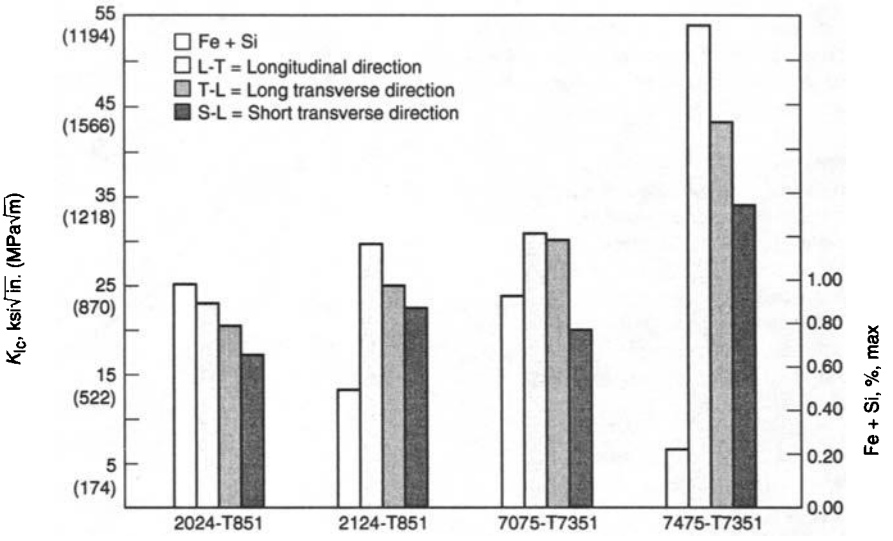

Fig. 7 Aluminum alloys 2124 and 7475 are tougher versions of alloys 2024 and 7075. High-purity metal (low iron and silicon) and special processing techniques are needed to optimize toughness in these materials. Source: Ref 14

Table 6 Effect of purity on the fracture toughness of some high-strength wrought aluminum alloys

Alloy and temper	% Fe, %, max	% Si, %, max	0.2% proof stress, MPa	Tensile strength, MPa	Fracture toughness, MPa√m	
					Longitudinal	Short transverse
2024-T8	0.50	0.50	450	480	22-27	18-22
2124-T8	0.30	0.20	440	490	31	25
2048-T8	0.20	0.15	420	460	37	28
7075-T6	0.50	0.40	500	570	26-29	17-22
7075-T73	0.50	0.40	430	500	31-33	20-23
7175-T736	0.20	0.15	470	540	33-38	21-29
7050-T736	0.15	0.12	510	550	33-39	21-29

Source: M.O. Speidel, *Met. Trans.*, Vol 6A, 1975, p 631

Table 7 Nominal compositions of aluminum alloys used in low-temperature service

Alloy designation	Nominal composition, %								
	Si	Cu	Mn	Mg	Cr	Zn	Ti	Zr	Others
Wrought alloys									
1100	...	0.12	...	...	...	...	...	...	...
2014	0.8	4.4	0.8	0.5	...	...	...	...	...
2024	...	4.4	0.6	1.5	...	...	...	...	...
2219	...	6.3	0.3	...	...	...	0.06	0.18	0.1V
3003	...	0.12	1.2	...	...	...	...	...	...
5083	...	...	0.7	4.4	0.15	...	...	...	...
5456	...	...	0.8	5.1	0.12	...	...	...	...
6061	0.6	0.28	...	1.0	0.20	...	...	...	...
7005	...	...	0.45	1.4	0.13	4.5	0.04	0.14	...
7039	0.1	0.05	0.25	2.8	0.20	3.0	0.05	...	0.2Fe
7075	...	1.6	...	2.5	0.23	5.6	...	...	...
Cast alloys									
355	5.0	1.2	...	0.5	...	...	...	...	...
C355	5.0	1.3	...	0.5	...	...	...	...	...
356	7.0	...	...	0.3	...	...	...	...	...
A356	7.0	...	...	0.3	...	...	...	...	...

and PFZ's (which adversely affect fracture toughness) at the desired strength level.

Alloy 2124 was the first 2XXX alloy developed to have high fracture toughness. The principal contribution to high toughness was increased purity (low iron and silicon), which minimizes formation of relatively large insoluble constituents (>1 μm). The detrimental effect of large constituent phases on the fracture toughness of aluminum alloys has been documented by many investigators. Constituent particles participate in the fracture process through void formation at particle/matrix interfaces or by fracturing during primary processing. Their volume fraction can be minimized by reducing impurity elements, e.g., iron and silicon, and excess solute. The detrimental effect of dispersoids also depends on their size and the details of their interface with the matrix. For example, the strength-toughness relationships in Fig. 6(b) were determined for 7075 variants containing different dispersoid-forming elements. Because Zr particles are small and coherent with the matrix (strong interface), they are usually not involved in the fracture process.

Resultant improvement for production materials is shown in Fig. 7 (Ref 14). Minimization of insoluble constituents by process control was used to develop 2419 and 2214 as higher-toughness versions of 2219 and 2014, respectively. Biggest gains in fracture toughness of 2XXX alloys by process control have been to the precipitation-hardened T8 tempers which are widely used in applications requiring good resistance to exfoliation corrosion and SCC. The effect of impurity on toughness of other alloys is shown in Table 6.

Grain size and degree of recrystallization can have a significant effect on fracture toughness.

The desired degree of recrystallization depends on product thickness, i.e., whether the part is under plane stress or plane strain. In thin products under plane stress, fracture is controlled by plasticity and a small recrystallized grain size is preferable. If the grain size is small enough, plasticity will be enhanced without detrimental, low energy, intergranular fracture. However, for thick products under plane strain, fracture is usually controlled by coarse particles and an unrecrystallized grain structure is preferable.

Alloy 7475 represents one of the most successful applications of alloy design techniques. Its composition and properties are modified from those of alloy 7075 by

- Reducing iron and silicon contents
- Optimizing dispersoids
- Altering precipitates
- Controlling quenching rate
- Controlling grain size

These modifications result in the toughest aluminum alloy available commercially at high strength levels. For designers this influence is shown most clearly by information on crack lengths for unstable crack growth at specific design stresses, such as that shown in Fig. 8. The crack tolerance of the 7475-T761 alloy sheet is almost three times greater than that of conventional 7075-T6. Similar effects have been noted for plate.

Alloy 7475 represents the highest strength-toughness combinations available in a commercial aluminum alloy. However, patented process controls (in addition to controlling the purity of iron and silicon) are necessary to achieve highest toughness levels in 7475. In comparison to conventional high-strength alloys, the effectiveness of alloy 7475 in developing high toughness at high strength is shown by plane-strain fracture toughness (K_{Ic}) data (Fig. 9), plane-stress fracture toughness (K_c) data from wide center crack panel tests (Fig. 10), and crack resistance curves (Fig. 11). This advantage is demonstrated by the critical stress-flaw size relationships in Fig. 8. The effect of heat treatment on crack propagation energy is shown in Fig. 6. Controls on production processes for high-toughness alloys 2124 and 7475 should also improve fatigue crack growth resistance.

7150-T77 Plate. In response to a need for improved corrosion resistance, another temper was developed for 7150. Alloy 7150-T77 plate develops the same mechanical properties as does 7150-T6 with significantly improved resistances to both exfoliation corrosion and SCC. The first application was on the C17 cargo transport. This saved a considerable amount of weight because corrosion performance of 7150-T6 and T61 was deemed to be inadequate by the Air Force for this application, and strength of 7050-T76 is considerably lower. The combination of strength and corrosion characteristics of 7150-T77 is attributed to proprietary processing. This processing promotes the development of a precipitate structure which effectively resists the passage of dislocations equivalent to that provided by the T6 temper and simultaneously minimizes the electrochemical differences between the matrix and grain boundaries. Extruded products in T77 do not develop the 70 MPa strength advantage.

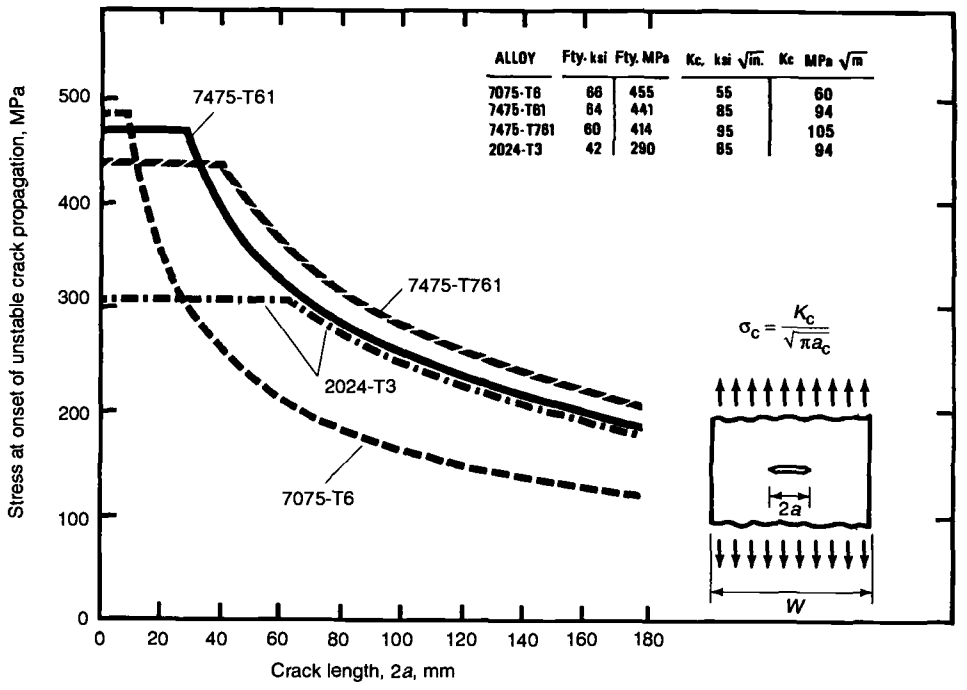

Fig. 8 Gross section stress at initiation of unstable crack propagation vs. crack length for wide sheet panels of four aluminum alloy/temper combinations. Source: Ref 13

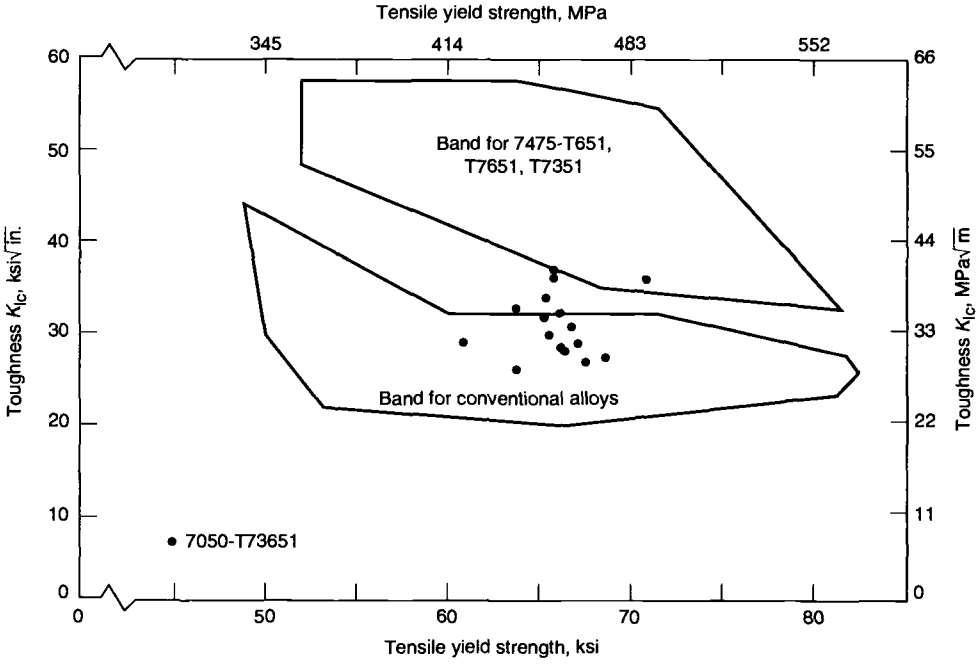

Fig. 9 Fracture toughness vs. yield strength for high-strength aluminum alloy plate (L-T orientation)

7055-T77 Plate. The implementation of the T77 temper for 7150 was followed by development of a proprietary material for compressively loaded structures. Alloy 7055-T77 plate offers a strength increase of about 10% relative to that of 7150-T6 (almost 30% higher than that of 7075-T76). It also provides a high resistance to exfoliation corrosion similar to that of 7075-T76 with fracture toughness and resistance to the growth of fatigue cracks similar to that of 7150-T6. In contrast to the usual loss in toughness of 7XXX products at low temperatures, fracture toughness of 7055-T77 at –65 °F (220 K) is similar to that at room temperature. Resistance to SCC is intermediate to those of 7075-T6 and 7150-T77. The

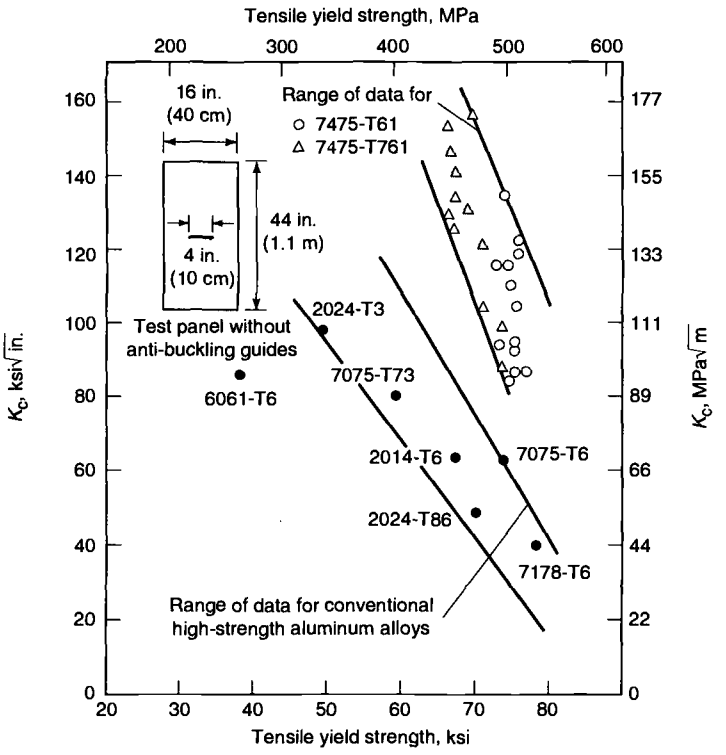

Fig. 10 Critical stress intensity factor, K_c, vs. tensile yield strength for 1.0 to 4.7 mm (0.040 to 0.188 in.) aluminum alloy sheet. Improved alloy 7475 is compared to other commercial alloys. Source: Ref 10

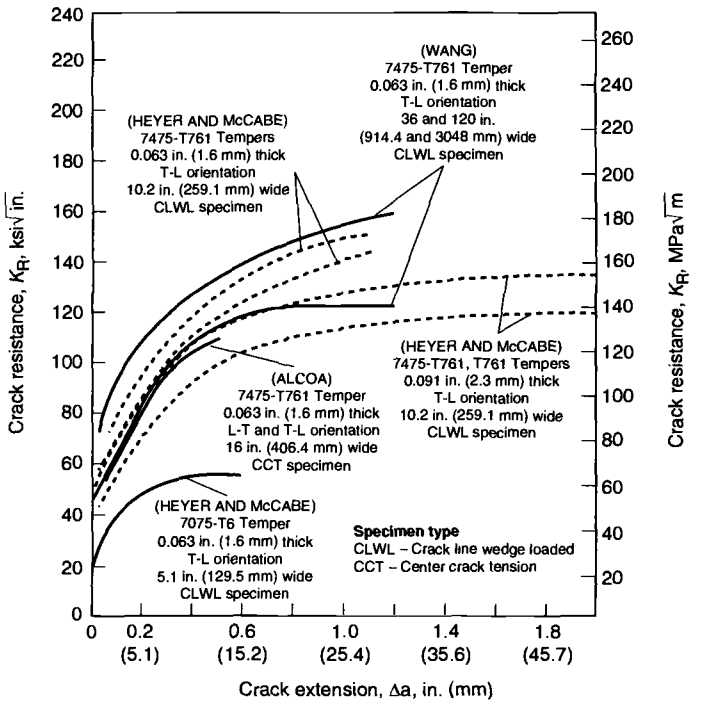

Fig. 11 Crack resistance curves for aluminum alloy 7475 sheet

Table 8 Fracture toughness of aluminum alloy plate

Alloy and condition	Room-temperature yield strength		Specimen design	Orientation	Fracture toughness, K_{Ic} or $K_{Ic}(J)$ at: 24 °C (75 °F)		−196 °C (−320 °F)		−253 °C (−423 °F)		−269 °C (−452 °F)	
	MPa	ksi			MPa√m	ksi√in.	MPa√m	ksi√in.	MPa√m	ksi√in.	MPa√m	ksi√in.
2014-T651	432	62.7	Bend	T-L	23.2	21.2	28.5	26.1	...	...	...	...
2024-T851	444	64.4	Bend	T-L	22.3	20.3	24.4	22.2	...	...	...	...
2124-T851(a)	455	66.0	CT	T-L	26.9	24.5	32.0	29.1	...	...	...	...
	435	63.1	CT	L-T	29.2	26.6	35.0	31.9	...	...	...	...
	420	60.9	CT	S-L	22.7	20.7	24.3	22.1	...	...	...	...
2219-T87	382	55.4	Bend	T-S	39.9	36.3	46.5	42.4	52.5	48.0	...	...
			CT	T-S	28.8	26.2	34.5	31.4	37.2	34.0	...	...
	412	59.6	CT	T-L	30.8	28.1	38.9	32.7	...	...	...	...
5083-O	142	20.6	CT	T-L	27.0(b)	24.6(b)	43.4(b)	39.5(b)	...	...	48.0(b)	43.7(b)
6061-T651	289	41.9	Bend	T-L	29.1	26.5	41.6	37.9	...	...	...	...
7039-T6	381	55.3	Bend	T-L	32.3	29.4	33.5	30.5	...	...	...	...
7075-T651	536	77.7	Bend	T-L	22.5	20.5	27.6	25.1	...	...	...	...
7075-T7351	403	58.5	Bend	T-L	35.9	32.7	32.1	29.2	...	...	...	...
7075-T7351	392	56.8	Bend	T-L	31.0	28.2	30.9	28.1	...	...	...	...

(a) 2124 is similar to 2024, but with higher-purity base and special processing to improve fracture toughness. (b) $K_{Ic}(J)$. Source: *Metals Handbook*, 9th ed., Vol 3, American Society for Metals, 1980, p 746, compiled from several references

attractive combination of properties of 7055-T77 is attributed to its high ratios of Zn/Mg and Cu/Mg. When aged by the proprietary T77 process this composition provides a microstructure at and near grain boundaries that is resistant to intergranular fracture and to intergranular corrosion. The matrix microstructure resists strain localization while maintaining a high resistance to the passage of dislocations. The extruded products in T77 do not develop the 70 MPa strength advantage.

Low-Temperature Toughness. Aluminum alloys represent a very important class of structural metals for subzero-temperature applications. Aluminum and aluminum alloys have face-centered-cubic (fcc) crystal structures. Most fcc metals retain good ductility at subzero temperatures. Aluminum can be strengthened by alloying and heat treatment while still retaining good ductility along with adequate toughness at subzero temperatures. Nominal compositions of aluminum alloys that are most often considered for subzero service are presented in Table 7.

Data on fracture toughness of several aluminum alloys at room and subzero temperatures are summarized in Table 8. The room-temperature yield strengths for the alloys in this table range from 142 to 536 MPa (20.6 to 77.7 ksi), and room-temperature plane-strain fracture toughness values for both bend and compact tension specimens range from 22.3 to 39.9 MPa√m (20.3 to 36.3 ksi√in.). This range in numerical values is not as impressive as actual service performances.

Of the alloys listed in Table 8, 5083-O has substantially greater toughness than the others. Because this alloy is too tough to obtain valid K_{Ic} data, the values shown for 5083-O were converted from J_{Ic} data. The fracture toughness of this alloy increases as exposure temperature de-

creases. Of the other alloys, which were evaluated in various heat-treated conditions, 2219-T87 has the best combination of strength and fracture toughness, both at room temperature and at −196 °C (−320 °F); this alloy can be readily welded.

Alloy 6061-T651 is another weldable alloy. It has good fracture toughness at room temperature and at −196 °C (−320 °F), but its yield strength is lower than that of alloy 2219-T87. Alloy 7039 also is weldable and has a good combination of strength and fracture toughness at room temperature and at −196 °C (−320 °F). Alloy 2124 is similar to 2024 but with a higher-purity base and special processing for improved fracture toughness. Tensile properties of 2124-T851 at subzero temperatures can be expected to be similar to those for 2024-T851.

Several other aluminum alloys, including 2214, 2419, 7050, and 7475, have been developed in order to obtain room-temperature fracture toughness superior to that of other 2000 and 7000 series alloys. Information on subzero properties of these alloys is limited, but it is expected that these alloys would have improved fracture toughness at subzero temperatures as well as at room temperature.

Stress-Corrosion Cracking of Aluminum Alloys

Stress-corrosion cracking (SCC) is a complex synergistic interaction of corrosive environment and sustained tensile stress at an exposed surface of metal resulting in cracking and premature failure at stresses below yield. In high-strength aluminum alloys, SCC is known to occur in ordinary atmospheres and aqueous environments. Both initiation and crack propagation may be accelerated by chlorides, temperature, and certain other chemical species. Susceptibility to SCC places a limitation on use of high-strength materials in certain applications. However, proper alloy/temper selection, good design and assembly practices, and environmental protection, combined with regular inspections, have proved to be highly successful techniques for the prevention of SCC failure in high-strength parts (Ref 15, 16).

The exact mechanisms responsible for SCC of a susceptible aluminum alloy in a particular environment remains controversial. However, most proposed mechanisms are variations of two basic theories: crack advance by anodic dissolution or hydrogen embrittlement. The controlling factors in these two SCC models are as follows:

Anodic dissolution is characterized by:

- Grain boundary precipitate size, spacing, and/or volume fraction
- Grain boundary PFZ width, solute profile or deformation mode
- Matrix precipitate size/distribution and deformation mode
- Oxide rupture and repassivation kinetics,

while *hydrogen embrittlement* is characterized by:

- Hydrogen absorption leading to grain boundary or transgranular decohesion
- Internal void formation via gas pressurization
- Enhanced plasticity (adsorption and absorption arguments exist)

An important fact to remember is that pure aluminum does not stress corrode, and for any given system, susceptibility usually increases with solute content. This fact, coupled with data and the controlling factors of the two models, suggests that microstructural alterations may influence SCC behavior for a given composition.

It is possible that hydrogen may contribute in the SCC of certain alloys and tempers of aluminum, although a detailed mechanistic understanding of SCC in aluminum alloys still requires more research (Ref 17). Recent literature surveys indicate considerable dispute as to how much, if at all, high-strength Al alloys are embrittled by hydrogen (Ref 18, 19, 20). There has not been enough evidence of hydrogen embrittlement to restrict commercialization of high-strength Al alloys (Ref 21).

SCC Resistance Ratings

An important step in controlling SCC by proper alloy selection is the SCC ranking of candidate materials. To establish performance that can be expected in service, it is necessary to compare candidate materials with other materials for which either long-term service experience or appropriate laboratory test data are available. Such comparisons, however, can be influenced significantly by test procedures (Ref 22-24). Laboratory stress-corrosion tests are generally of two types: constant deflection tests of smooth tensile bars or *C*-ring specimens loaded in aggressive environments, or crack propagation tests of precracked fracture mechanics specimens in aggressive environments. Commonly used criteria for SCC resistance from these tests include:

- Stress threshold (σ_{th}) below which laboratory specimens do not fail in aggressive environments
- Stress intensity threshold (K_{th}) below which crack propagation does not occur in precracked specimens
- Crack velocity measurements (da/dt) versus stress intensity in aggressive environments

There presently are no foolproof stress-corrosion test methods that are free of special limitations on test conditions and free of problems on interpretation of test results. However, a system of ratings of resistance to SCC for high-strength aluminum alloy products based on σ_{th} of smooth test specimens has been developed by a joint task group of ASTM and the Aluminum Association to assist alloy and temper selection, and it has been incorporated into ASTM G64 (Ref 25). Definitions of these ratings, which range from A (highest resistance) to D (lowest resistance), are as follows (adapted from G64-91):

- *A: Very high.* No record of service problems; SCC is not anticipated in general applications.
- *B: High.* No record of service problems; SCC is not anticipated at stresses of the magnitude caused by solution heat treatment. Precautions must be taken to avoid high sustained tensile stresses (exceeding 50% of the minimum specified yield strength) produced by any combination of sources including heat treatment, straightening, forming, fit-up, and sustained service loading.
- *C: Intermediate.* Stress-corrosion cracking is not anticipated if total sustained tensile stress is maintained below 25% of minimum specified yield strength. This rating is designated for the short-transverse direction in products used primarily for high resistance to exfoliation corrosion in relatively thin structures, where appreciable stresses in the short-transverse direction are unlikely.
- *D: Low.* Failure due to SCC is anticipated in any application involving sustained tensile stress in the designated test direction. This rating is currently designated only for the short-transverse direction in certain products.

Ratings are based on service experience, if available, or on standard SCC tests (ASTM G47, Ref 26) as required by many materials specifications. This exposure represents a severe control environment commonly used in alloy development and quality control. To rate a new material and test direction, according to G47, tests are performed on at least ten random lots and the test results must have 90% compliance at a 95% level of confidence for one of the following stress levels:

- A: Up to and including 75% of the specified minimum yield strength
- B: Up to and including 50% of the specified minimum yield strength
- C: Up to and including 25% of the specified minimum yield strength
- D: Fails to meet the criterion for rating C

It is cautioned, however, that these generalized SCC ratings may involve an oversimplification in regard to the performance in unusual chemical environments. In this rating system, a quantitative (numerical) ranking was avoided because current SCC test methods do not justify finite values. Table 9 contains a tabulation of alloys and tempers, product forms, and stressing directions,

Table 9 Relative stress-corrosion cracking ratings for high-strength wrought aluminum products

The associated stress levels for rankings A, B, C, D (see text) are not to be interpreted as threshold stresses and are not recommended for design. Documents such as MIL-HANDBOOK-5, MIL-STD-1568, NASC SD-24, and MSFC-SPEC-552A should be consulted for design recommendations. Resistance ratings are as follows: A, very high; B, high; C, intermediate; D, low (see text)

Alloy and temper(a)	Test direction(b)	Rolled plate	Rod and bar(c)	Extruded shapes	Forgings
2011-T3, -T4	L	(d)	B	(d)	(d)
	LT	(d)	D	(d)	(d)
	ST	(d)	D	(d)	(d)
2011-T8	L	(d)	A	(d)	(d)
	LT	(d)	A	(d)	(d)
	ST	(d)	A	(d)	(d)
2014-T6	L	A	A	A	B
	LT	B(e)	D	B(e)	B(e)
	ST	D	D	D	D
2024-T3, -T4	L	A	A	A	(d)
	LT	B(e)	D	B(e)	(d)
	ST	D	D	D	(d)
2024-T6	L	(d)	A	(d)	A
	LT	(d)	B	(d)	A(e)
	ST	(d)	B	(d)	D
2024-T8	L	A	A	A	A
	LT	A	A	A	A
	ST	B	A	B	C
2048-T851	L	A	(d)	(d)	(d)
	LT	A	(d)	(d)	(d)
	ST	B	(d)	(d)	(d)
2124-T851	L	A	(d)	(d)	(d)
	LT	A	(d)	(d)	(d)
	ST	B	(d)	(d)	(d)
2219-T3, -T37	L	A	(d)	A	(d)
	LT	B	(d)	B	(d)
	ST	D	(d)	D	(d)
2219-T6	L	(d)	(d)	(d)	A
	LT	(d)	(d)	(d)	A
	ST	(d)	(d)	(d)	A
2219-T87, -T8	L	A	A	A	A
	LT	A	A	A	A
	ST	A	A	A	A
6061-T6	L	A	A	A	A
	LT	A	A	A	A
	ST	A	A	A	A
7005-T53, -T63	L	(d)	(d)	A	A
	LT	(d)	(d)	A(e)	A(e)
	ST	(d)	(d)	D	D
7039-T63, -T64	L	A	(d)	A	(d)
	LT	A(e)	(e)	A(e)	(d)
	ST	D	(d)	D	(d)
7049-T73	L	A	(d)	A	A
	LT	A	(d)	A	A
	ST	A	(d)	B	A
7049-T76	L	(d)	(d)	A	(d)
	LT	(d)	(d)	A	(d)
	ST	(d)	(d)	C	(d)
7149-T73	L	(d)	(d)	A	A
	LT	(d)	(d)	A	A
	ST	(d)	(d)	B	A
7050-T74	L	A	(d)	A	A
	LT	A	(d)	A	A
	ST	B	(d)	B	B
7050-T76	L	A	A	A	(d)
	LT	A	B	A	(d)
	ST	C	B	C	(d)
7075-T6	L	A	A	A	A
	LT	B(e)	D	B(e)	B(e)
	ST	D	D	D	D
7075-T73	L	A	A	A	A
	LT	A	A	A	A
	ST	A	A	A	A

(continued)

(a) Ratings apply to standard mill products in the types of tempers indicated and also in TX5X and TX5XX (stress-relieved) tempers. They may be invalidated in some cases by use of nonstandard thermal treatments, or mechanical deformation at room temperature, by the user. (b) Test direction refers to orientation of direction in which stress is applied relative to the directional grain structure typical of wrought alloys, which for extrusions and forgings may not be predictable on the basis of the cross-sectional shape of the product: L, longitudinal; LT, long transverse; ST, short transverse. (c) Sections with width-to-thickness ratios equal to or less than two, for which there is no distinction between LT and ST properties. (d) Rating not established because product not offered commercially. (e) Rating is one class lower for thicker sections; extrusions, 25 mm (1 in.) and thicker; plate and forgings, 38 mm (1.5 in.) and thicker

with the classification of each into one of four categories from ASTM G64-91.

Precracked specimens and linear elastic fracture mechanics (LEFM) methods of analysis have also been widely used for SCC testing in recent years. It was anticipated that this new technique would provide a more quantitative measure of the resistance to the propagation of SCC of an alloy in the presence of a flaw. The test results are generally presented in a graph of the crack velocity versus the crack driving force in terms of a stress-intensity factor, K. Although the full diagram is required to describe the performance of an alloy, numbers derived from the diagram such as the "plateau velocity" and the "threshold stress intensity" (K_{th} or K_{Iscc}) can be used to compare materials. Effective use of the precracked specimen testing procedures, however, have proven very difficult to standardize, and there currently is no commonly accepted rating system for rating the resistance to SCC based on these descriptors. It is noteworthy that ranking of alloys by these criteria corresponds well with the ratings obtained with smooth specimens in ASTM G64.

Alloy Selection for SCC Resistance

In general, high-purity aluminum and low-strength aluminum alloys are not susceptible to SCC. Occurrence of SCC is chiefly confined to higher-strength alloy classes, such as 2XXX and 7XXX alloys and 5XXX Al-Mg alloys containing 3% or more Mg, particularly when loaded in the short-transverse orientation. Historically, in higher-strength alloys (e.g., aircraft structures) most service failures involving SCC of aluminum alloys have resulted from assembly or residual stresses acting in a short-transverse direction relative to the grain flow of the product (Ref 15, 18, 21). This is generally more troublesome for parts machined from relatively thick sections of rolled plate, extrusions, or forgings of complex shape where short-transverse grain orientation may be exposed. The specific alloy/temper combinations 7079-T6 (now obsolete), 7075-T6, and 2024-T3 have contributed to 90% of all service SCC failures of aluminum alloy products.

Within the high-strength alloy classes (2XXX, 7XXX, 5XXX), broad generalizations that relate susceptibility to SCC and strength or fracture toughness do not appear possible (Fig. 12). However, for certain alloys useful correlations of these properties with SCC resistance may be made over restricted ranges of the alloy's strength capability. For example, progressively overaging 7075 products from the T6 peak strength temper to T76 and T73 lowers strength but increases SCC resistance. However, "underaging" 7075 plate to T76 and T73 strength levels does not improve resistance to SCC.

Controls on alloy processing and heat treatment are key to assurance of high resistance to SCC without appreciable loss in mechanical properties and great accomplishments have been made. General developments are discussed below in several alloy classes.

Table 9 (continued)

Alloy and temper(a)	Test direction(b)	Rolled plate	Rod and bar(c)	Extruded shapes	Forgings
7075-T74	L	(d)	(d)	(d)	A
	LT	(d)	(d)	(d)	A
	ST	(d)	(d)	(d)	B
7075-T76	L	A	(d)	A	(d)
	LT	A	(d)	A	(d)
	ST	C	(d)	C	(d)
7175-T74	L	(d)	(d)	(d)	A
	LT	(d)	(d)	(d)	A
	ST	(d)	(d)	(d)	B
7475-T6	L	A	(d)	(d)	(d)
	LT	B(e)	(d)	(d)	(d)
	ST	D	(d)	(d)	(d)
7475-T73	L	A	(d)	(d)	(d)
	LT	A	(d)	(d)	(d)
	ST	A	(d)	(d)	(d)
7475-T76	L	A	(d)	(d)	(d)
	LT	A	(d)	(d)	(d)
	ST	C	(d)	(d)	(d)
7178-T6	L	A	(d)	A	(d)
	LT	B(e)	(d)	B(e)	(d)
	ST	D	(d)	D	(d)
7178-T76	L	A	(d)	A	(d)
	LT	A	(d)	A	(d)
	ST	C	(d)	C	(d)
7079-T6	L	A	(d)	A	A
	LT	B(e)	(d)	B(e)	B(e)
	ST	D	(d)	D	D

(a) Ratings apply to standard mill products in the types of tempers indicated and also in TX5X and TX5XX (stress-relieved) tempers. They may be invalidated in some cases by use of nonstandard thermal treatments, or mechanical deformation at room temperature, by the user. (b) Test direction refers to orientation of direction in which stress is applied relative to the directional grain structure typical of wrought alloys, which for extrusions and forgings may not be predictable on the basis of the cross-sectional shape of the product: L, longitudinal; LT, long transverse; ST, short transverse. (c) Sections with width-to-thickness ratios equal to or less than two, for which there is no distinction between LT and ST properties. (d) Rating not established because product not offered commercially. (e) Rating is one class lower for thicker sections; extrusions, 25 mm (1 in.) and thicker; plate and forgings, 38 mm (1.5 in.) and thicker

2XXX Alloys (Ref 28). Thick-section products of 2XXX alloys in the naturally aged T3 and T4 tempers have low ratings of resistance to SCC in the short-transverse direction. Ratings of such products in other directions are higher, as are ratings of thin-section products in all directions. These differences are related to the effects of quenching rate (largely determined by section thickness) on the amount of precipitation that occurs during quenching. If 2XXX alloys in T3 and T4 tempers are heated for short periods in the temperature range used for artificial aging, selective precipitation along grain or subgrain boundaries may further impair their resistance.

Artificial aging of 2XXX alloys to precipitation-hardened T8 tempers provides relatively high resistance to exfoliation, SCC, and superior elevated-temperature characteristics with modest strength increase over their naturally aged counterparts (Ref 27). Longer heating, as specified for T6 and T8 tempers, produces more general precipitation and significant improvements in resistance to SCC. Precipitates are formed within grains at a greater number of nucleation sites during treatment to T8 tempers. These tempers require stretching, or cold working by other means, after quenching from the solution heat treatment temperature and before artificial aging. These tempers provide the highest resistance for SCC and the highest strength in 2XXX alloys. This significant progress in improving fracture toughness of 2XXX alloys in T8 tempers is demonstrated by alloy 2124-T851 (also known as Alcoa 417 Process 2024-T851), which has had over 30 years of experience in military aircraft with no record of SCC problems. Typical data on 2XXX alloys are shown in Fig. 13.

Aluminum-Lithium Alloys. Some studies on aluminum-copper-lithium alloys indicate that these alloys have their highest resistance to SCC at or near peak-aged tempers. Underaging of these alloys (e.g., 2090) is detrimental; overaging decreases resistance only slightly. The susceptibility of the underaged microstructure has been attributed to the precipitation of an intermetallic constituent, Al_2CuLi, on grain boundaries during the early stages of artificial aging. This constituent is believed to be anodic to the copper-rich matrix of an underaged alloy, causing preferential dissolution and SCC. As aging time increases, copper-bearing precipitates form in the interior of the grains, thus increasing the anode-cathode area ratio in the microstructure to a more favorable value that avoids selective grain-boundary attack. Similar studies of stress-corrosion behavior are being conducted on aluminum-lithium-copper-magnesium alloys (e.g., 8090).

Newer Al-Li alloys have been developed that have lower lithium concentrations than 8090,

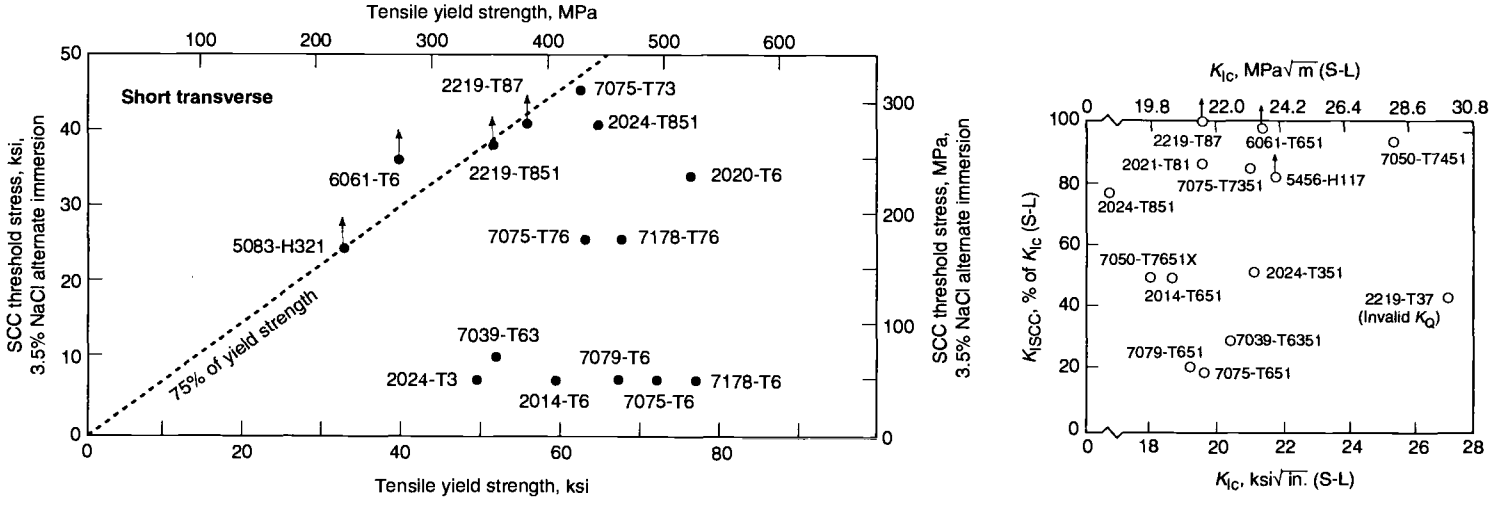

Fig. 12 Relationship between estimated stress-corrosion cracking "threshold stresses" and the tensile yield strength (a) and fracture toughness (b) of a wide variety of aluminum alloys and tempers. Data show that there is no general correlation. Source: Ref 16

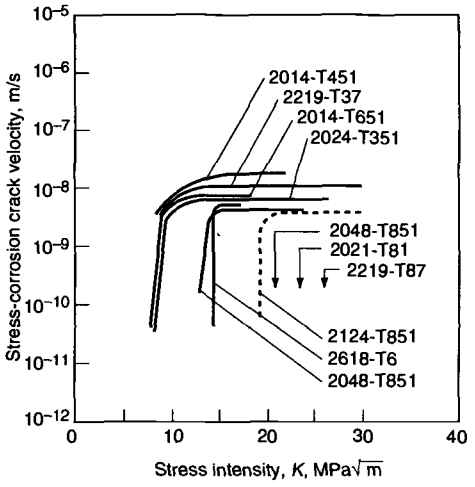

Fig. 13 Crack propagation rates in stress corrosion tests using precracked specimens of high-strength 2XXX series aluminum alloys, 25 mm thick, double cantilever beam, TL(S-L) orientation of plate, wet twice a day with an aqueous solution of 3.5% NaCl, 23 °C

2090, and 2091. These alloys do not appear to suffer from the same technical problems. The first of the newer generation was Weldalite 049 which can attain a yield strength as high as 700 MPa and an associated elongation of 10%. A refinement of the original alloy, 2195, is being considered for cryogenic tanks for the U.S. Space Shuttle. Alloy 2195 offers many advantages over 2219 for cryogenic tanks. Its higher strength coupled with higher modulus and lower density can lead to significant weight savings. Alloy 2195 also has good corrosion resistance, excellent fatigue properties, has a higher strength and fracture toughness at cryogenic temperatures than at room temperature, can be near-net shaped formed, and can be welded with proper precautions. However, further development work is required to identify optimum processing conditions that will ensure that the required combination of strength and fracture properties is obtained in the final product.

Other alloys containing less than 2% Li are being considered. Preliminary work indicates that new Al-Li alloy plate can be developed to provide a superior combination of properties for the bulkheads of high-performance aircraft, and analyses indicate that new Al-Li alloy flat-rolled products and extrusions would be competitive with polymer matrix composites for the horizontal stabilizer of commercial jetliners.

5XXX Alloys (Ref 28). These strain-hardening alloys do not develop their strength through solution heat treatment; rather, they are processed to H3 tempers, which require a final thermal stabilizing treatment to eliminate age softening, or to H2 tempers, which require a final partial annealing. The H116 or H117 tempers are also used for high-magnesium 5XXX alloys and involve special temperature control during fabrication to achieve a microstructural pattern of precipitate that increases the resistance of the alloy to intergranular corrosion and SCC. The alloys of the 5XXX series span a wide range of magnesium contents, and the tempers that are standard for each alloy are primarily established by the magnesium content and the desirability of microstructures highly resistant to SCC and other forms of corrosion.

Although 5XXX alloys are not heat treatable, they develop good strength through solution hardening by the magnesium retained in solid solution, dispersion hardening by precipitates, and strain-hardening effects. Because the solid solutions in the higher-magnesium alloys are more highly supersaturated, the excess magnesium tends to precipitate out as Mg_2Al_3, which is anodic to the matrix. Precipitation of the phase with high selectivity along grain boundaries, accompanied by little or no precipitation within grains, may result in susceptibility to SCC.

The probability that a susceptible microstructure will develop in a 5XXX alloy depends on magnesium content, grain structure, amount of strain hardening, and subsequent time/temperature history. Alloys with relatively low magnesium contents, such as 5052 and 5454 (2.5 and 2.7% Mg, respectively), are only mildly supersaturated; consequently, their resistance to SCC is not affected by exposure to elevated temperatures. In contrast, alloys with magnesium contents exceeding about 3%, when in strain-hardened tempers, may develop susceptible structures as a result of heating or even after very long times at room temperature. For example, the microstructure of alloy 5083-O (4.5% Mg) plate stretched 1% is relatively free of precipitate (no continuous second-phase paths), and the material is not susceptible to SCC. Prolonged heating below the solvus, however, produces continuous precipitate, which results in susceptibility.

6XXX Alloys (Ref 28). The service record of 6XXX alloys shows no reported cases of SCC. In laboratory tests, however, at high stresses and in aggressive solutions, cracking has been demonstrated in 6XXX alloys of particularly high alloy content, containing silicon in excess of the Mg_2Si ratio and/or high percentages of copper.

7XXX Alloys Containing Copper (Ref 28). The 7XXX series alloy that has been used most extensively and for the longest period of time is 7075, an aluminum-zinc-magnesium-copper-chromium alloy. Introduced in 1943, this aircraft construction alloy was initially used for products with thin sections, principally sheet and extrusions. In these products, quenching rate is normally very high, and tensile stresses are not encountered in the short-transverse direction; thus, SCC is not a problem for material in the highest-strength (T6) tempers. When 7075 was used in products of greater size and thickness, however, it became apparent that such products heat treated to T6 tempers were often unsatisfactory. Parts that were extensively machined from large forgings, extrusions, or plate were frequently subjected to continuous stresses, arising from interference misfit during assembly or from service loading, that were tensile at exposed surfaces and aligned in unfavorable orientations. Under such conditions, SCC was encountered in service with significant frequency (Ref 29).

The problem resulted in the introduction (in about 1960) of the T73 tempers for thick-section 7075 products. The precipitation treatment used to develop these tempers requires two-stage artificial aging, the second stage of which is done at a higher temperature than that used to produce T6 tempers. During the preliminary stage, a fine, high-density precipitation dispersion is nucleated, producing high strength. The second stage is then used to develop resistance to SCC and exfoliation. The additional aging treatment required to produce 7075 in T73 tempers, reduces strength to levels below those of 7075 in T6 tempers. Excellent test results for 7075-T73 have been confirmed by extensive service experience in various applications. Environmental testing has demonstrated that 7075-T73 resists SCC even when stresses are oriented in the least favorable direction, at stress levels up to 300 MPa (44 ksi). Under similar conditions, the maximum stress at which 7075-T6 resists cracking is about 50 MPa (7 ksi).

Utilizing T7-type overaged tempers is a primary way to ensure improved resistance to exfoliation and SCC in 7XXX alloys. The T73 temper for alloy 7075 was the first aluminum alloy temper specifically developed to provide high resistance to stress-corrosion cracking with acceptable strength reduction from the T6 temper. Favorable evidence of this alloy's high resistance covers over 35 years of testing experience and extensive use in critical applications with no reported instances of failure in service by stress-corrosion cracking. This experience surpasses that of all other high-strength aluminum alloys and has become a standard of comparison for rating newer alloys and tempers (Ref 30).

Several commercial 7XXX alloys (7049-T73 and T76, 7175-T74 and 7050-T73, T74, and T76) offer combinations of strength, fracture toughness, and resistance to SCC superior to those combinations provided by conventional high-strength alloys, such as 7075-T6 and 7079-T6 (Ref 27). Alloys 7*x*49 and 7*x*50 were developed specifically for optimum combinations of the above properties in thick sections. Increased copper content provided good balance of strength and SCC resistance, while restriction of the impurity elements iron and silicon provided high toughness. Of particular note are 7149-T7451 and 7150-T7451 plate alloys, which offers optimum combinations of toughness, SCC resistance, and strength. Certain high-strength 7XXX alloys with lower copper content, such as 7079 and weldable 7005, exhibit excessive strength reduction when overaged to a T73-type temper, and a commercial stress-corrosion-resistant temper does not exist for these alloys. When using these alloys in existing commercial tempers, appreciable short-transverse tensile stresses, about 10 ksi (69 MPa) or above, should be avoided where exposure to an aggressive environment is of concern.

Alloy 7175, a variant of 7075, was developed for forgings. In the T74 temper, 7175 alloy forgings have strength nearly comparable to that of 7075-T6 and has better resistance to SCC (Fig.

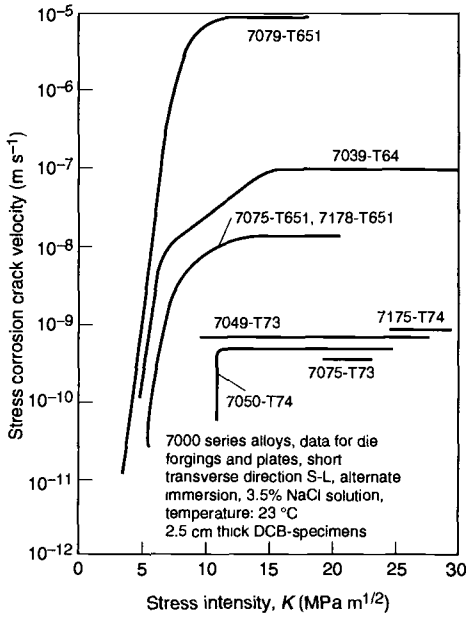

Fig. 14 Crack propagation rates in stress corrosion tests using 7XXX series aluminum alloys, 25 mm thick, double cantilever beam, short-transverse orientation of die transverse orientation of die forgings and plate, alternate immersion tests, 23 °C. Source: M.O. Speidel, *Met. Trans.*, Vol 6A, 1975, p 631

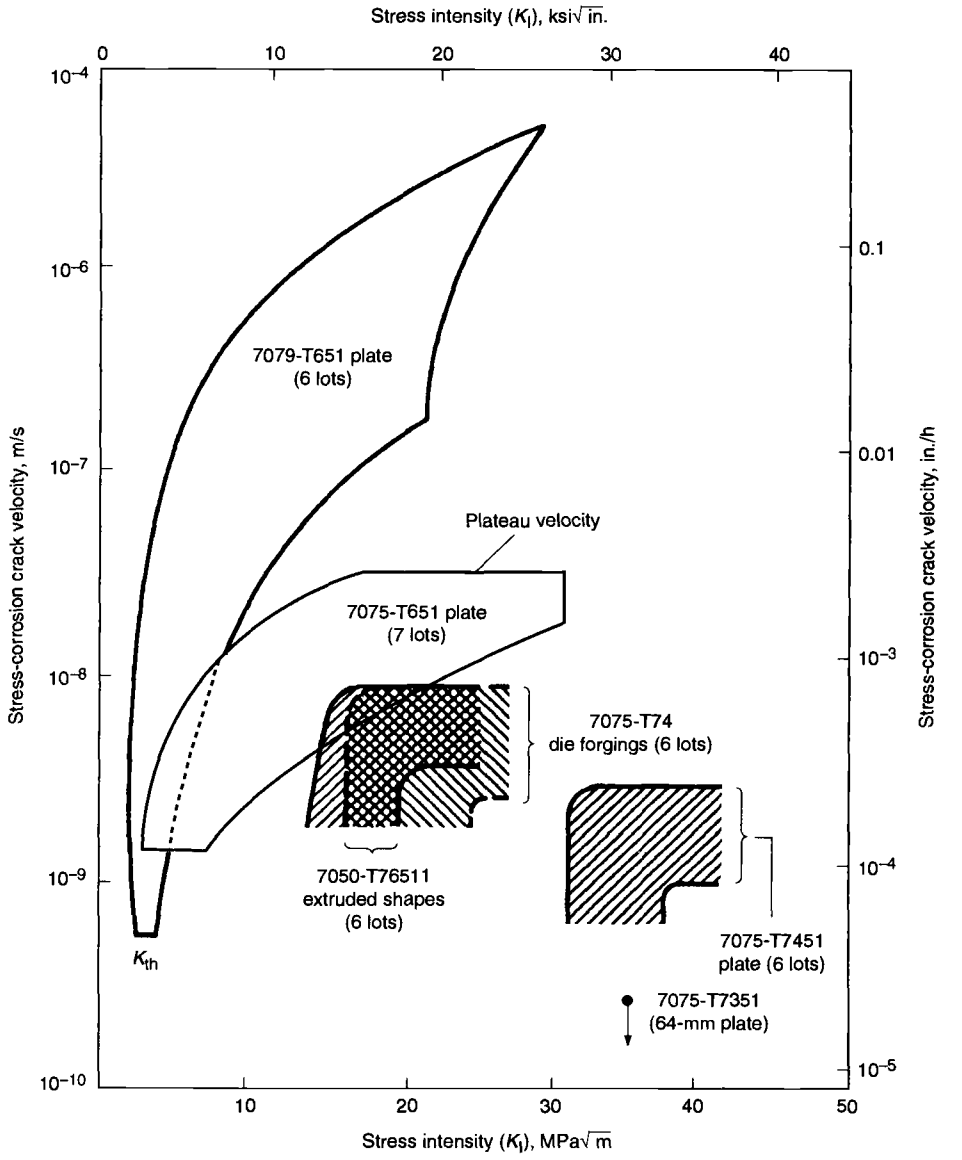

Fig. 15 SCC propagation rates for various aluminum alloy 7050 products. Double-beam specimens (S-L) bolt-loaded to pop-in and wetted three times daily with 3.5% NaCl. Plateau velocity averaged over 15 days. The right-hand end of the band for each product indicates the pop-in starting stress intensity (K_{Io}) for the tests of that material. Data for alloys 7075-T651 and 7079-T651 are from Ref 31. Source: Ref 32

14). Newer alloys—such as 7049 and 7475, which are used in the T73 temper, and 7050, which is used in the T74 temper—couple high strength with very high SCC resistance and improved fracture toughness. The superior performance is evident for alloys in the T7 tempers (Fig. 15) (Ref 31, 32).

The T76 tempers, which also require two-stage artificial aging and which are intermediate to the T6 and T73 tempers in both strength and resistance to SCC, are developed in copper-containing 7XXX alloys for certain products. Comparative ratings of resistance for various products of all these alloys, as well as for products of 7178, are given in Table 9.

The microstructural differences among the T6, T73, and T76 tempers of these alloys are differences in size and type of precipitate, which changes from predominantly Guinier-Preston (GP) zones in T6 tempers to η', the metastable transition form of $\eta(MgZn_2)$, in T73 and T76 tempers. None of these differences can be detected by optical metallography. In fact, even the resolutions possible in transmission electron microscopy are insufficient for determining whether the precipitation reaction has been adequate to ensure the expected level of resistance to SCC. For quality assurance, copper-containing 7XXX alloys in T73 and T76 tempers are required to have specified minimum values of electrical conductivity and, in some cases, tensile yield strengths that fall within specified ranges. The validity of these properties as measures of resistance to SCC is based on many correlation studies involving these measurements, laboratory and field stress-corrosion tests, and service experience.

T77 Tempers. Until recently, overaging to T76, T74, and T73 tempers increased exfoliation resistance with a compromise in strength; strength was sacrificed from 5 to 20% to provide adequate resistance. The T77 temper, however, provides resistance to exfoliation with no sacrifice in strength, and resistance to SCC superior to that of 7075-T6 and 7150-T6. The highest strength aluminum alloy products, 7055 plate and extrusions, are supplied primarily in the T77 temper. Alloy 2024 products are also resistant to intergranular corrosion in the T8 temper, but fracture toughness and resistance to the growth of fatigue cracks suffer relative to 2024-T3.

New processing for 7150, resulting in 7150-T77, offers a higher strength with the durability and damage tolerance characteristics matching or exceeding those of 7050-T76. Extrusions of 7150-T77 have been selected by Boeing as fuselage stringers for the upper and lower lobes of the new 777 jetliner because of the superior combination of strength, corrosion and SCC characteristics, and fracture toughness. Alloy 7150-T77 plate and extrusions are being used on the new C17 cargo transport. Use of this material saved considerable weight because corrosion performance of 7150-T6 was deemed to be inadequate.

The implementation of the T77 temper for 7150 was followed by development of new 7XXX products for compressively loaded structures. Alloy 7055-T77 plate and extrusions offer a strength increase of about 10% relative to that of 7150-T6 (almost 30% higher than that of 7075-T76). They also provide a high resistance to exfoliation corrosion similar to that of 7075-T76 with fracture toughness and resistance to the

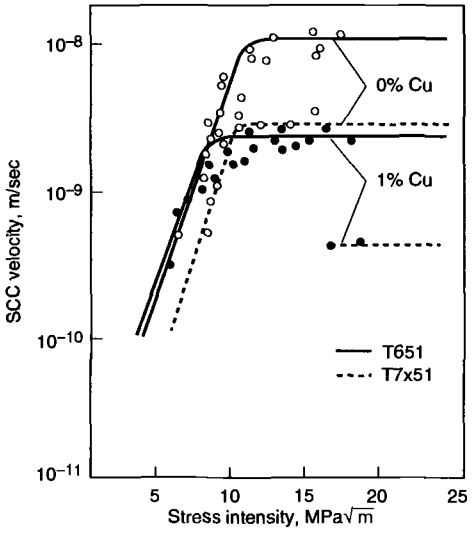

Fig. 16 Effect of overaging and copper content on SCC resistance of an Al-Zn-Mg alloy in 3.5% NaCl solution. Source: Ref 33

growth of fatigue cracks similar to that of 7150-T6. In contrast to the usual loss in toughness of 7XXX products at low temperatures, fracture toughness of 7055-T77 at –65 °F (220 K) is similar to that at room temperature. Resistance to SCC is intermediate to those of 7075-T6 and 7150-T77 products. The attractive combination of properties of 7055-T77 is attributed to its high ratios of Zn/Mg and Cu/Mg. When aged to T77 this composition provides a microstructure at and near grain boundaries that is resistant to intergranular fracture and to intergranular corrosion.

Copper-free 7XXX Alloys (Ref 28). Wrought alloys of the 7XXX series that do not contain copper are of considerable interest because of their good resistance to general corrosion, moderate-to-high strength, and good fracture toughness and formability. Alloys 7004 and 7005 have been used in extruded form and, to a lesser extent, in sheet form for structural applications. More recently introduced compositions, including 7016, 7021, 7029, and 7146, have been used in automobile bumpers formed from extrusions or sheet.

As a group, copper-free 7XXX alloys are less resistant to SCC than other types of aluminum alloys when tensile stresses are developed in the short-transverse direction at exposed surfaces. Resistance in other directions may be good, particularly if the product has an unrecrystallized microstructure and has been properly heat treated. Products with recrystallized grain structures are generally more susceptible to SCC as a result of residual stress induced by forming or mechanical damage after heat treatment. When cold forming is required, subsequent solution heat treatment or precipitation heat treatment is recommended. Applications of these alloys must be carefully engineered, and consultation among designers, application engineers and product producers, or suppliers is advised in all cases.

Overaging (T7*x* tempers) improves the SCC resistance of copper-containing alloys such as 7075, whereas for the low-copper alloys, like 7079, a considerable amount of overaging is required with severe strength penalty to improve the stress-corrosion resistance. In general, increasing the copper content decreases the crack velocity (Fig. 16) (Ref 33). The effect can be mainly attributed to the change in the electrochemical activity of the precipitates as a function of their copper content. In the 7XXX series alloys the η phase is very active and anodic with respect to the film-covered matrix. If the alloy contains copper, copper both dissolves in the matrix and enters the η phase, making both more noble. As a result, the mixed potential at the crack tip shifts to a more noble value. The decrease in the crack velocity can then be attributed to the reduced rate of dissolution of the more noble precipitates, or reduced rate of hydrogen ion reduction and hydrogen adsorption at the crack tip at the more noble potential.

Casting Alloys (Ref 28). The resistance of most aluminum casting alloys to SCC is sufficiently high that cracking rarely occurs in service. The microstructures of these alloys are usually nearly isotropic; consequently, resistance to SCC is unaffected by orientation of tensile stresses.

Accelerated laboratory tests, natural-environment testing, and service experience indicate that alloys of the aluminum-silicon 4XX.X series, 3XX.X alloys containing only silicon and magnesium as alloying additions, and 5XX.X alloys with magnesium contents of 8% or lower have virtually no susceptibility to SCC. Alloys of the 3XX.X group that contain copper are rated as less resistant, although the numbers of castings of these alloys that have failed by SCC have not been significant.

Significant SCC of aluminum alloy castings in service has occurred only in the highest-strength aluminum-zinc-magnesium 7XX.X alloys and in the aluminum-magnesium alloy 520.0 in the T4 temper. For such alloys, factors that require careful consideration include casting design, assembly and service stresses, and anticipated environmental exposure.

Fatigue Life of Aluminum Alloys

Although high-strength aluminum alloys with high toughness have drastically lowered the probability of catastrophic failures in high-performance structures, corrosion fatigue requirements will continue to bear the burden for low-maintenance, durable, long-life structures. Good design, attention to structural details, and reliable inspection are of primary importance to controlling fatigue, and designers have traditionally considered these factors more important than alloy choice. However, a primary challenge facing designers and the materials engineer alike is extension of fatigue life and/or increased structural efficiency through optimum selection and use of fatigue-resistant alloys.

Differences in the fatigue performance of engineering materials can be translated into longer life, reduced weight, and reduced maintenance costs of present engineering structures. Fatigue improvements in aluminum, titanium, and steel alloys have been demonstrated through modifications to alloy composition, fabricating practice, and processing controls. Better understanding of fatigue mechanics has led to new hypotheses having the potential to lead to commercialization of improved alloys for fatigue.

Early work at Alcoa on large numbers of smooth and notched specimens demonstrated that wide variations in commercial aluminum alloys caused little or no detectable difference in fatigue strengths (Ref 34, 35). When early fatigue crack growth experiments categorized fatigue crack growth rates of aluminum alloys into one band, for example Fig. 17, it was generalized that fatigue resistance of all aluminum alloys were alike (Ref 36, 37). As a consequence of these early beliefs, further efforts to develop fatigue-resistant aluminum alloys were minimized, and though several conceptual improvements have been advanced in laboratory experiments (Ref 13), none to date have reached commercial levels. For alloys developed to provide improved combinations of properties such as strength, corrosion resistance, and fracture toughness, fatigue resistance was determined as a last step before products were offered for sale, only to ensure that fatigue resistance was not degraded.

Despite early conclusions from laboratory data, users discovered that certain aluminum alloys performed decidedly better than others in

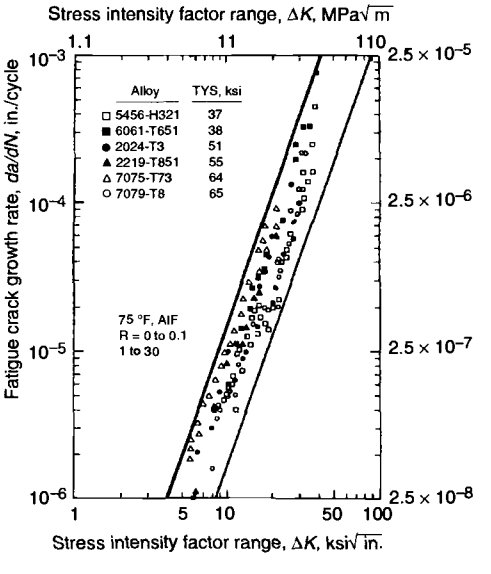

Fig. 17 Scatter band limits for fatigue crack growth rate behavior for a range of aluminum alloys. Source: Ref 26

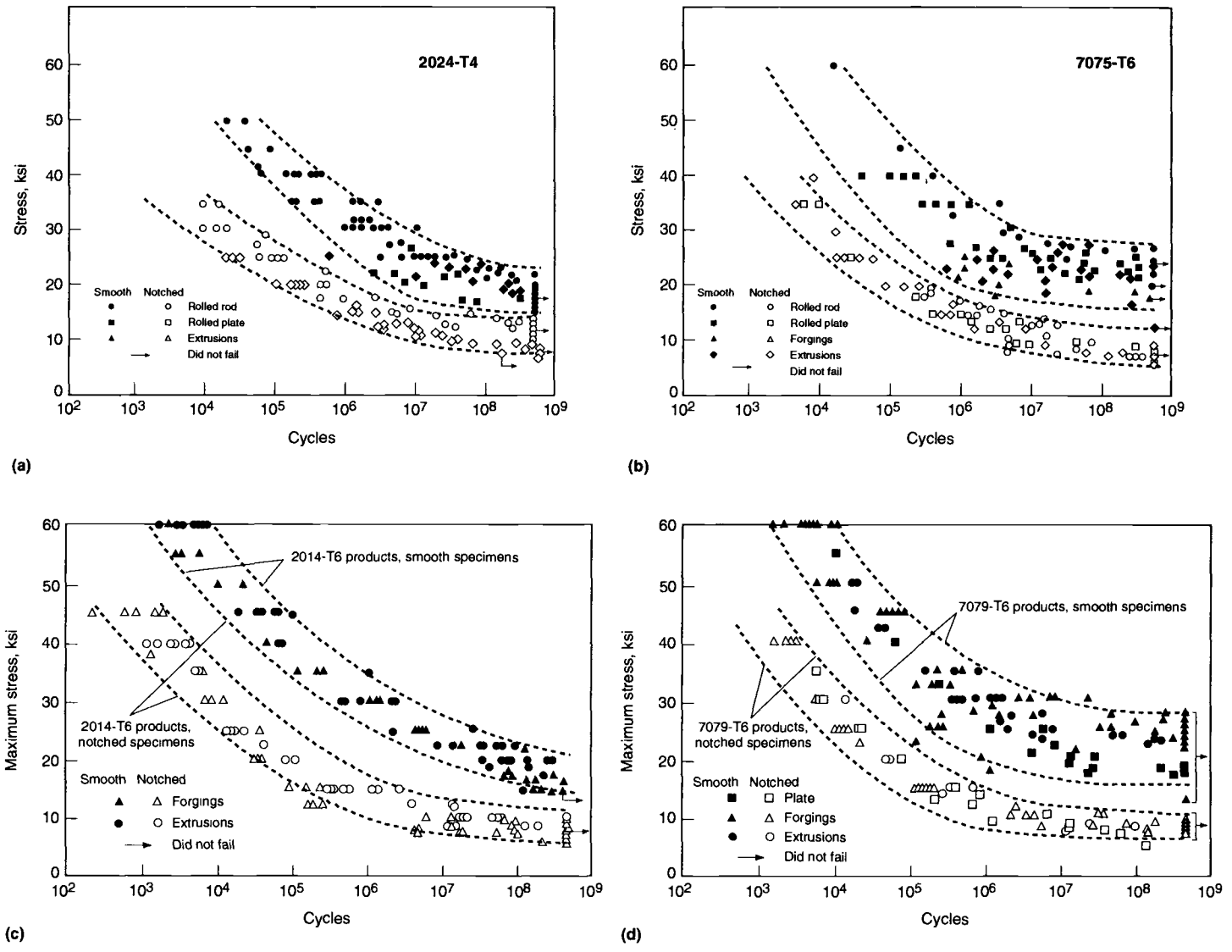

Fig. 18 Variation in rotating-beam fatigue for (a) 2024-T4, (b) 7075-T6, (c) 2014-T6, and (d) 7079-T6 alloys. Notches (60°) were very sharp ($K_t > 12$) with a radius of about 0.0002 in. Results are from over a thousand rotating-beam tests performed in the 1940s. Sources: R. Templin, F. Howell, and E. Hartmann, "Effect of Grain-Direction on Fatigue Properties of Aluminum Alloys," Alcoa, 1950 and *ASTM Proceedings*, Vol 64, p 581-593

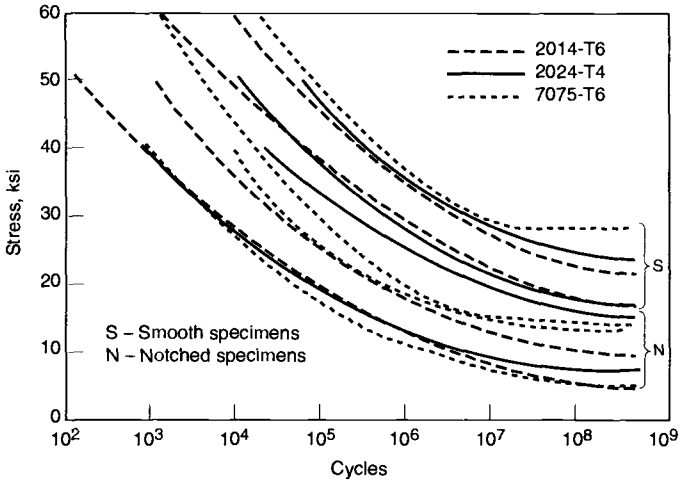

Fig. 19 Comparison of fatigue strength bands for 2014-T6, 2024-T4, and 7075-T6 aluminum alloys for rotating-beam tests. Source: R. Templin, F. Howell, and E. Hartmann, "Effect of Grain-Direction on Fatigue Properties of Aluminum Alloys," Alcoa, 1950

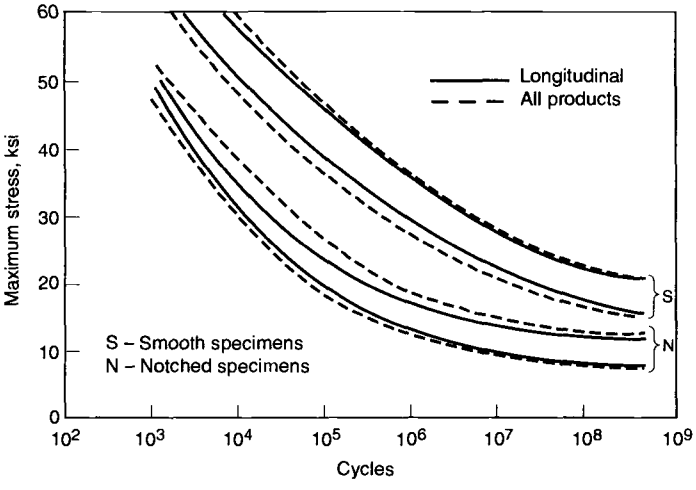

Fig. 20 Comparison of fatigue strength bands for 2014-T6 aluminum alloy products, showing effects of direction. Source: *ASTM Proceedings*, Vol 64, p 581-593

service when fluctuating loads were encountered, and therefore any generalization that all aluminum alloys are alike in fatigue is not wholly appropriate for design use. For example, alloy 2024-T3 has long been recognized as a better fatigue performer in service than alloy 7075-T6. In part, this may be explained by designers using higher design stresses on the basis of higher static strength of 7075-T6. However, results of Fig. 18(b) show alloy 7075-T6 to have broader scatter for smooth specimens and a lower bound of performance for severely notched specimens that is below that for alloy 2024-T4 (Fig. 18a). Broader scatter is also evident for 7079 compared to 2014 (Fig. 18c and d).

Most fatigue data were obtained from the basic stress-controlled cycling of notched and unnotched coupons in rotating-beam, axial, and flexure-type sheet tests. Test results from coupon specimens are useful for rating fatigue resistance of materials. However, material selection by the traditional *S-N* approach requires large numbers of material characterization tests for each material to simulate a myriad of possible service conditions. *S-N* data are also strongly influenced by many factors, such as specimen configuration, test environment, surface condition, load type, and stress ratio. Therefore, caution is required when translating coupon test results to a particular application. Evaluation of more than one material in component testing is needed to assist in final accurate material selection.

Nonetheless, extensive efforts have led to major improvements in the ability to characterize cyclic behavior and fatigue resistance of materials. Recognition of the importance of controlling basic elements of test procedure have led to development of recommended practices for establishing basic *S-N* fatigue data (Ref 38). The emerging disciplines of strain control fatigue and fracture mechanics have greatly enhanced understanding of fatigue processes. The strain control approach is aimed primarily at low-cycle fatigue crack initiation and early fatigue crack growth, while fracture mechanics concepts address the propagation of an existing crack to final failure. Each of these approaches is reviewed in the following sections.

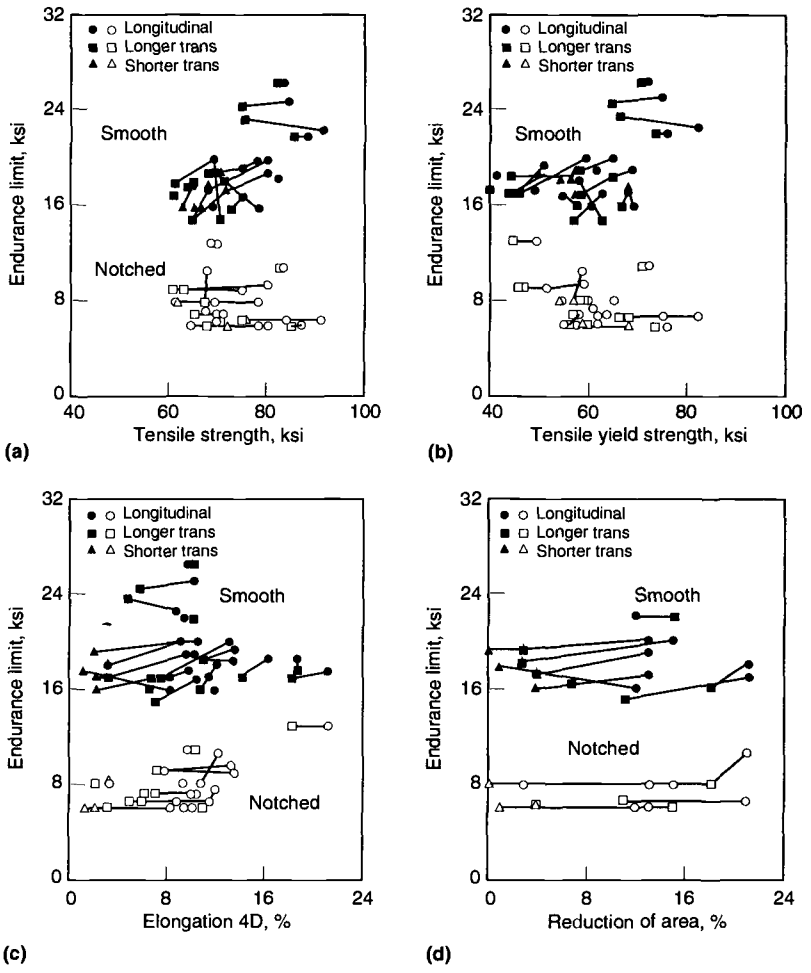

Fig. 21 Plots of fatigue with static mechanical properties for 2014, 2024, and 7075 aluminum alloys. (a) Endurance limit vs. tensile strength. (b) Endurance limit vs. yield strength. (c) Endurance limit vs. Elongation. (d) Endurance limit vs. reduction of area. Sharp notches ($K_t > 12$). Source: R. Templin, F. Howell, and E. Hartmann, "Effect of Grain-Direction on Fatigue Properties of Aluminum Alloys," Alcoa, 1950

S-N Fatigue

High-cycle fatigue characteristics commonly are examined on the basis of cyclic *S-N* plots of rotating-beam, axial, or flexure-type sheet tests. Many thousands of tests have been performed, and a collection of aluminum alloy *S-N* data is contained in the publication *Fatigue Data Book: Light Structural Alloys* (ASM, 1995). Early work on rotating-beam tests is summarized in Fig. 19. There seems to be greater spread in fatigue strengths for unnotched specimens than for notched specimens. This appears to be evidence that the presence of a notch minimizes differences, thus suggesting similar crack propagation after crack initiation with a sharp notch. In this context, the spread in smooth fatigue life is partly associated with variations in crack initiation sources (at surface imperfections or strain localizations). In general, however, the *S-N* approach does not provide clear distinctions in characterizing the crack initiation and crack propagation stages of fatigue.

The *S-N* response curves for rotating-beam fatigue strength of unnotched aluminum alloys tend to level out as the number of applied cycles approaches 500 million. This allows some rating of fatigue endurance, and estimated fatigue limits from rotating-beam tests have been tabulated for many commercial aluminum alloys (Table 10). Fatigue limits should not be expected in aggressive environments, as *S-N* response curves don't tend to level out when corrosion fatigue occurs. Rotating-beam strengths determined in the transverse direction are not significantly different from test results in the longitudinal direction. The scatter band limits in Fig. 20 show relatively small effects attributable to working direction, particularly for the notched fatigue data.

Rotating-beam data have also been analyzed to determine whether fatigue strength can be correlated with static strength. From a plot of average endurance limits (at 5×10^8 cycles) plotted against various tensile properties (Fig. 21), there does not appear to be any well-defined quantitative relation between fatigue limit and static strength. This is consistent with results for most nonferrous alloys. It should be noted that proportionate increases in fatigue strength from tensile strengths do appear lower for age-hardened aluminum alloys than for strain-hardened alloys (Fig. 22). A similar trend appears evident for fatigue strength at 5×10^7 cycles (Fig. 23).

Effect of Environment. A key source of variability in *S-N* data is environment (Ref 39-41). Even atmospheric moisture is recognized to have a little corrosive effect on fatigue performance of aluminum alloys. Much high-cycle *S-N* testing has been carried out in uncontrolled ambient lab air environments, thereby contributing to scatter in existing data. This factor should be recognized when comparing results of different investigations.

Most aluminum alloys experience some reduction of fatigue strength in corrosive environments such as seawater, especially in low-stress, long-life tests (e.g., Fig. 24). Unlike sustained-load SCC, fatigue degradation by environment may occur even when the direction of principal loading with respect to grain flow is other than short-

Table 10 Typical tensile properties and fatigue limit of aluminum alloys

Alloy and temper	Ultimate tensile strength		Tensile yield strength		Elongation in 50 mm (2 in.), %		Fatigue endurance limit(a)	
					1.6 mm (1/16 in.) thick specimen	1.3 mm (1/2 in.) diam specimen		
	MPa	ksi	MPa	ksi			MPa	ksi
1060-0	70	10	30	4	43	...	20	3
1060-H12	85	12	75	11	16	...	30	4
1060-H14	95	14	90	13	12	...	35	5
1060-H16	110	16	105	15	8	...	45	6.5
1060-H18	130	19	125	18	6	...	45	6.5
1100-0	90	13	35	5	35	45	35	5
1100-H12	110	16	105	15	12	25	40	6
1100-H14	125	18	115	17	9	20	50	7
1100-H16	145	21	140	20	6	17	60	9
1100-H18	165	24	150	22	5	15	60	9
1350-0	85	12	30	4	...	(d)	...	...
1350-H12	95	14	85	12	...	...	...	...
1350-H14	110	16	95	14	...	...	...	...
1350-H16	125	18	110	16	...	...	...	...
1350-H19	185	27	165	24	...	(e)	50	7
2011-T3	380	55	295	43	...	15	125	18
2011-T8	405	59	310	45	...	12	125	18
2014-0	185	27	95	14	...	18	90	13
2014-T4, T451	425	62	290	42	...	20	140	20
2014-T6, T651	485	70	415	60	...	13	125	18
Alclad 2014-0	175	25	70	10	21	...	...	...
Alclad 2014-T3	435	63	275	40	20	...	...	...
Alclad 2014-T4, T451	420	61	255	37	22	...	...	...
Alclad 2014-T6, T651	470	68	415	60	10	...	...	...
2017-0	180	26	70	10	...	22	90	13
2017-T4, T451	425	62	275	40	...	22	125	18
2018-T61	420	61	315	46	...	12	115	17
2024-0	185	27	75	11	20	22	90	13
2024-T3	485	70	345	50	18	...	140	20
2024-T4, T351	470	68	325	47	20	19	140	20
2024-T361(b)	495	72	395	57	13	...	125	18
Alclad 2024-0	180	26	75	11	20	...	...	...
Alclad 2024-T3	450	65	310	45	18	...	...	...
Alclad 2024-T4, T351	440	64	290	42	19	...	...	...
Alclad 2024-T361(b)	460	67	365	53	11	...	...	...
Alclad 2024-T81, T851	450	65	415	60	6	...	...	...
Alclad 2024-T861(b)	485	70	455	66	6	...	...	...
2025-T6	400	58	255	37	...	19	125	18
2036-T4	340	49	195	28	24	...	125(c)	18(c)
2117-T4	295	43	165	24	...	27	95	14
2125	...	...	...	...	...	...	90	13(d)
2124-T851	485	70	440	64	...	8	...	...
2214	...	...	...	...	...	...	103	15(d)
2218-T72	330	48	255	37	...	11	...	...
2219-0	175	25	75	11	18	...	...	...
2219-T42	360	52	185	27	20	...	...	...
2219-T31, T351	360	52	250	36	17	...	...	...
2219-T37	395	57	315	46	11	...	...	...
2219-T62	415	60	290	42	10	...	105	15
2219-T81, T851	455	66	350	51	10	...	105	15
2219-T87	475	69	395	57	10	...	105	15
2618-T61	440	64	370	54	...	10	125	18
3003-0	110	16	40	6	30	40	50	7
3003-H12	130	19	125	18	10	20	55	8
3003-H14	150	22	145	21	8	16	60	9
3003-H16	180	26	170	25	5	14	70	10
3003-H18	200	29	185	27	4	10	70	10
Alclad 3003-0	110	16	40	6	30	40	...	...
Alclad 3003-H12	130	19	125	18	10	20	...	...
Alclad 3003-H14	150	22	145	21	8	16	...	...
Alclad 3003-H16	180	26	170	25	5	14	...	...
Alclad 3003-H18	200	29	185	27	4	10	...	...
3004-0	180	26	70	10	20	25	95	14
3004-H32	215	31	170	25	10	17	105	15
3004-H34	240	35	200	29	9	12	105	15
3004-H36	260	38	230	33	5	9	110	16
3004-H38	285	41	250	36	5	6	110	16
Alclad 3004-0	180	26	70	10	20	25	...	...
Alclad 3004-H32	215	31	170	25	10	17	...	...

(continued)

(a) Based on 500,000,000 cycles of completely reversed stress using the R.R. Moore type of machine and specimen. (b) Tempers T361 and T861 were formerly designated T36 and T86, respectively. (c) Based on 10 cycles using flexural type testing of sheet specimens. (d) Unpublished Alcoa data. (e) Data from CDNSWRC-TR619409, 1994, cited below. (f) T7451, although not previously registered, has appeared in literature and some specifications as T73651. (g) Sheet flexural. Sources: *Aluminum Standards and Data*, Aluminum Association, and E. Czyryca and M. Vassilaros, *A Compilation of Fatigue Information for Aluminum Alloys*, Naval Ship Research and Development Center, CDNSWC-TR619409, 1994

Table 10 (Continued)

Alloy and temper	Ultimate tensile strength		Tensile yield strength		Elongation in 50 mm (2 in.), %		Fatigue endurance limit(a)	
					1.6 mm (1/16 in.) thick specimen	1.3 mm (1/2 in.) diam specimen		
	MPa	ksi	MPa	ksi			MPa	ksi
Alclad 3004-H34	240	35	200	29	9	12	...	...
Alclad 3004-H36	260	38	230	33	5	9	...	...
Alclad 3004-H38	285	41	250	36	5	6	...	...
3105-0	115	17	55	8	24	...	...	...
3105-H12	150	22	130	19	7	...	...	...
3105-H14	170	25	150	22	5	...	...	...
3105-H16	195	28	170	25	4	...	...	...
3105-H18	215	31	195	28	3	...	...	...
3105-H25	180	26	160	23	8	...	...	...
4032-T6	380	55	315	46	...	9	110	16
4043-0	...	...	...	...	...	...	40	6(d)
4043-H38	...	...	...	...	...	...	55	8(d)
5005-0	125	18	40	6	25	...	...	...
5005-H12	140	20	130	19	10	...	...	...
5005-H14	160	23	150	22	6	...	...	...
5005-H16	180	26	170	25	5	...	...	...
5005-H18	200	29	195	28	4	...	...	...
5005-H32	140	20	115	17	11	...	...	...
5005-H34	160	23	140	20	8	...	...	...
5005-H36	180	26	165	24	6	...	...	...
5005-H38	200	29	185	27	5	...	...	...
5005-0	145	21	55	8	24	...	85	12
5050-H32	170	25	145	21	9	...	90	13
5050-H34	195	28	165	24	8	...	90	13
5050-H36	205	30	180	26	7	...	95	14
5050-H38	220	32	200	29	6	...	95	14
5052-0	195	28	90	13	25	30	110	16
5052-H32	230	33	195	28	12	18	115	17
5052-H34	260	38	215	31	10	14	125	18
5052-H36	275	40	240	35	8	10	130	19
5052-H38	290	42	255	37	7	8	140	20
5056-0	290	42	150	22	...	35	140	20
5056-H18	435	63	405	59	...	10	150	22
5056-H38	415	60	345	50	...	15	150	22
5083-0	290	42	145	21	...	22	160	23
5083-H11	303	44	193	28	...	16	150	22(e)
5083-H112	295	43	160	23	...	20	150	22(e)
5083-H113	317	46	227	33	...	16	160	23(e)
5083-H32	317	46	227	33	...	16	150	22(e)
5083-H34	358	52	283	41	...	8	...	...
5083-H321, H116	315	46	230	33	...	16	160	23
5086-0	260	38	115	17	22	...	145	21(e)
5086-H32, H116	290	42	205	30	12	...	50	22(e)
5086-H34	325	47	255	37	10	...	...	...
5086-H112	270	39	130	19	14	...	...	...
5086-H111	270	39	170	25	17	...	145	21(e)
5086-H343	325	47	255	37	10-14	...	160	23(e)
5154-0	240	35	115	17	27	...	115	17
5154-H32	270	39	205	30	15	...	125	18
5154-H34	290	42	230	33	13	...	130	19
5154-H36	310	45	250	36	12	...	140	20
5154-H38	330	48	270	39	10	...	145	21
5154-H112	240	35	115	17	25	...	115	17
5252-H25	235	34	170	25	11	...	...	...
5252-H38, H28	285	41	240	35	5	...	...	...
5254-0	240	35	115	17	27	...	115	17
5254-H32	270	39	205	30	15	...	125	18
5254-H34	290	42	230	33	13	...	130	19
5254-H36	310	45	250	36	12	...	140	20
5254-H38	330	48	270	39	10	...	145	21
5254-H112	240	35	115	17	25	...	115	17
5454-0	250	36	115	17	22	...	140	20(e)
5454-H32	275	40	205	30	10	...	140	20(e)
5454-H34	305	44	240	35	10	...	...	...
5454-H111	260	38	180	26	14	...	...	...
5454-H112	250	36	125	18	18	...	...	...
5456-0	310	45	160	23	...	24	150	22(e)
5456-H112	310	45	165	24	...	22	...	...

(continued)

(a) Based on 500,000,000 cycles of completely reversed stress using the R.R. Moore type of machine and specimen. (b) Tempers T361 and T861 were formerly designated T36 and T86, respectively. (c) Based on 10 cycles using flexural type testing of sheet specimens. (d) Unpublished Alcoa data. (e) Data from CDNSWRC-TR619409, 1994, cited below. (f) T7451, although not previously registered, has appeared in literature and some specifications as T73651. (g) Sheet flexural. Sources: *Aluminum Standards and Data*, Aluminum Association, and E. Czyryca and M. Vassilaros, *A Compilation of Fatigue Information for Aluminum Alloys*, Naval Ship Research and Development Center, CDNSWC-TR619409, 1994

Table 10 (Continued)

Alloy and temper	Ultimate tensile strength		Tensile yield strength		Elongation in 50 mm (2 in.), %		Fatigue endurance limit(a)	
					1.6 mm (1/16 in.) thick specimen	1.3 mm (1/2 in.) diam specimen		
	MPa	ksi	MPa	ksi			MPa	ksi
5456-H321, H116, H32	350	51	255	37	...	16	160	23(e)
5457-0	130	19	50	7	22	...	...	...
5457-H25	180	26	160	23	12	...	...	...
5457-H38, H28	205	30	185	27	6	...	...	...
5652-0	195	28	90	13	25	30	110	16
5652-H32	230	33	195	28	12	18	115	17
5652-H34	260	38	215	31	10	14	125	18
5652-H36	275	40	240	35	8	10	130	19
5652-H38	290	42	255	37	7	8	140	20
5657-H25	160	23	140	20	12	...	...	...
5657-H38, H28	195	28	165	24	7	...	...	...
6061-0	125	18	55	8	25	30	60	9
6061-T4, T451	240	35	145	21	22	25	95	14
6061-T6, T651	310	45	275	40	12	17	95	14
Alclad 6061-0	115	17	50	7	25	...	...	...
Alclad 6061-T4, T451	230	33	130	19	22	...	...	...
Alclad 6061-T6, T651	290	42	255	37	12	...	...	...
6063-0	90	13	50	7	...	...	55	8
6063-T1	150	22	90	13	20	...	60	9
6063-T4	170	25	90	13	22	...	...	...
6063-T5	185	27	145	21	12	...	70	10
6063-T6	240	35	215	31	12	...	70	10
6063-T83	255	37	240	35	9	...	...	...
6063-T831	205	30	185	27	10	...	...	...
6063-T832	290	42	270	39	12	...	...	...
6066-0	150	22	85	12	...	18	...	...
6066-T4, T451	360	52	205	30	...	18	...	...
6066-T6, T651	395	57	360	52	...	12	110	16
6070-T6	380	55	350	51	10	...	95	14
6101-H111	95	14	75	11	...	...	...	...
6101-T6	220	32	195	28	15	...	...	...
6151-T6	...	...	...	...	...	...	83	12
6201-T81	...	...	...	...	...	...	105	15
6262-T9	...	...	...	...	...	...	95	14
6351-T4	250	36	150	22	20	...	...	...
6351-T6	310	45	285	41	14	...	90	13
6463-T1	150	22	90	13	20	...	70	10
6463-T5	185	27	145	21	12	...	70	10
6463-T6	240	35	215	31	12	...	70	10
7002-T6	440	64	365	53	9-12	...	...	...
7039-T6	415	60	345	50	14	...	...	...
7049-T73	515	75	450	65	...	12	...	...
7049-T7352	515	75	435	63	...	11	...	...
7050-T73510, T73511	495	72	435	63	...	12	...	...
7050-T7451(f)	525	76	470	68	...	11	...	...
7050-T7651	550	80	490	71	...	11	...	...
7075-0	230	33	105	15	17	16	117	17(e)
7075-T6, T651	570	83	505	73	11	11	160	23
7072-H14	...	...	...	...	...	...	35	5(g)
7075-T73	503	73	435	63	13	...	150	22(e)
7076-T6	...	...	...	...	...	...	138	20(d)
Alclad 7075-0	220	32	95	14	17	...	...	...
Alclad 7075-T6, T651	525	76	460	67	11	...	...	...
7079-T6	490	71	428	62	10	...	160	23(e)

(a) Based on 500,000,000 cycles of completely reversed stress using the R.R. Moore type of machine and specimen. (b) Tempers T361 and T861 were formerly designated T36 and T86, respectively. (c) Based on 10 cycles using flexural type testing of sheet specimens. (d) Unpublished Alcoa data. (e) Data from CDNSWRC-TR619409, 1994, cited below. (f) T7451, although not previously registered, has appeared in literature and some specifications as T73651. (g) Sheet flexural. Sources: *Aluminum Standards and Data*, Aluminum Association, and E. Czyryca and M. Vassilaros, *A Compilation of Fatigue Information for Aluminum Alloys*, Naval Ship Research and Development Center, CDNSWC-TR619409, 1994

transverse. Fatigue response to environment varies with alloy, so final alloy selection for design should address this important interaction. When accumulating data for this purpose, it is recommended that any testing be conducted in a controlled environment, and preferably the environment of the intended application. However, an environment known to be more severe than that encountered in service is often used to conservatively establish baseline data and design guidelines. Because environmental interaction with fatigue is a rate-controlled process, interaction of time-dependent fatigue parameters such as frequency, waveform, and load history should be factored into the fatigue analysis (Ref 39-41).

Typically, the fatigue strengths of the more corrosion-resistant 5XXX and 6XXX aluminum alloys and tempers are less affected by corrosive environments than are higher-strength 2XXX and 7XXX alloys, as indicated by Fig. 25. Corrosion fatigue performance of 7XXX alloys may, in general, be upgraded by overaging to the more corrosion-resistant T7 tempers (Ref 42-47), as indicated by results shown in Fig. 26 and 27. With 2XXX alloys, the more corrosion-resistant, precipitation-hardened T8-type tempers provide a better combination of strength and fatigue resistance at high endurances than naturally aged T3 and T4 tempers. However, artificial aging of 2XXX alloys is accompanied by loss in toughness with resultant decrease in fatigue crack growth resistance at intermediate and high stress intensities (Ref 45, 46).

Table 11 Summary of the 7050 plate materials used in the study of the effect of microporosity on fatigue

Material	Product thickness, in.	Key microstructural features
Old-quality plate	5.7	Large porosity
New-quality plate	5.7	Porosity
Low-porosity plate	6.0	Small porosity, constituent particles
Low-particle plate	6.0 (T/4)	Small constituents, thick plate grain structure
Thin plate	1.0	Refined grain size and constituent particles

Interaction of a clad protective system with fatigue strength of alloys 2024-T3 and 7075-T6 in air and seawater environments is shown in Fig. 24. In air, the cladding appreciably lowers fatigue resistance. In seawater, benefits of the cladding are readily apparent.

Reduced Porosity Materials*. The size of microporosity in commercial products is affected by the forming processes used in their production. A recent program was undertaken to determine whether the fatigue strength could be improved by the control of microporosity. Five variants of 7050 plate were produced to provide a range of microstructures to quantify the effects of intrinsic microstructural features on fatigue durability (Table 11). The first material, designated "old-quality" material, was produced using production practices typical of those used in 1984. The material is characterized by extensive amounts of centerline microporosity. Despite the centerline microporosity, this material still meets all existing mechanical property specifications for thick 7050 plate. Current quality production material, designated "new-quality" material, was also used, characterized by reduced levels of centerline microporosity compared to the old-quality material. The new-quality material represents the current benchmark for commercially available material. The processing methods used in the production of the new-quality material are a result of a statistical quality control effort to improve 7050 alloy thick plate (Ref 48). Material taken from two plant-scale production lots of each quality level provided the material for this program. Both materials are 5.7 in. thick 7050-T7451 plate. Static mechanical property characterization of the two 7050 plate pedigrees showed no significant differences in properties other than an increase in short transverse elongation for the new-quality material (Ref 49), and both materials meet the AMS material specification minimums. The fact that both materials meet the property requirements of the AMS specification underscores the limitation of existing specifications in that they do not differentiate intrinsic metal quality.

Effect of Microporosity on Fatigue. Smooth axial stress fatigue tests were performed for both the old-quality and the new-quality plate materials. The tests were done on round bars with a gage diameter of 12.7 mm (0.5 in.). Gage sections were sanded longitudinally to remove circumferential machining marks. Testing was done at a maximum stress of 240 MPa (35 ksi), a stress ratio $R = 0.1$, and cyclic frequency of 10 Hz in laboratory air. The specimen orientation was long-transverse (L-T) relative to the parent plate. The specimens were removed from the midthickness (T/2) plane of the plate where microporosity concentration is the greatest (Ref 49). The lifetimes of the specimens are plotted in Fig. 28 on a cumulative failure plot, where the data are sorted in order of ascending lifetime and ordinate is the percentile ranking of the specimens relative to the total number of tests. Thus, the lifetime corresponding to the 50% point on the ordinate represents the median lifetime, where half of the specimens failed prior to that lifetime and half failed at longer lifetimes. The data show that the cumulative distribution of fatigue lifetimes for the new-quality material is substantially longer than for the old-quality material.

Fatigue tests were also performed for the old- and new-quality materials using flat specimens containing open holes. Tests were performed at four stress levels for each material pedigree at a stress ratio of $R = 0.1$ and cyclic frequency of 25 Hz in laboratory air. As with the round specimens, L-T specimens were removed from the T/2 plane of the plate. The holes were deburred by polishing with diamond compound only on the corners and not in the bore of the hole; this resulted in slight rounding of the corners. The fatigue lifetime data are plotted in Fig. 29 as an *S-N* plot. Also plotted for both materials are the 95% confidence limits for the *S-N* curves. The confidence limits were obtained from a Box-Cox analysis of the data, which enables statistical determination of the mean *S-N* response and the 95% confidence limits (Ref 39). The data clearly show that, at equivalent stresses, the new-quality material exhibited longer lifetimes than the old-quality material.

*"Effect of Porosity" is adapted from J.R. Brockenbrough, R.J. Bucci, A.J. Hinkle, J. Liu, P.E. Magnusen, and S.M. Mixasato, "Role of Microstructure on Fatigue Durability of Aluminum Aircraft Alloys," Progress Report, ONR Contract N00014-91-C-0128, 15 April 1993

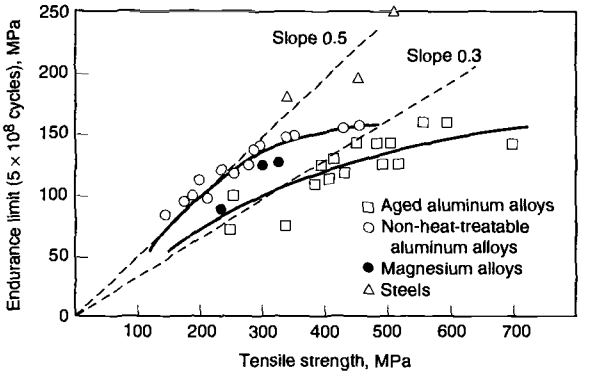

Fig. 22 Fatigue ratios (endurance limit/tensile strength) for aluminum alloys and other materials. Source: P.C. Varley, *The Technology of Aluminum and Its Alloys*, Newnes-Butterworths, London, 1970

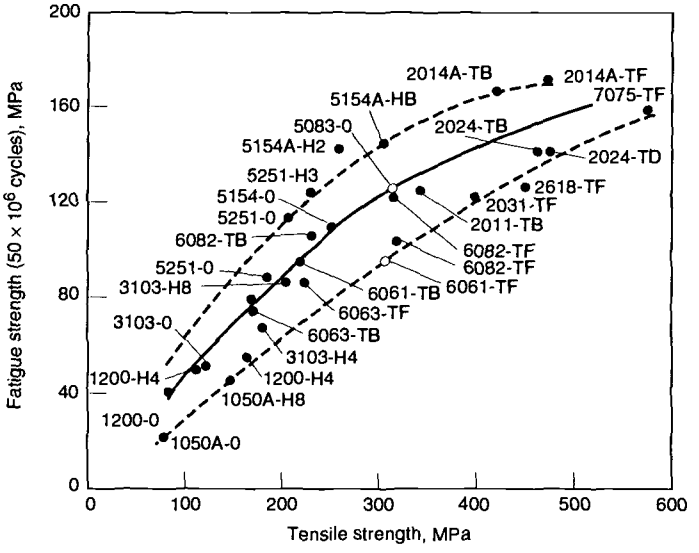

Fig. 23 Relationships between the fatigue strength and tensile strength of some wrought aluminum alloys

Strain Control Fatigue

Considerable evidence suggests that failure data are more usefully presented in the form of strain-life curves, and that strain-based cumula-

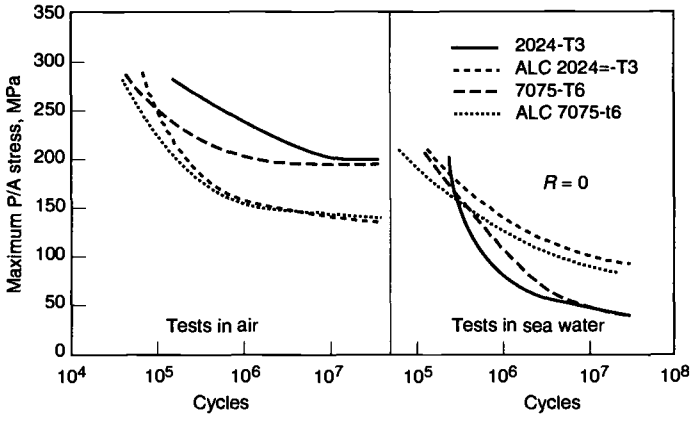

Fig. 24 Axial stress fatigue strength of 0.8 mm 2024, 7075, and clad sheet in air and seawater, $R = 0$. Source: Ref 33

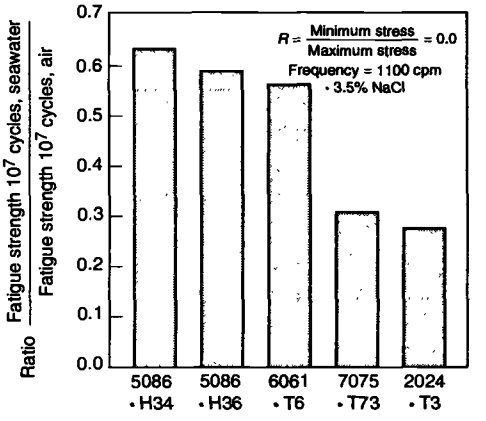

Fig. 25 Comparison of axial-stress fatigue strengths of 0.032 in. aluminum alloy sheet in seawater and air. Source: Ref 33

tive-damage life predictions are generally more reliable than conventional stress-based approaches (Ref 51-53). Strain-based prediction methods are capable of addressing interaction effects of variable load history and are better suited to handle "what if" situations than traditional stress approaches. In addition, they require a significantly reduced number of material characterization and component verification tests to make a material selection and/or design decision. Strain control fatigue is also essential in the understanding of crack initiation because, without localized plastic strain at areas of stress concentration in a structure, failure cannot occur. At high plastic strains, fatigue experiments on aluminum alloys (Ref 54) have shown that homogeneous slip (i.e., distribute plastic strain and avoid strain concentration sites) prolongs fatigue life to crack initiation. Recognized factors that promote homogeneous slip and/or increase low-cycle fatigue life are decreased coherency of strengthening particles, increased magnesium content, and minimization and more uniform distribution of second-phase particles, which serve as initiation sites. Effects of alloy microstructure on fatigue initiation life depend on the level of strain.

In general, strain-life fatigue is based on the division of cyclic stress-strain response into plastic and elastic components (Fig. 30a), where the relation between stress and strain depends on the strength-ductility properties of the material (Fig. 30b) and also the cyclic hardening or softening of the material. For most metals, stress-strain hysteresis behavior (Fig. 30) is not constant, as cyclic softening or hardening can occur by reversed loading and cyclic straining. Generally (Ref 55-57), materials that are initially soft exhibit cyclic hardening, and materials that are initially hard undergo cyclic softening.

With strain-life fatigue, the elastic and plastic components may be separated and plotted on a strain life curve (Fig. 31). A plot on logarithmic coordinates of the plastic portion of the strain amplitude (half the plastic strain range) versus the fatigue life often yields a straight line, described by the equation

$$\frac{\Delta\varepsilon_p}{2} = \varepsilon'_f (2N_f)^c \qquad \text{(Eq 3)}$$

where ε'_f is the fatigue ductility coefficient, c is the fatigue ductility exponent, and N_f is the number of cycles to failure ($2N_f$ is the number of load reversals). In contrast, elastic strains influence fatigue behavior under long-life conditions, where a stress-based analysis of fatigue is charted by plotting stress amplitude (half the stress range) versus fatigue life on logarithmic coordinates. The result is a straight line having the equation

$$\frac{\Delta\sigma}{2} = \sigma'_f (2N_f)^b \qquad \text{(Eq 4)}$$

where σ'_f is the fatigue strength coefficient and b is the fatigue strength exponent.

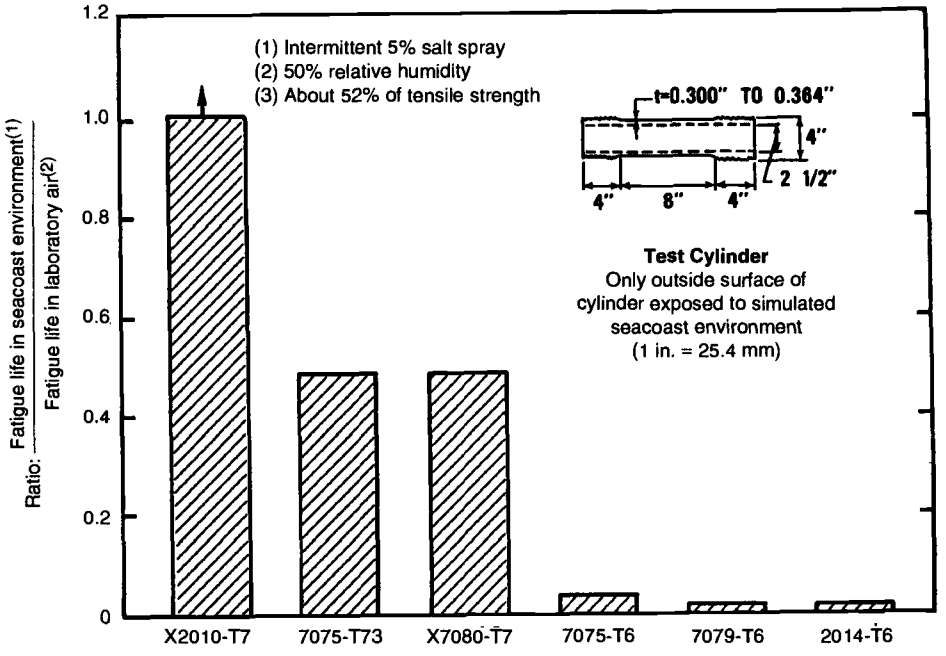

Fig. 26 Comparisons of fatigue lives of pressurized hydraulic cylinders in laboratory air and simulated seacoast environments at 80% design stress. Sources: Ref 3, 42

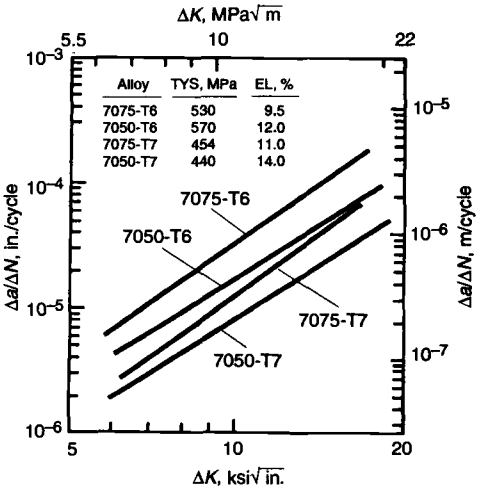

Fig. 27 Cyclic stress intensity range, ΔK, vs. cyclic fatigue crack growth rate, $\Delta a/\Delta N$, of laboratory-fabricated high-strength 7XXX aluminum alloys

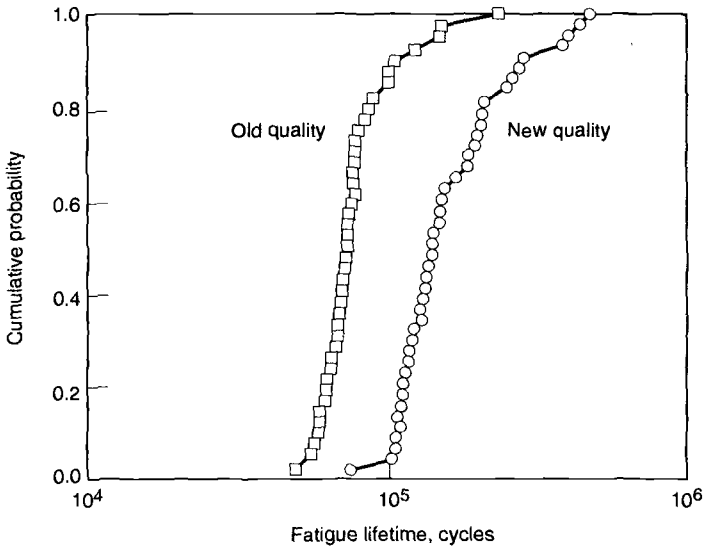

Fig. 28 Cumulative smooth fatigue lifetime distributors for old-quality and new-quality plate (see text for definitions). Tests conducted at 240 MPa (35 ksi) max stress, $R = 0.1$

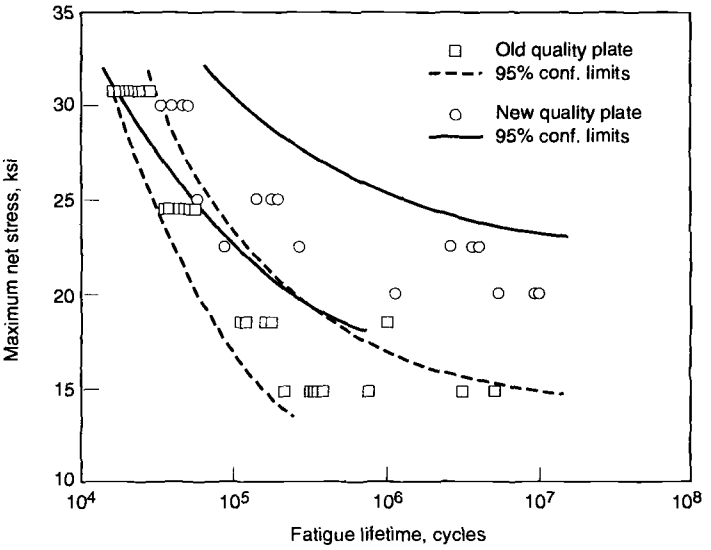

Fig. 29 Open-hole fatigue lifetimes for new-quality and old-quality plate (see text for definitions). Tests conducted at $R = 0.1$

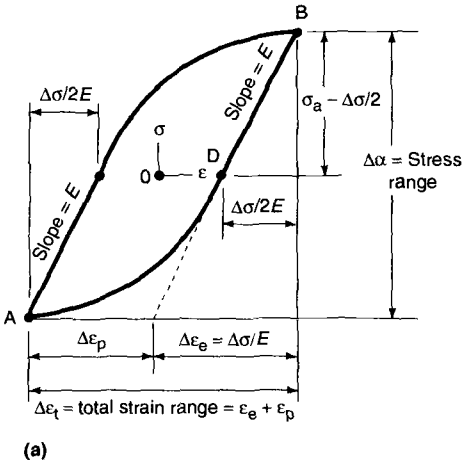

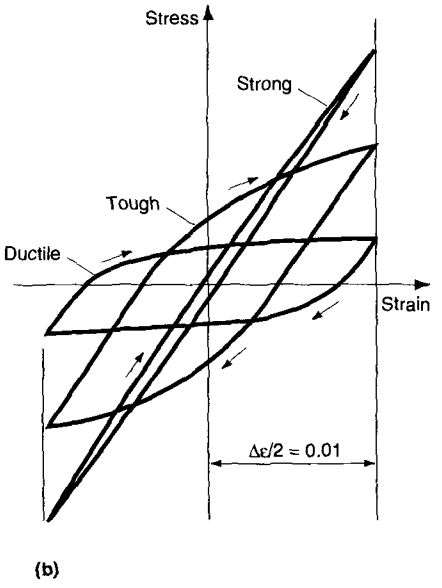

Fig. 30 Stress-strain hysteresis loop under cyclic loading. (a) Elastic and plastic strain range. (b) Hysteresis loops showing idealized stress-strain behavior for different types of materials

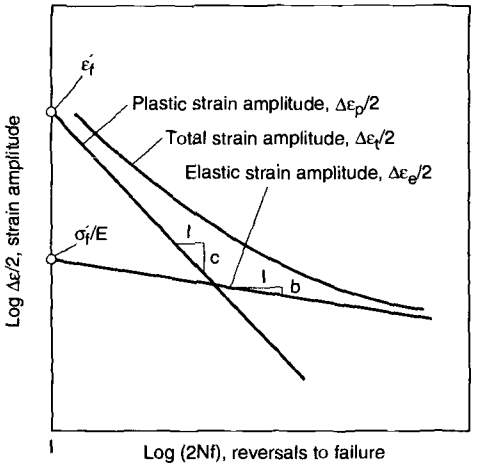

$$\frac{\Delta\varepsilon_t}{2} = \frac{\Delta\varepsilon_e}{2} + \frac{\Delta\varepsilon_p}{2}$$

$$= \frac{\sigma_f'}{E}(2Nf)^b + \varepsilon_f'(2Nf)^c$$

Where: σ_f' = Fatigue strength ductility coefficient

ε_f' = Fatigue ductility coefficient

b = Fatigue strength exponent

c = Fatigue ductility exponent

Fig. 31 Strain control fatigue life as a function of elastic-, plastic-, and total-strain amplitude

The elastic strain range is obtained by dividing Eq 4 by Young's modulus E:

$$\frac{\Delta\varepsilon_e}{2} = \frac{\sigma_f'}{E}(2N_f)^b \qquad \text{(Eq 5)}$$

The total strain range is the sum of the elastic and plastic components, obtained by adding Eq 3 and 5 (see Fig. 31):

$$\frac{\Delta\varepsilon}{2} = \varepsilon_f'(2N_f)^c - \frac{\sigma_f'}{E}(2N_f)^b \qquad \text{(Eq 6)}$$

For low-cycle fatigue conditions (frequently fewer than about 1000 cycles to failure), the first term of Eq 6 is much larger than the second; thus, analysis and design under such conditions must use the strain-based approach. For long-life fatigue conditions (frequently more than about 10,000 cycles to failure), the second term dominates, and the fatigue behavior is adequately described by Eq 4. Thus, it becomes possible to use Eq 4 in stress-based analysis and design.

This approach offers the advantage that both high-cycle and low-cycle fatigue can be characterized in one plot. From this relationship it is seen that long-life fatigue resistance is governed by the elastic line, while short-life fatigue resistance is governed by the plastic line (Ref 58). Within a bounded range of alloy types and microstructures, controlled strain fatigue lives greater than 10^4 cycles typically increase with increasing strength. On the other hand, low-cycle controlled strain fatigue lives for the same alloys generally increase with increasing ductility where ductility can be defined as $\ln(1/1\text{-}RA)$, RA being reduction of area determined from the standard tension test. The reciprocal strength-ductility relationship implies that materials selected on the basis of long-life resistance may not perform as well in low-cycle applications, and vice-versa. This is illustrated in Fig. 32 by the crossover in the strain-life relationships of X7046, a high-strength alloy, and 5083, a moderate-strength/high-ductility alloy. Results of strain control fatigue experiments on high-strength 7XXX laboratory-fabricated microstructures (Fig. 33) show similar crossover trends that can be correlated with strength and ductility. The observed crossovers imply that alloy selection, dependent on estimation of fatigue initiation life, requires identification of the most damaging cycles in the component fatigue spectrum for proper interpretation of mechanical property tradeoffs. This is accomplished using knowledge of the component strain

spectrum, from strain gaged parts and/or stress analysis, and cumulative damage assessment of strain-life data. A compilation of fatigue strain-life parameters for various aluminum alloys is given in Table 12 and the appendix "Parameters for Estimating Fatigue Life" in this Volume. Corresponding monotonic properties are given in Table 13. Additional details on state-of-the-art fatigue analysis methods are given in Ref 59-62 and Section 3 "Fatigue Strength Prediction and Analysis" in this Volume.

Microstructure and Strain Life*

Plastic strain has been recognized as a controlling parameter in fatigue, and microstructures that homogeneously distribute the strain are desirable. Any microstructural feature that concentrates plastic strain or that results in an inhomogeneous distribution of plastic strain leads to undesirable local stress concentrations and large slip offsets at surfaces. Mechanisms representing these effects are illustrated schematically in Fig. 34, which shows two microstructural features that can result in strain localization: shearable precipitates, Fig. 34(a) and precipitate free zones (PFZs), Fig 34(b). These can lead to early crack nucleation and enhanced metal/environment interactions.

The following discussions briefly review the effect of shearable precipitates and PFZs on the strain life of aluminum alloys. These two microstructural features are considered because of their importance in commercial alloys. Inhomogeneous deformation similar to that in Fig. 34(a) can also occur in irradiated materials in which glide dislocations remove radiation defects, forming cleared channels of defect-free material. Low-stacking-fault-energy materials may also exhibit planar slip, but inhomogeneous deformation is not prevalent because softening in the slip plane does not occur. Inhomogeneous deformation similar to that in Fig. 34(b) may occur in two-phase materials having a soft and a hard phase. To some extent, localized deformation occurs in *all* materials at low stress and strain amplitudes.

The effect of shearable precipitates and PFZs on plastic-strain localization can be reduced by microstructural modification to improve fatigue life (see Table 14). The degree of plastic strain localization is primarily determined by the slip length and degree of age hardening. Because extensive age hardening and corresponding high yield strength are desirable, focus is placed on ways of improving the fatigue life by reducing the slip length. A reduction in grain size seems to be the most effective method for alloys that can contain both shearable precipitates and PFZs.

To definitively determine the influence of microstructure on fatigue life, it may be necessary to test in the low-cycle fatigue (LCF) regime under stress as well as strain control. Some microstructural features, through their effect on cyclic deformation behavior and resulting softening and/or hardening, may improve or reduce the observed fatigue life, depending on the control mode. In addition, high-cycle fatigue (HCF) tests are important because in this region the influence of the yield stress usually dominates. It should also be emphasized that the microstructural parameters that accelerate or delay fatigue crack nucleation may have the opposite effect on fatigue crack propagation.

*Adapted from *Fatigue and Microstructure*, ASM, 1979, p 469-490

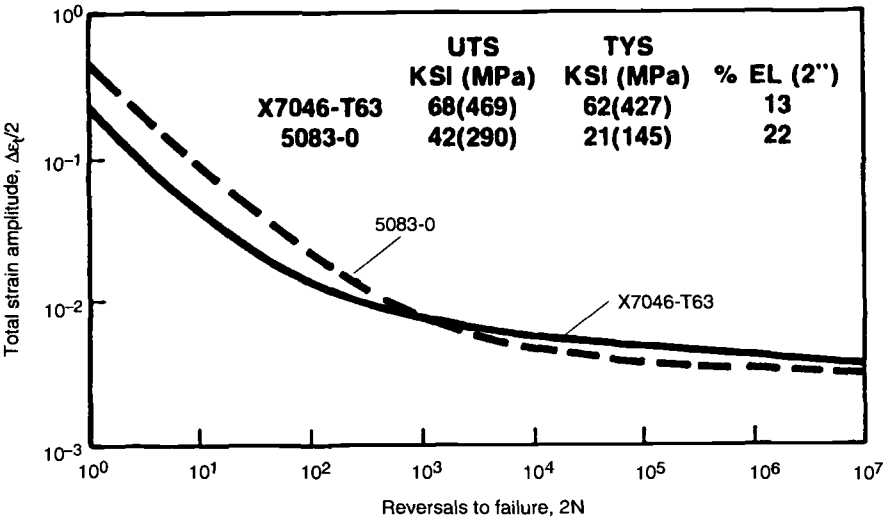

Fig. 32 Cyclic strain vs. life curve for X7046-T63 and 5083-O aluminum alloys

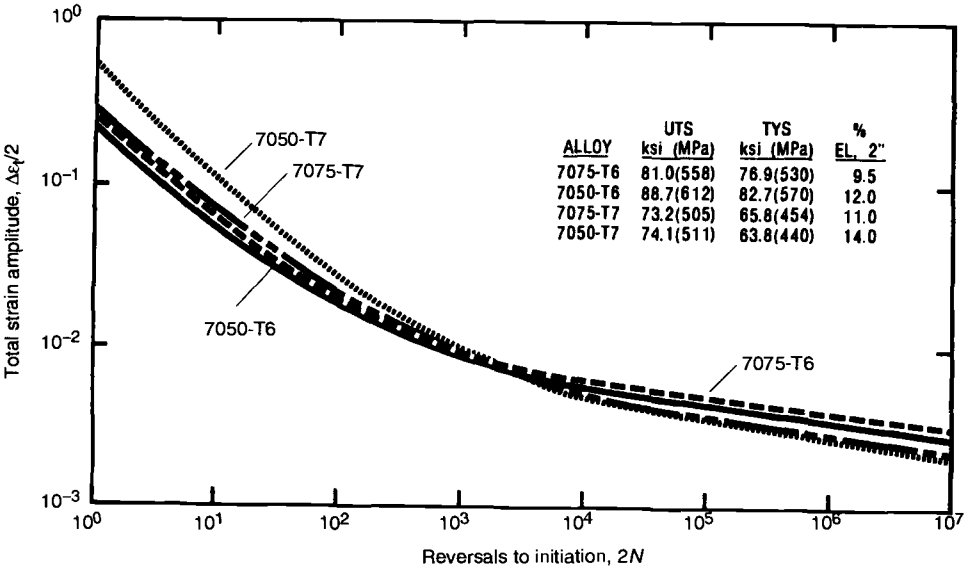

Fig. 33 Cyclic strain vs. initiation life for laboratory-fabricated high-strength 7XXX aluminum alloys. Fatigue resistance at low total strain amplitude is governed by the elastic-strain amplitude. Fatigue lives for total strain amplitudes less than about 5×10^{-3} generally increase with increasing strength. On the other hand, fatigue lives for total strain amplitude greater than about 10^{-2} generally increase with increasing ductility. Source: T.H. Sanders, Jr. and J.T. Staley, "Review of Fatigue and Fracture Research on High-Strength Aluminum Alloys," *Fatigue and Microstructure*, American Society for Metals, 1979, p 472

Precipitate Shearing

Overaging homogenizes slip and increases fatigue resistance in the low-cycle region where "ductility-controlled" fatigue dominates. This behavior, as it relates to the formation of nonshearable precipitates, alters fatigue properties, as shown in the Coffin-Manson life plots of Fig. 35. The two curves are for an underaged (with shearable precipitates) and an overaged (with nonshearable precipitates) 7050 alloy having identical yield strengths and strain to fracture (Ref 63). The fatigue life of the overaged alloy is consistently longer than that of the underaged alloy. The curves converge at low and high plastic strain amplitudes in these strain-controlled tests for the following reasons: For large strain amplitudes, all slip is homogeneous, regardless of the deformation mechanism, primarily due to multiple-slip activation. For small strain amplitudes, the sample with nonshearable precipitates hardens more extensively (due to the generation of geometrically necessary dislocations) than the sample with shearable precipitates (which normally softens). Consequently, for a strain-controlled test, failure occurs earlier than anticipated for the samples with nonshearable precipitates.

Table 12 Room-temperature cyclic parameters of various aluminum alloys (strain control, $R = -1$, unnotched)

Alloy/ temper	Form	Condition	Fatigue failure criterion	Ultimate tensile strength, MPa (ksi)	Tensile yield strength, MPa (ksi)	Fatigue strength coefficient, σ_f', MPa (ksi)	Fatigue strength exponent, b	Fatigue ductility coefficient, ε_f'	Fatigue ductility exponent, c	Cyclic strain hardening coefficient, K', MPa (ksi)(a)	Cyclic strain hardening exponent, n' (a)
99.5% Al	Sheet	Cold rolled	Crack initiation(b)	73 (25)	19 (2.75)	95 (13.8)	–0.088	0.022	–0.328	255 (37)	0.265
99.5% Al	Sheet	Cold rolled	Crack initiation(c)	73 (25)	19 (2.75)	117 (17)	–0.109	0.017	–0.315	453 (65.7)	0.337
1100	Bar stock	As received	Rupture	110 (16)	97 (14)	159 (23)	–0.092	0.467	–0.613	184 (26.6)	0.159
2014-T6	Bar stock	As received	Rupture	511 (74)	463 (67)	776 (112.5)	–0.091	0.269	–0.742	704 (102)	0.072
2024-T3	Sheet	As received	5% load decrease	490 (71)	345 (50)	835 (121)	–0.096	0.174	–0.644	843 (122)	0.109
2024-T3	Sheet	5% cold formed	Crack initiation at 1 mm depth	490 (71)	476 (69)	891 (129)	–0.103	4.206	–1.056	669 (97)	0.074
2024-T3	Sheet	...	Crack initiation, 0.5 mm length	486 (70.5)	378 (55)	1044 (151)	–0.114	1.765	–0.927	590 (85.5)	0.040
2024-T4	Rod	Heat treated	...	476 (69)	304 (44)	764 (110.8)	–0.075	0.334	–0.649	808 (117)	0.098
2024-T351	Plate	Solution heat treated and cold worked(d)	...	455 (66)	380 (55)	927 (134)	–0.1126	0.4094	–0.7134	1067 (155)	0.1578
5454-H32	...	...	...	275 (40)	175 (26)	537 (77.8)	–0.0920	0.324	–0.6596	628 (91.1)	0.1394
5456-H311	Bar stock	As received	Rupture	400 (58)	235 (34)	702 (101.8)	–0.102	0.200	–0.655	635 (92)	0.084
6061-T6	...	ASTM grain size 3 to 5	...	328 (48)	300 (44)	654 (94.8)	–0.100	4.2957	–1.0072	566 (82)	0.0993
7075-T6	...	...	...	578 (84)	469 (68)	971 (140.8)	–0.072	0.7898	–0.9897	987 (143.2)	0.0728
7075-T6	Sheet	As received	5% load decrease	572 (83)	512 (74)	1048 (152)	–0.106	3.1357	–1.045	1500 (217.5)	0.186
7075-T6	Plate	As received	5% load decrease	572 (83)	512 (74)	776 (112.5)	–0.095	2.565	–0.987	521 (75.5)	0.045
7075-T6	Rod	Heat treated	...	580 (84)	470 (68)	886 (128.5)	–0.076	0.446	–0.759	913 (132)	0.088
7075-T7351	Plate	...	Crack initiation, 0.5 mm length	462 (67)	382 (55)	989 (143)	–0.140	6.812	–1.198	695 (100)	0.094
7475-T761	Sheet	As received	5% load decrease	475 (69)	414 (60)	983 (142.5)	–0.107	4.246	–1.066	675 (98)	0.059

(a) Stress-strain behavior at half-failure life. (b) Strain control, initiation criterion not specified. (c) Stress control, initiation criterion not specified. (d) Stress relieved by stretching 1.5% to 3% permanent set. Sources: MarTest Inc., test data for Materials Properties Council; *J. of Materials*, Vol 4, 1969, p 159; and *Materials Data for Cyclic Loading Part D; Aluminum and Titanium Alloys*, Elsevier, 1987

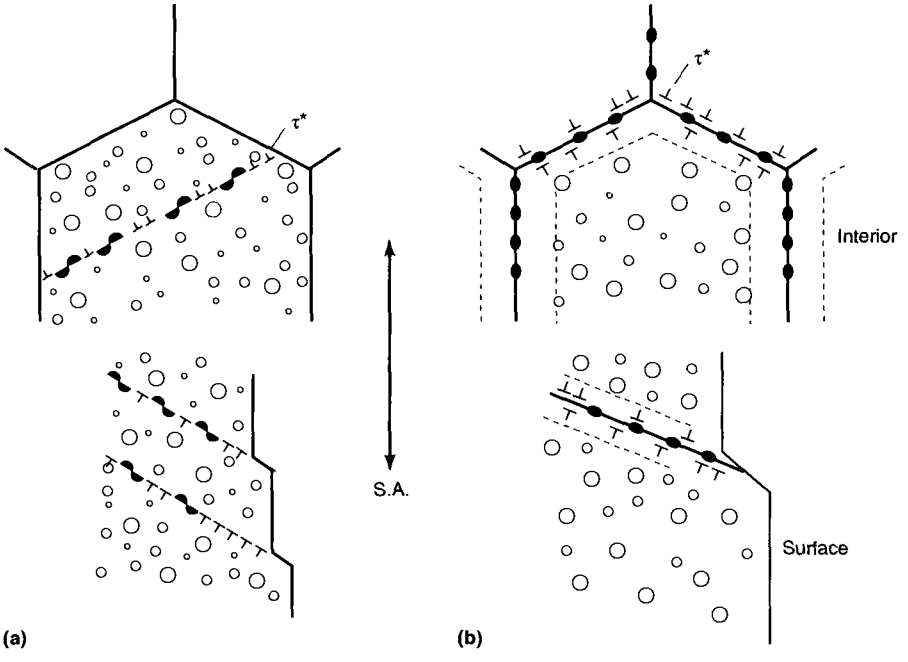

Fig. 34 Schematic representation of two microstructural features that result in strain localization. τ^* represents stress concentration at indicated areas of grain boundaries. (a) Shearable precipitates. (b) Precipitate-free zones

Larger differences between the two heat treatments would occur under stress-controlled conditions, because the samples that harden would resist plastic deformation and those that soften would not.

Aggressive environments enhance the differences in fatigue life when one compares alloys having shearable precipitates (inhomogeneous deformation) with alloys having nonshearable precipitates (homogeneous deformation). This is illustrated by the Coffin-Manson life plots of LCF samples cycled in dry air and distilled water (Fig. 36). The aggressive H_2O environment decreases the fatigue life of the alloy with shearable precipitates by almost an order of magnitude when compared with the inert environment for the same plastic strain amplitude. The aggressive environment has little or no effect on the alloy with nonshearable precipitates. The degree of coherency in these Al-Zn-Mg-Cu alloys (Ref 64) was modified by changing the copper concentration. Increasing the copper content in the strengthening precipitates of 7XXX alloys results in earlier loss of coherency (Ref 63) and increases the probability of dislocation looping when compared with alloys containing lesser amounts of

Table 13 Room-temperature monotonic properties of various aluminum alloys

Alloy/ temper	Form	Condition	Ultimate tensile strength, MPa (ksi)	Tensile yield strength, MPa (ksi)	Elongation (EL) /reduction in area (RA), %	Static strain hardening coefficient, K, MPa (ksi)	Static strain hardening exponent, n	Cyclic strain hardening coefficient, K', MPa (ksi)(a)	Cyclic strain hardening exponent, n'(a)
99.5% Al	Sheet	Cold rolled	73 (25)	19 (2.75)	43% EL in 5D	42 (6)	0.117	255 (37)(b)	0.265(b)
99.5% Al	Sheet	Cold rolled	73 (25)	19 (2.75)	43% EL in 5D	42 (6)	0.117	453 (65.7)(c)	0.337(c)
1100	Bar stock	As received	110 (16)	97 (14)	87.6% RA	...	...	184 (26.6)	0.159
2014-T6	Bar stock	As received	511 (74)	463 (67)	25% RA	610 (88.5)	0.043	704 (102)	0.072
2024-T3	Sheet	As received	490 (71)	345 (50)	19% EL in 5D	...	...	843 (122)	0.109
2024-T3	Sheet	5% cold formed	490 (71)	476 (69)	16% EL in 5D/ 16% RA	476 (69)	0.0	669 (97)	0.074
2024-T3	Sheet	...	486 (70.5)	378 (55)	17.3% EL in 5D	627 (91)	0.074	590 (85.5)	0.040
2024-T4	Rod	Heat treated	476 (69)	304 (44)	35% RA	...	0.20	808 (117)	0.098
2024-T351	Plate	Solution heat treated and cold worked(d)	455 (66)	380 (55)	24.5% RA	455 (66)	0.032	1067 (155)	0.1578
5454-H32	...	...	275 (40)	175 (26)	28% RA	238 (34.5)	0.0406	628 (91.1)	0.1394
5456-H311	Bar stock	As received	400 (58)	235 (34)	34.6% RA	591 (85.7)	0.166	635 (92)	0.084
6061-T6	...	ASTM grain size 3 to 5	328 (48)	300 (44)	51.8%	...	...	566 (82)	0.0993
7075-T6	...	...	578 (84)	469 (68)	33% RA	827 (120)	0.1130	987 (143.2)	0.0728
7075-T6	Sheet	As received	572 (83)	512 (74)	10.8% EL in 5D	...	...	1500 (217.5)	0.186
7075-T6	Plate	As received	572 (83)	512 (74)	10.8% EL in 5D	...	...	521 (75.5)	0.045
7075-T6	Rod	Heat treated	580 (84)	470 (68)	33% RA	...	0.113	913 (132)	0.088
7075-T7351	Plate	...	462 (67)	382 (55)	8.4% EL in 5D	633 (91.8)	0.055	695 (100)	0.094
7475-T761	Sheet	As received	475 (69)	414 (60)	13.5% EL in 5D	...	...	675 (98)	0.059

(a) Stress-strain behavior at half-failure life, see accompanying table with fatigue characteristics. (b) Strain control, initiation criterion not specified. (c) Stress control, initiation criterion not specified. (d) Stress relieved by stretching 1.5% to 3% permanent set. Sources: MarTest Inc., test data for Materials Properties Council: *J. of Materials*, Vol 4, 1969, p 159; and *Materials Data for Cyclic Loading Part D; Aluminum and Titanium Alloys*, Elsevier, 1987

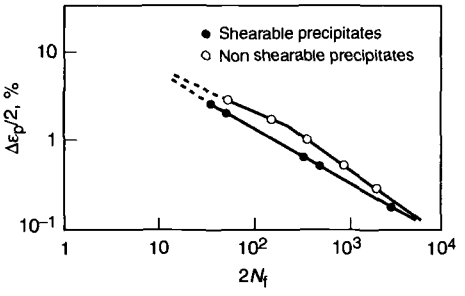

Fig. 35 Strain-life curves for samples of 7050 alloy with shearable precipitates (4 h at 120 °C, or 250 °F) and nonshearable precipitates (96 h at 150 °C, or 300 °F)

Table 14 Effect of microstructural modifications on the fatigue resistance of alloys containing shearable precipitates and PFZs

Modification to microstructure	Shearable precipitates	Precipitate-free zones
Overaging	Improves	No effect
Dispersoids	Improves	No effect
Unrecrystallized structures	Improves	Improves
Reduction of grain size	Improves	Improves
Steps in grain boundaries	No effect	Improves
Alignment of grain boundaries	No effect	Improves

copper with the same aging treatment. Cyclic deformation of the lower-copper-content alloys with shearable precipitates produced localized slip bands (Ref 64), which intensified metal/environment interactions. The nonshearable precipitates of the high-copper-content alloy prevented the occurrence of such inhomogeneous deformation.

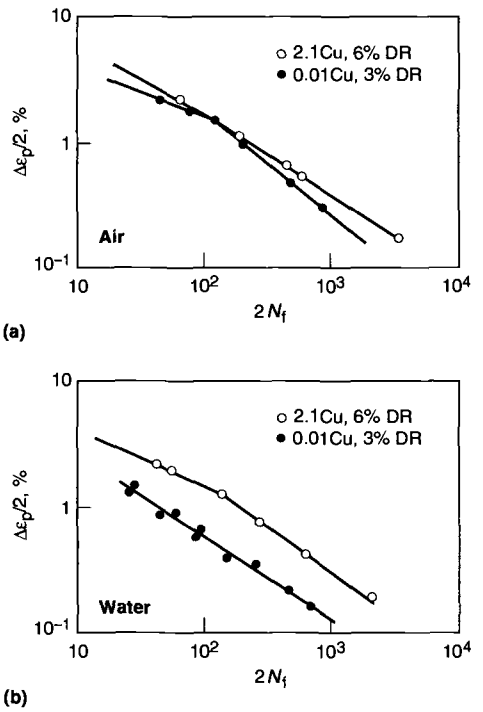

Fig. 36 Strain-life curves for samples of Al-Zn-Mg-x Cu alloys with shearable precipitates (0.01% Cu) and nonshearable precipitates (2.1% Cu). DR, degree of recrystallization. (a) Cycled in dry air. (b) Cycled in distilled water. Source: Ref 64

Addition of Nonshearable Precipitates. Although overaging homogenizes slip and increases the resistance of an alloy to fatigue crack nucleation, it normally results in a reduction in

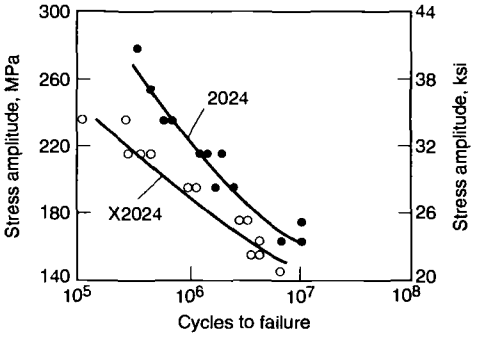

Fig. 37 S-N curves for commercial and experimental 2024 alloys with comparable tensile strengths. Both alloys contained a distribution of 5 μm diam iron- and silicon-rich inclusions; the commercial alloy also contained 0.1 to 0.2 m diam manganese-rich inclusions. Experimental alloy X2024 was free of the manganese inclusions and exhibited lower fatigue strength due to high crack density from sharp slip bands. Source: Pelloux and Stoltz Ref 65

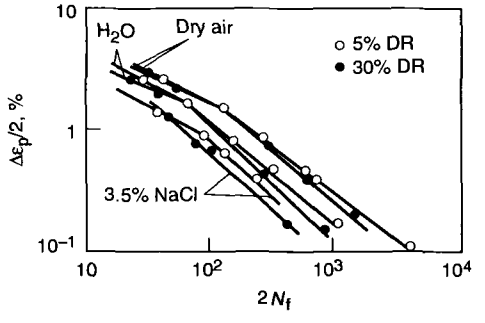

Fig. 38 Influence of degree of recrystallization (DR) and environment on the strain-life behavior of an Al-Zn-Mg-1.6 Cu alloy with shearable precipitates

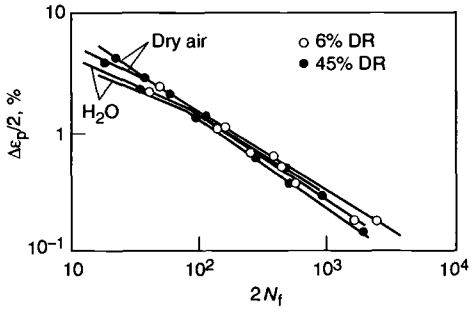

Fig. 39 Influence of degree of recrystallization (DR) and environment on the strain-life behavior of an Al-Zn-Mg-2.1 Cu alloy with nonshearable precipitates

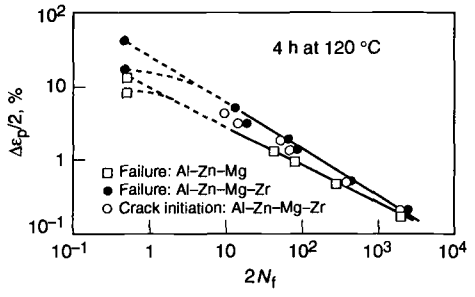

Fig. 40 Effect of grain size on the strain-life behavior of an alloy with shearable precipitates. The Al-Zn-Mg alloy had large grain size; the Al-Zn-Mg-Zr alloy, small grain size. Source: Ref 68

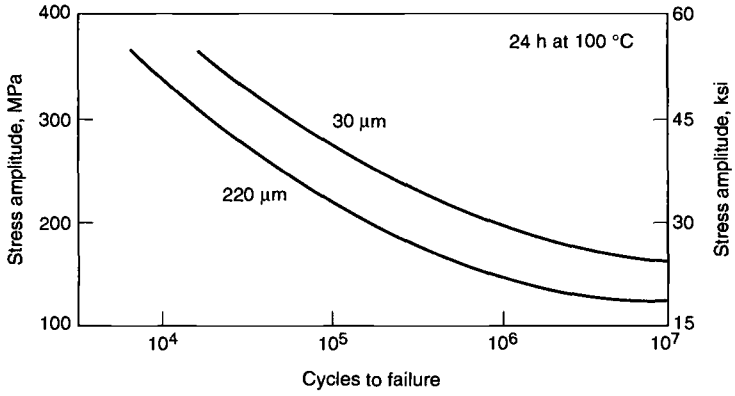

Fig. 41 Effect of grain size on the stress-life behavior of an X7075 alloy with shearble precipitates. Source: Ref 69

static strength. Consequently, it is sometimes beneficial to have a dispersion of nonshearable precipitates intermixed with shearable precipitates. Some commercial alloys have alloying additions (for example, manganese and chromium in 2XXX and 7XXX aluminum alloys, respectively) that form small (0.1 to 0.2 μm), incoherent dispersoids during high-temperature homogenization treatments. The primary purpose of these small intermetallic compounds is to control grain size and shape. However, they also disperse slip and inhibit the formation of intense slip bands. Therefore, plastic deformation is more homogeneous, and early crack nucleation due to intense slip bands is avoided.

Figure 37 shows the results of a stress-controlled test of two 2XXX alloys—one (X2024) contains only shearable precipitates and the other (2024) both shearable and nonshearable precipitates. At all stress levels, alloy 2024 has a much longer fatigue life than X2024. It is important to note that the alloys have comparable tensile strengths—a necessity for a valid comparison in a stress-controlled test. The X2024 alloy having only shearable precipitates developed sharp, intense slip bands and a higher density of crack nuclei earlier in the fatigue life than did the alloy containing nonshearable dispersoids.

Unrecrystallized Structures. Figure 36 demonstrates that an alloy containing shearable precipitates has lower fatigue strength than a similar alloy containing nonshearable precipitates. Those results were obtained on material having a low (3 to 6%) degree of recrystallization. A larger difference in fatigue lives would have been observed if the alloys were fully recrystallized. Unrecrystallized structures also promote homogeneous deformation and reduce the influence of the type (shearable or nonshearable) of precipitates.

Figure 38 shows Coffin-Manson life plots of an Al-Zn-Mg-Cu alloy with shearable precipitates (Ref 64). Two different degrees of recrystallization were tested in three different environments. The specimens having the largest volume fraction of unrecrystallized structure showed the greatest fatigue resistance in each environment. However, as expected, an aggressive environment enhanced the difference observed between specimens having a mostly unrecrystallized structure (homogeneous deformation) and those with a more recrystallized structure (inhomogeneous deformation). The dislocation substructure in the unrecrystallized regions and the nonshearable precipitates along subgrain boundaries reduce slip lengths and thus homogenize deformation. On the other hand, localized planar slip occurred in the recrystallized grains, resulting in an enhanced environmental effect and early crack nucleation.

For alloys with nonshearable precipitates, the degree of recrystallization has no effect on fatigue life, regardless of environment (Fig. 39). Further, the effect of the environment was small. Slip distances, which are controlled by the spacings of the nonshearable precipitates, are much smaller than the mean intercept length between subgrain boundaries.

Grain Size. A reduction in grain size results in beneficial effects that delay crack nucleation in alloys containing shearable precipitates. Reduced grain size reduces the slip length, and thus the stress concentration, by reducing the number of dislocations in a pileup. A reduction in slip length also reduces the number of dislocations that can egress at a free surface (and thus the slip-step height and extrusion/intrusion size). Another beneficial effect of grain-size reduction involves the volume of material needed to satisfy the von Mises criterion (Ref 66). In essence, this criterion requires multiple slip to occur in polycrystalline materials in order to preserve the external form of the specimen and maintain cohesion at the grain boundaries. However, as Calnan and Clews (Ref 67) have suggested, multiple-slip systems need only operate in the immediate vicinity of the grain boundary, whereas slip may occur on either

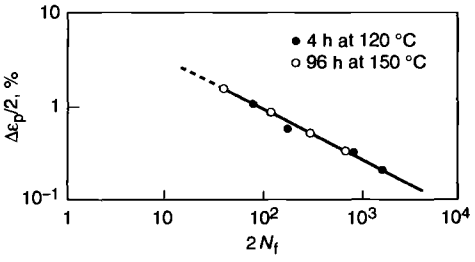

Fig. 42 Strain-life curves of large-grained Al-Zn-Mg alloy with shearable precipitates when underaged (4 h at 120 °C, or 250 °F) and nonshearable precipitates plus PFZs when overaged (96 h at 150 °C, or 300 °F). Source: Ref 64

duplex or single systems in the body of the grains. Consequently, the smaller the grain size, the larger the volume fraction of material deformed by multiple slip and the more homogeneous the overall deformation.

Figure 40 illustrates the beneficial effect of reducing grain size for an alloy containing shearable precipitates (Ref 68). The ternary alloy had an equiaxed grain structure with a mean intercept length of 0.5 mm. Coarse planar slip and intense slip bands, which were later sites for crack nuclei, occurred early in the life of the large-grained material. The Al-Zn-Mg-Zr alloy had smaller elongated grains with mean grain dimensions of approximately 0.03 by 0.05 by 0.10 mm. Slip in the fine-grained material was less intense, and crack initiation was delayed. This is further illustrated in Fig. 40 by the fact that cycles to initiation for the fine-grained material exceeded cycles to failure for the coarse-grained material under the same plastic strain amplitude.

Again it is noted that the two curves converge at low plastic amplitudes (long life) for this strain-controlled test. As mentioned previously, this is due to differences in cyclic-hardening behavior. The strain-hardening exponent, n', of the Al-Zn-Mg-Zr alloy is approximately twice that of the ternary alloy, a fact attributed to a larger degree of multiple slip and more frequent dislocation-dislocation interactions in the Al-Zn-Mg-Zr alloy than in the Al-Zn-Mg alloy. The convergence would not have been observed in a stress-controlled test.

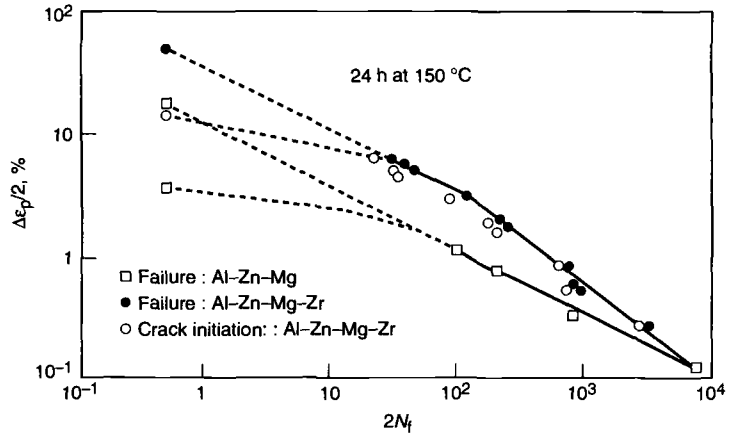

Fig. 43 Effect of grain size on the strain-life behavior of an alloy with nonshearable precipitates plus PFZs. The Al-Zn-Mg alloy had large grain size; the Al-Zn-Mg-Zr, small grain size. Source: Ref 68

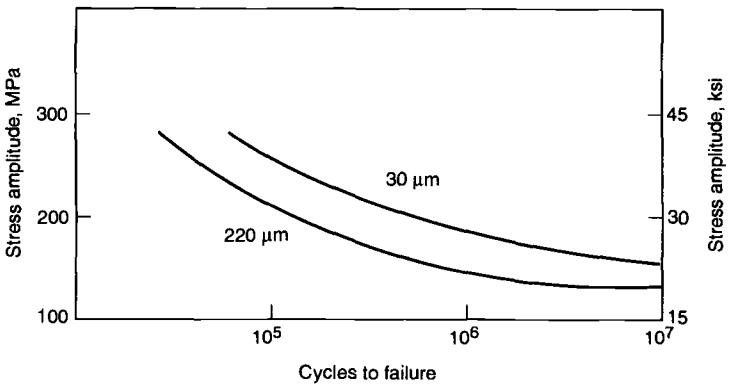

Fig. 44 Effect of grain size on the stress-life behavior of an X7075 alloy with nonshearable precipitates plus PFZs. Source: Ref 69

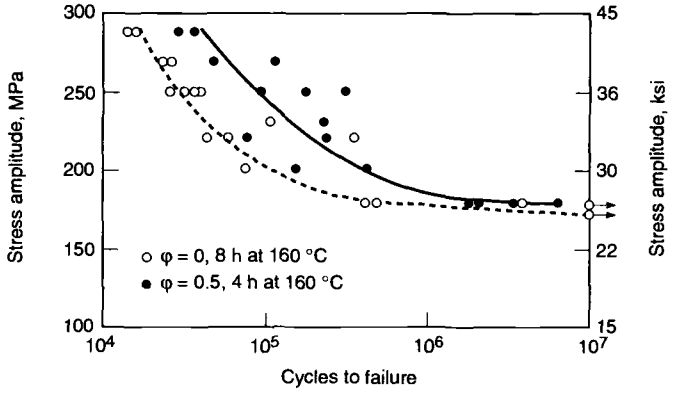

Fig. 45 Effect of grain-boundary ledges on the stress-life behavior of an X7075 alloy containing nonshearable precipitates and PFZs

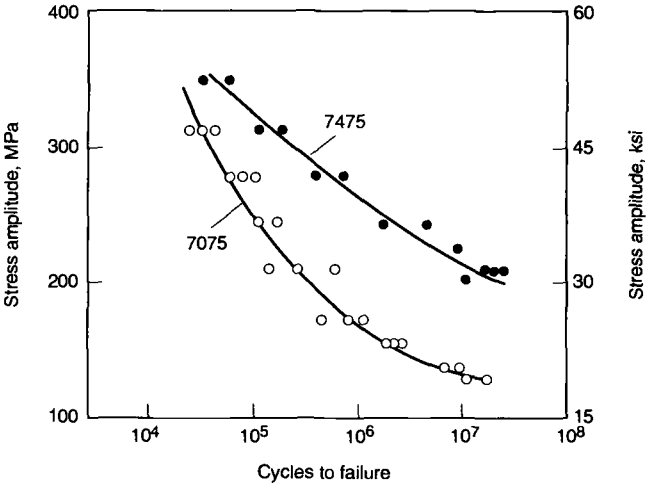

Fig. 46 Effect of inclusion density on the stress-life behavior of two 7XXX alloys: high inclusion density, alloy 7075; low inclusion density, alloy 7475

Figure 41 shows the grain-size effect in a stress-controlled test for a high-purity 7075 alloy (X7075) aged to contain shearable precipitates (Ref 69). Since the flow stress is determined by the interaction of dislocations with the coherent precipitates, the yield stress is approximately the same for both alloys. Optical examinations of the specimen surfaces show that cracks nucleate much earlier in specimens having the large grain size. Cracks nucleated at intense slip bands for both grain sizes. However, the slip bands were much more pronounced in specimens with a large grain size of 200 μm. For specimens with small grain size (30 μm), cracks at slip bands could be detected only in grains that were statistically larger than average.

Precipitate-Free Zones

A solute-depleted PFZ is weaker than the matrix and can be the site of preferential deformation. This preferential plastic deformation leads to high stress concentrations at grain-boundary triple points (Fig. 34) and to early crack nucleation. The magnitude of the stress concentrations will be a function of the grain-boundary length and the difference in shear strength of the age-hardened matrix and the soft PFZ.

Because the strain localization occurs in a region free of solute, overaging the matrix precipitates or adding dispersoids does not homogenize the deformation. This is clearly illustrated by comparing results for underaged and overaged specimens of large-grained Al-Zn-Mg alloy (Fig. 42). The tensile yield strength and strain to fracture are approximately the same for both specimens. As mentioned previously, the underaged alloy has shearable precipitates, which results in strain localization, the formation of intense slip bands, and early crack nucleation under cyclic loading. Overaging was one method described for homogenizing deformation; however, this method is not effective for large-grained material. Preferential deformation in the PFZ also leads to strain localization and results, for this particular case, in the same fatigue life. For the same reason dispersoids distributed throughout the matrix would not inhibit strain localization in the PFZ.

Reduction of grain size is a very effective method of reducing early crack nucleation due to preferential deformation in the PFZ. This reduces the slip distance and lowers the stress concentrations at grain-boundary triple points. The fracture mode can likewise change from a low-energy intergranular to a higher-energy transgranular mode.

The effectiveness of reducing the grain size is illustrated in Fig. 43, which shows Coffin-Manson life plots of two overaged Al-Zn-Mg alloys, described previously (Ref 68). The small-grained Al-Zn-Mg-Zr alloy has a much longer life than does the large-grained Al-Zn-Mg alloy. The improvement in life is attributed to increasing the cycles to crack initiation. For the lower plastic strain amplitudes, a convergence is noted for long lives (10^4 cycles) for this strain-controlled test. Since the fine-grained material hardens more at low strains, the stress to enforce the applied strain is greater at long lives, and this affects the life improvement due to the fine grains.

No such convergence is observed for a stress-controlled test (Fig. 44) for a similar alloy

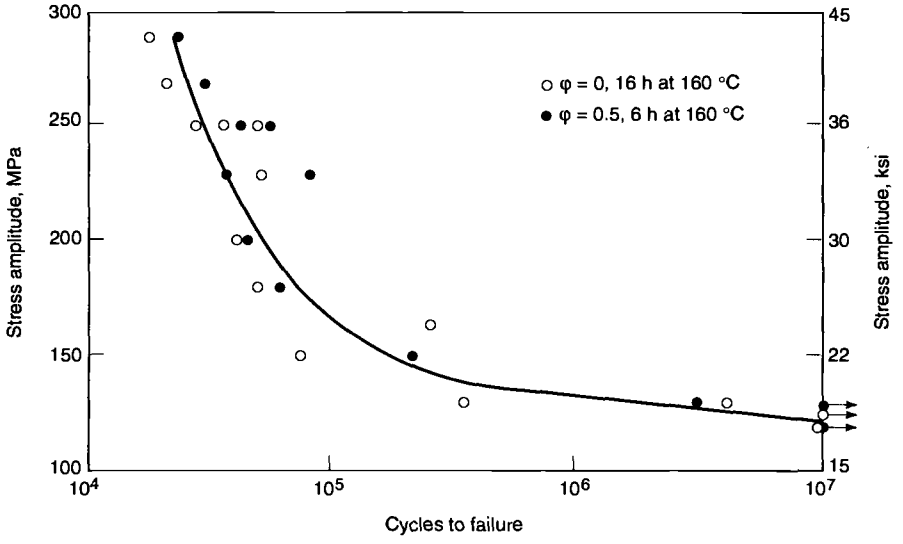

Fig. 47 Effect of alignment of grain boundaries—and alignment plus steps in grain boundaries—on the stress-life behavior of a 7475 alloy containing nonshearable precipitates and PFZs

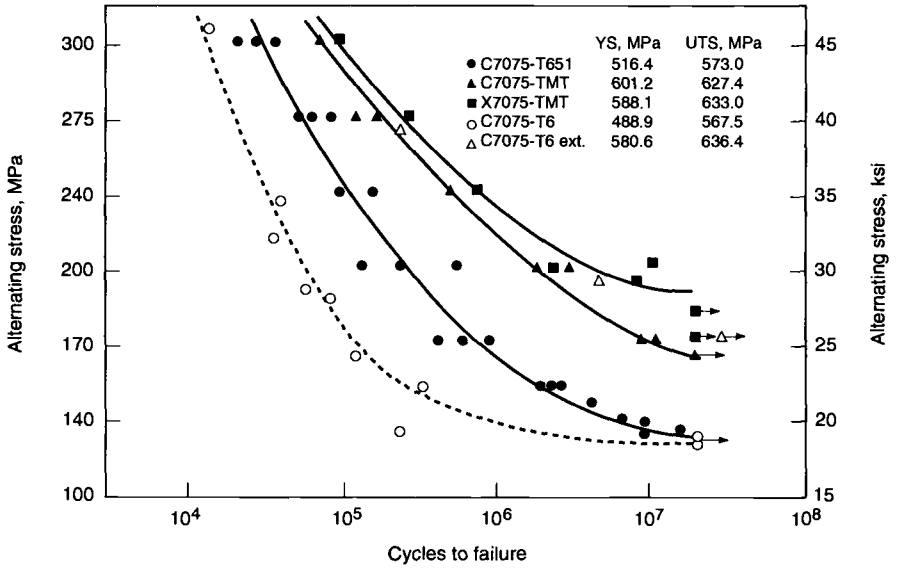

Fig. 48 S-N curves of 7075 aluminum alloys with and without TMTs. Axial loading with $R = 1$. Threaded 13 mm (0.5 in.) round, 75 mm (3 in.) long hourglass specimens (50 mm, or 2 in., radius) with 5 mm (0.2 in.) net section diameter were machined and longitudinally polished. A TMT was given to both commercial and high-purity bars by solution annealing at 460 °C (860 °F) for 1 h, water quenching, aging at 100 °C (212 °F) for 1 h, swaging at room temperature, and aging at 120 °C (250 °F) for 16 h. The commercial alloy, C7075-TMT, was reduced 30% in cross section, whereas the high-purity alloy, X7075-TMT, was swaged only 10% because of specimen size limitations. Source: Ref 72

(X7075) and heat treatment (Ref 69). Optical examination revealed that cracks were nucleated at grain boundaries parallel and perpendicular to the stress axis for the large-grained material, but only at grain boundaries perpendicular to the stress axis for the fine-grained material. This is a direct result of reducing the slip length and thus the local stress concentration. Cracks appearing parallel to the stress axis are a result of the tension-compression employed and the high stress concentrations at triple points in the large-grained material (Ref 69).

Steps in Grain Boundaries. The previous section described the use of grain-size reduction as a means of decreasing the slip length in the PFZ and thus the local stress concentration. This resulted in improved resistance to fatigue crack nucleation and increased fatigue life. Thermomechanical processing is another method that can be used to reduce the slip length in the PFZ. If enough cold deformation is employed to introduce steps (or "ledges") into the grain boundaries, the effective slip length within the PFZ is drastically reduced (similar to a small grain size), with corresponding improvement in resistance to fatigue crack nucleation. Figure 45 shows the results of a stress-controlled test for two high-purity 7075 alloys, one cold worked 50% to produce grain-boundary steps. The cold work drastically reduced the incidence of grain-boundary cracking and improved the fatigue life at high stress amplitudes. At low stress amplitudes and long fatigue lives, crack nucleation occurred at inclusions for both alloys. This effect is most likely due to lower stress concentration at inclusions.

This raises another important point about microstructure. Many alloys have large inclusions, which may concentrate strain during cyclic deformation and lead to early crack nucleation. This detrimental effect can be reduced substantially by lowering the impurity levels. This is illustrated in Fig. 46, which shows that a significant improvement in the HCF life of 7075 alloy is obtained by lowering the iron and silicon content (7475 alloy).

Alignment of Grain Boundaries. Like many other commercial alloys, high-strength aluminum alloys have dispersoids that inhibit grain growth during high-temperature processing and subsequent heat treatment. For these alloys, the resulting grain shape is characteristic of the processing treatment; for rolled plate it has a pancake shape. If these alloys are aged to contain nonshearable precipitates and have a solute-denuded PFZ, detrimental strain localization could occur only in the PFZ parallel to the long grain dimension and only if the PFZ is inclined to the stress axis. If the stress axis is parallel or perpendicular to the long grain dimension, there will be no shear stress parallel to the grain boundary, and preferential deformation within the PFZ will be restricted. Grain-boundary alignment is then as effective in restricting deformation in the PFZ as are steps produced by thermomechanical treatment (TMT), as shown by the stress-life curves in Fig. 47.

Thermomechanical Processing. Fatigue strength of age-hardened aluminum alloys can be improved in some cases by TMT involving cold work before or during aging. McEvily et al. (Ref 70, 71) found that the fatigue life of Al-Mg and Al-Zn-Mg alloys is increased marginally by cold working prior to aging, perhaps because of partial elimination of grain-boundary PFZs. Ostermann (Ref 72) showed that the long-life fatigue strength and fatigue ratio of smooth 7075 aluminum specimens were increased about 25% by cold working in the partially aged condition (Fig. 48). On the other hand, Reimann and Brisbane (Ref 62) found that the fatigue-life curves for notched 7075 (K_t = 3) were essentially unchanged by TMT, and suggested that TMT may affect crack initiation rather than crack growth.

The benefit of TMT is, however, not necessarily limited to crack initiation retardation. Crack growth retardation also has been observed as a result of cold working 2024 aluminum samples prior to aging (Ref 74). DiRusso and coworkers (Ref 75) compared the behavior of T6 and TMT 7075 aluminum and concluded that smooth TMT specimens have lower strength than T6, whereas notched samples may have higher strength. Other results (Ref 76) also demonstrate a significant improvement in fatigue strength in the long-life regime for both smooth and notched (K_t = 8) specimens of 7075 as a result of TMT (Fig. 49). The underlying cause of improvement is probably refinement and homogenization of microstructure as a result of TMT, and the consequent

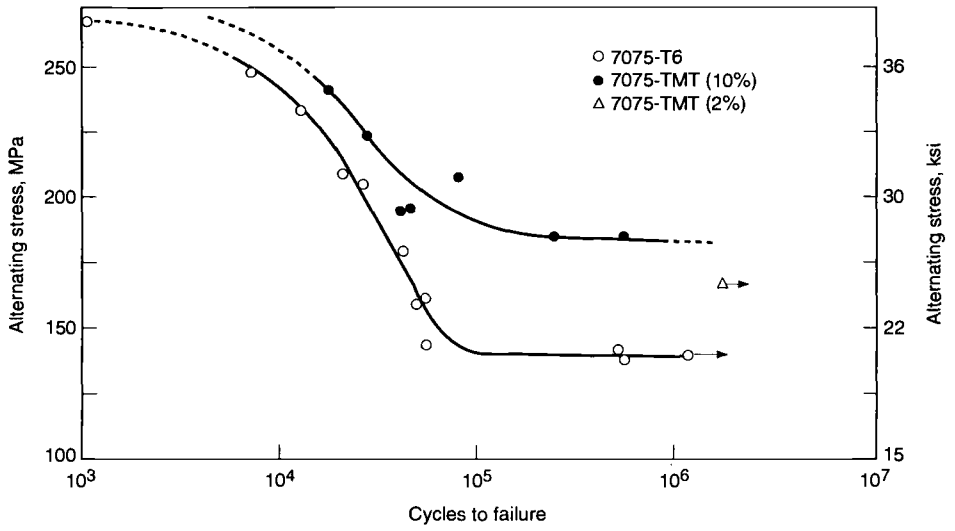

(a)

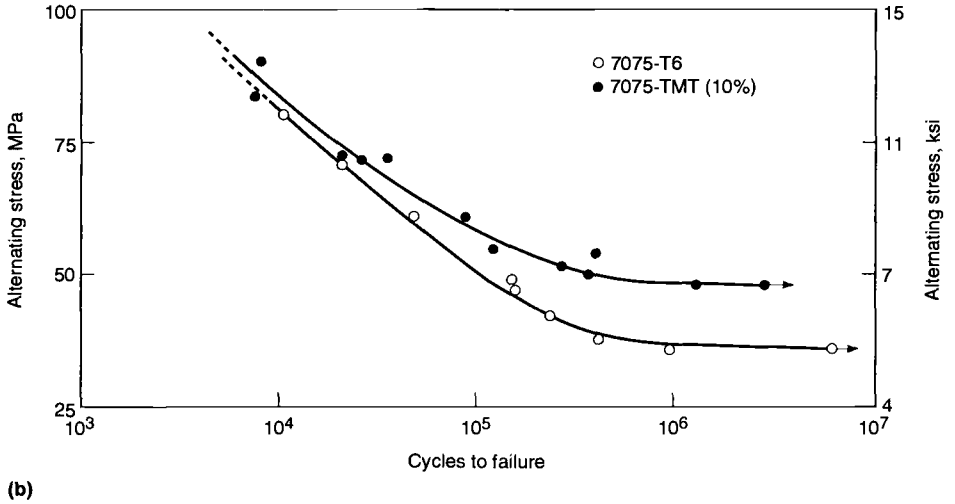

(b)

Fig. 49 Fatigue-life curves for 7075-T6 and 7075-TMT. (a) Unnotched. (b) Notched, $K_t = 8$

deformation by dispersed slip during cyclic loading (Ref 72). Other work (Ref 77) suggests that fatigue crack propagation rates in both 2024 and 2124 aluminum alloys depend on precipitate type and dislocation density. The substantial improvement in fatigue strength of notched samples tested at $R = 0$ strongly suggests that microstructural changes due to TMT can promote increased resistance to crack propagation as well as crack initiation during fatigue cycling of 7075.

Fatigue Crack Growth of Aluminum Alloys

A material's resistance to stable crack extension under cyclic loading is generally expressed either in terms of crack length, a, versus number of cycles, N, or as fatigue crack growth rate, da/dN, versus crack tip cyclic stress intensity factor range, ΔK, using fracture mechanics concepts. The latter approach is particularly useful in damage-tolerant design for estimating the influence of fatigue crack growth on the life of structural components. Baseline data for flaw growth predictions is usually established from constant load-amplitude cyclic loading of precracked specimens. Crack length is measured as a function of elapsed cycles, and these data are subjected to numerical analysis to establish rates of crack growth. Crack growth rates are expressed as function of the applied cyclic range in stress intensity factor, ΔK, calculated from expressions based on linear elastic stress analysis. Fracture mechanics assumes that fatigue crack growth in an engineering structure occurs at the same da/dN of the precracked specimen when the range and mean stress intensity factors for both configurations are the same. Component crack propagation life may therefore be estimated by numerical integration of crack growth rates established from the laboratory coupon specimen.

The typical relationship between fatigue crack growth rate and ΔK observed for most alloys when tested in a non-hostile environment is often classified by the three regions (Ref 78) as shown in Fig. 50. Within region A, crack growth rates become vanishingly small (approximately less than 10^{-5}mm/cycle) with decreasing ΔK, and there exists, within this region, a fatigue stress intensity threshold below which pre-existing cracks do not appear to grow. For many long and infinite life applications, growth of fatigue cracks at very slow rates comprise a major portion of component life, yet low fatigue crack growth rate data on aluminum alloys (and other structural alloys) are rather limited due to the relative high cost and time required to establish this information. Designers using fracture mechanics concepts are interested in low ΔK fatigue crack growth rate information since these rates correspond to early stages of crack formation and propagation where remedial measures can be instituted. In region B, behavior is often characterized by a linear relationship between log da/dN and log ΔK. Region B rates are of great practical interest, since they are generally associated with damage sizes for in-service inspection of high-performance parts. Final stages of fatigue crack propagation are characterized by region C as ΔK (or more specifically K_{max}) approaches the critical stress intensity, K_{Ic} or K_c. Region C growth rates are highly dependent on stress ratio, alloy toughness, and specimen thickness (if not plane strain). Tougher alloys exhibit better constant amplitude fatigue crack growth resistance in regions B and C (Ref 79-82) as indicated by 7075-T6 and high-toughness alloy 7475-T6 data of Fig. 51 (Ref 83).

In examining fatigue crack growth rate curves for many materials exhibiting very large differences in microstructure, the striking feature is the similarities between these curves, not the differences. This point is illustrated by Fig. 52, a compilation of data for 2XXX and 7XXX series aluminum alloys. The differences in crack growth rate between these alloys are important from the viewpoint of integrating along any one of them to obtain the lifetime of a structure, but from a mechanistic point of view, these differences are small. A larger range of metals can be represented by a single curve if the driving force (ΔK) is normalized by modulus. These data exclude the effect of environment (mainly water vapor) which is a major factor affecting fatigue crack growth rates.

The considerable use of the fracture mechanics approach in the evaluation of fatigue crack growth rates in aluminum alloys is evident from a four-part Compendium of Sources of Fracture Toughness and Fatigue-Crack Growth for Metallic Alloys published in the *International Journal of Fracture* (Ref 85-88). Another key reference is the *Damage Tolerant Design Handbook* (Ref 89).

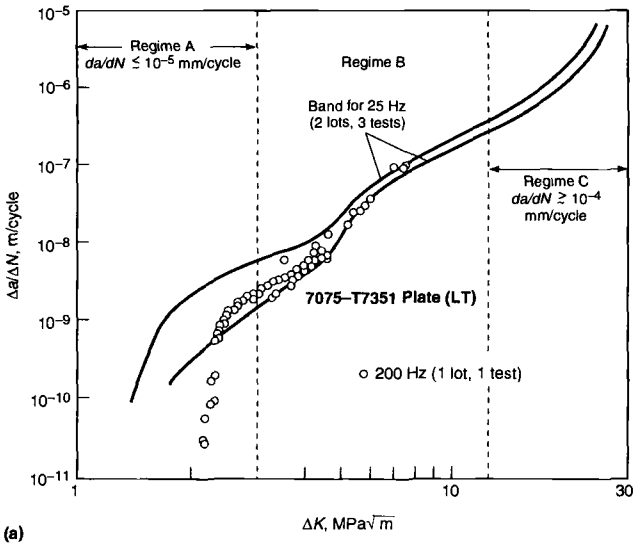

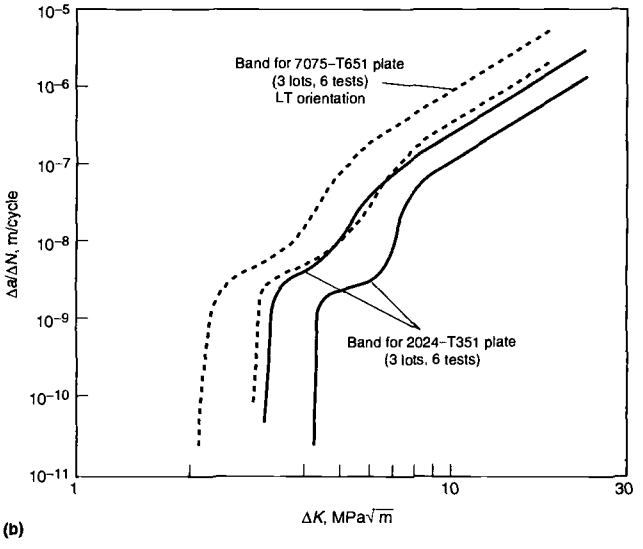

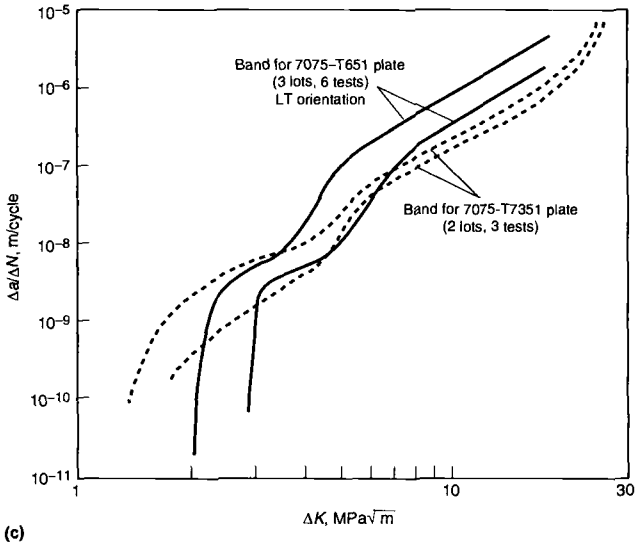

Fig. 50 Fatigue crack growth of 7075 and 2024 plate in moist air, $R = 0.33$ (a) 25 vs 200 Hz with crack growth regimes (b) and (c) typical scatterbands

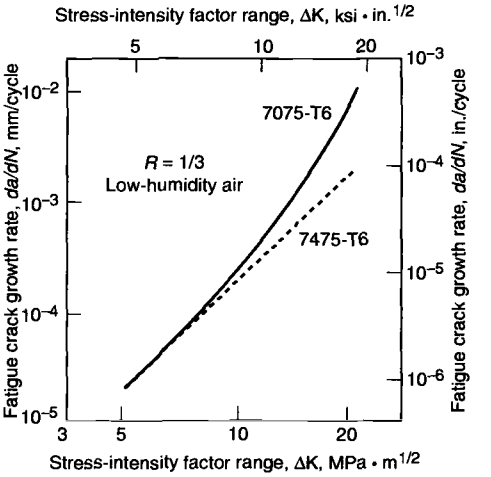

Fig. 51 Benefit of high-toughness alloy 7475 at intermediate and high stress intensity. Source: Ref 83

Effect of Composition, Microstructure, and Thermal Treatments. In general, fatigue crack growth rates in non-hostile environments fall within a relatively narrow scatter band, with only small systematic effects of composition, fabricating practice or strength, as illustrated by Fig. 52 to 54. There are many sources of fatigue crack growth rate data which show the effects of various physical and microstructural variables on fatigue life of aluminum alloys (Ref 92-105), but there is little agreement on the key variables and there are few significant approaches for improving the fatigue crack growth resistance of these alloys. However, some generalizations can be made.

As discussed in the section "Microstructure and Strain Life" in this article, metallurgical microstructures that distribute plastic strain and avoid strain concentration help reduce crack initiation. Those metallurgical factors which contribute to increased fracture toughness also generally contribute to increased resistance to fatigue crack propagation at relatively high ΔK levels. For example, as illustrated in Fig. 51, at low stress intensities the fatigue crack growth rates for 7475 are about the same as those for 7075. However, the factors that contribute to the higher fracture toughness of 7475 also contribute to the retardation of fatigue crack growth, resulting in two or more times slower growth for 7475 than for 7075 at ΔK levels equal to or greater than about 16 MPa $\cdot \sqrt{m}$ (15 ksi $\cdot \sqrt{in.}$). A similar trend has been observed for 2124-T851, which exhibits slower growth than 2024-T851. Smooth specimens of alloys 2024 and 2124 exhibit quite similar fatigue behavior. Because fatigue in smooth specimens is dominated by initiation, this suggests that the large insoluble particles may not be significant contributors to fatigue crack initiation. However, once the crack is initiated, crack propagation is slower in material with relatively few large particles (2124) than in material with a greater number of large particles (2024).

Staley (Ref 90) summarized the role of particle size in influencing fatigue crack growth in aluminum alloys, as shown in Fig. 55 (Ref 106). The influence of alloy composition on dispersoid effect is shown in Fig. 56. The general trend in Fig.

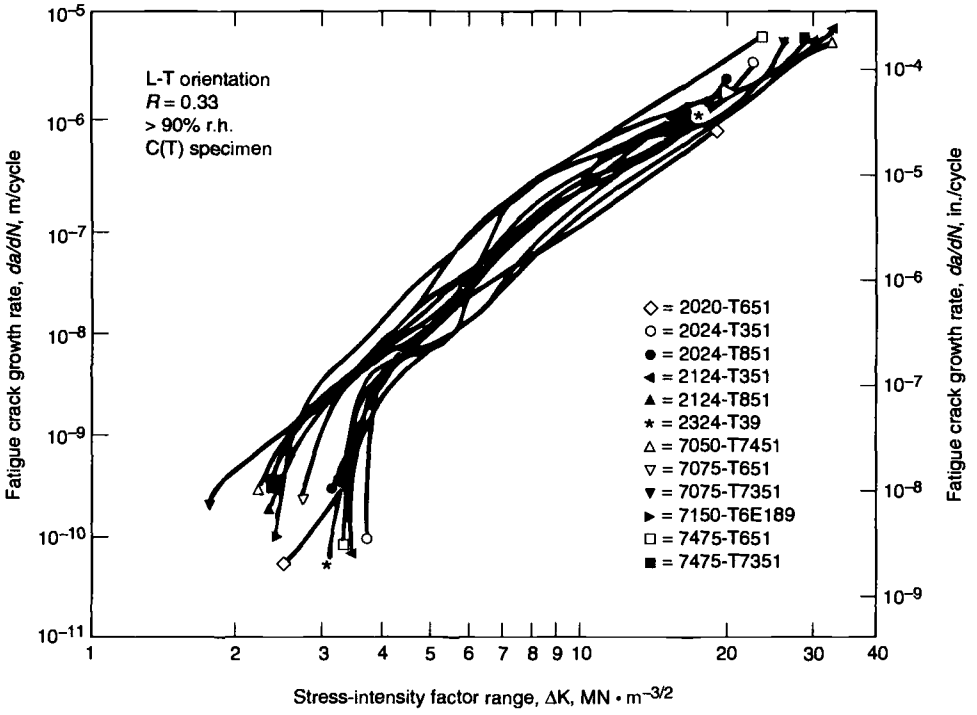

Fig. 52 Minor influences of differing microstructures on fatigue crack growth rate curves: data from twelve 2XXX and 7XXX aluminum alloys with different heat treatments. Source: Ref 73

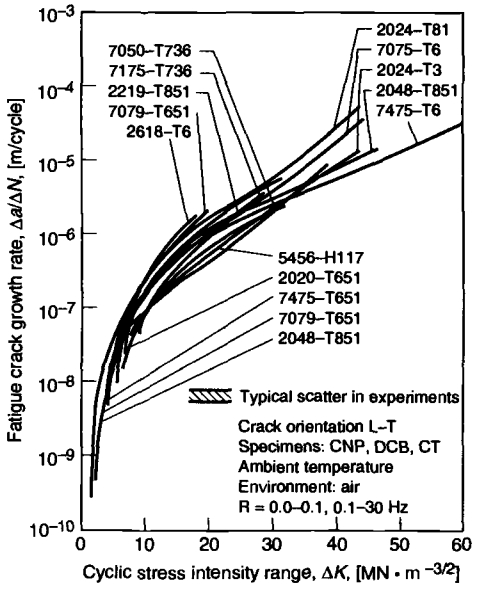

Fig. 53 Crack growth comparison. Many commercial aluminum alloys show similar fatigue crack propagation rates in air, as indicated above. Source: Ref 90

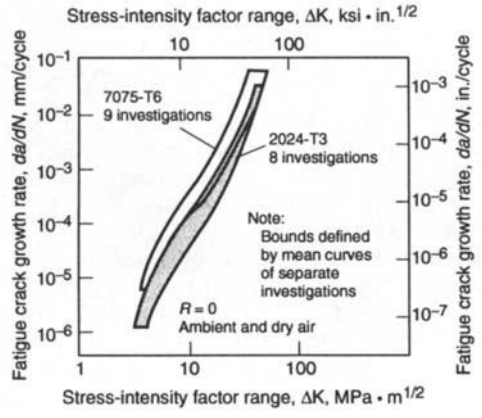

Fig. 54 Summary of fatigue crack growth rate data for aluminum alloys 7075-T6 and 2034-T3. Source: Ref 91

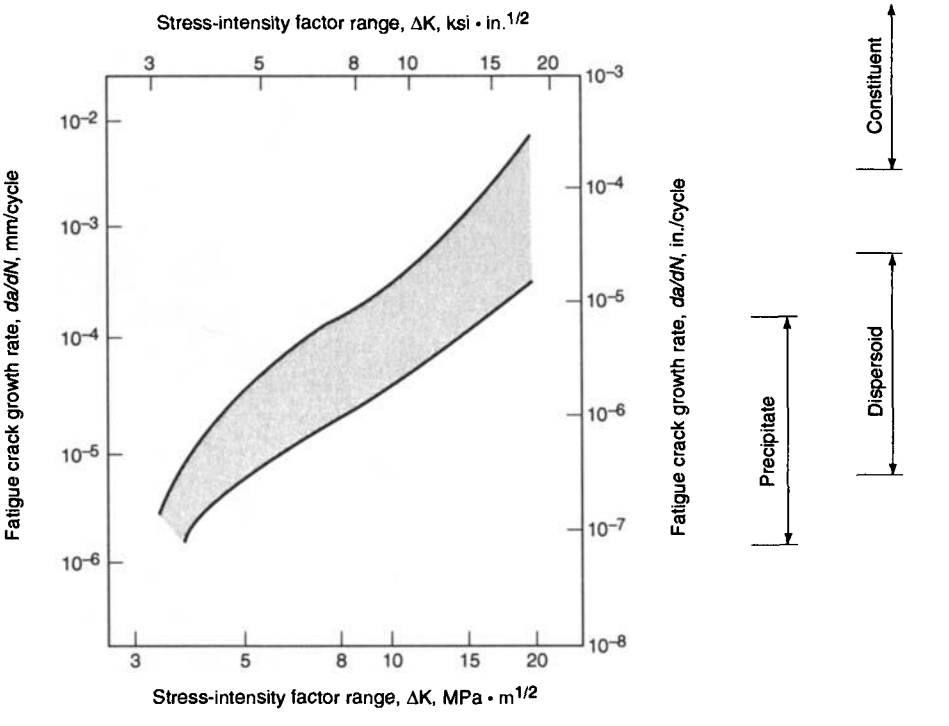

Fig. 55 Comparison of typical particle sizes in aluminum alloys with crack advance per cycle on fatigue loading. Source: Ref 106

56 is that for more finely dispersed particles, the fatigue crack propagation life is increased. Whereas dispersoid type appears to have a relatively small effect on mean calculated life, the smaller precipitates provided by aging produce a much larger effect.

Effect of Processing and Microstructure

The extensive use of age-hardenable aluminum alloys at high strength levels, i.e., greater than 520 MPa (75 ksi), has been hampered by poor secondary properties of toughness, stress-corrosion resistance, and fatigue resistance, particularly in the short transverse direction. Some secondary property improvements have been obtained by employing slight changes in alloy chemistry (Ref 107, 108), different grain refining elements (Ref 92), or removal of the impurity elements Fe and Si (Ref 109-111). Such research has led to the development of alloys with improved fracture toughness and stress-corrosion resistance compared to the extensively used 7075. However, significant improvements in fatigue resistance have not been realized with these methods.

Microstructure control through modification of conventional primary processing methods has

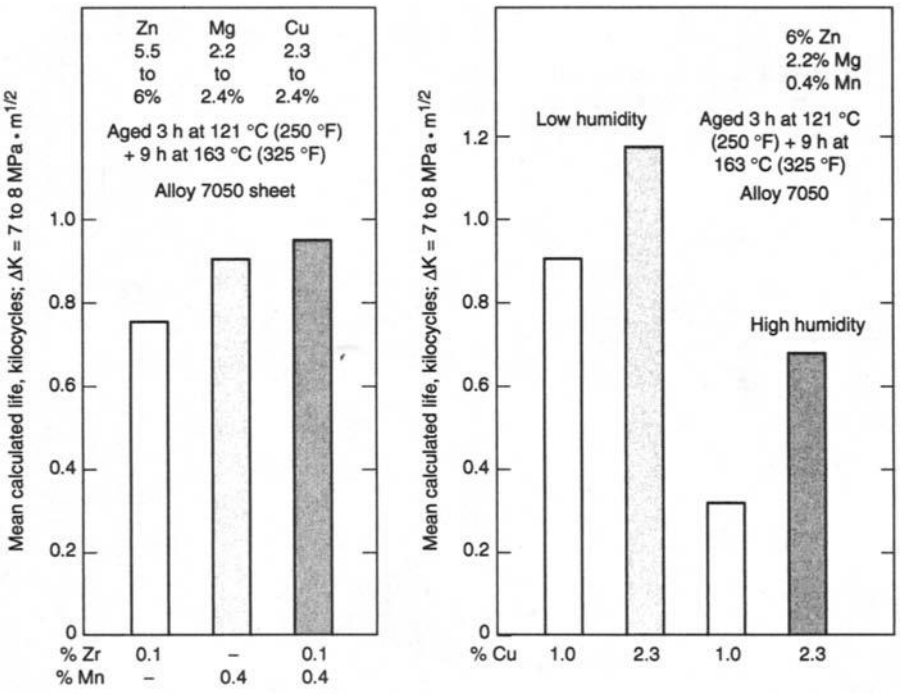

Fig. 56 Effect of dispersoid type (based on composition) on fatigue crack propagation life of 7050 alloy sheet. Source: Ref 106

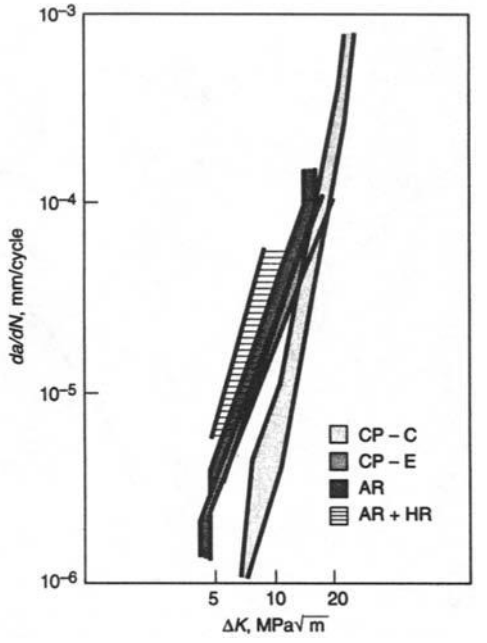

Fig. 57 Crack growth data for compact tension specimens from commercially processed (CP) plate and experimental intermediate thermomechanical treatment (ITMT) material in the as-recrystallized (AR) condition and the as-recrystallized plus hot-rolled (AR + HR) condition. The CP 7050 material was partially recrystallized (<50%) and specimens were from the center (CP-C) and the bottom or top edge (CP-E) of the plate. Scatter bands include data for specimens of both L-T and T-L orientations. Tests conducted at 10 cps and 20 cps in dry air with $R = 0.1$. Source: Ref 112

been examined as a way of upgrading the fatigue properties of these alloys. These methods, called thermomechanical treatments (TMT), include thermomechanical aging treatments (TMA) and intermediate thermomechanical treatments (ITMT), which are specialized ingot processing techniques applied before the final working operation. In general, for high-strength aluminum alloys, a fine grain structure produced by ITMT improves fatigue-crack-initiation resistance but reduces fatigue-crack-propagation resistance when compared with a typical pancake-shape, partially recrystallized, hot worked structure (Fig. 57) (Ref 112). This effect is more pronounced when the strengthening precipitates are shearable and the grain size determines the slip length. Figure 58(a) compares the LCF curves of ITMT and commercially pure (CP) 7XXX alloys. The ITMT material shows a significant increase in reversals to initiation for all strain amplitudes. The ITMT fine grain structure homogenizes the deformation, and the decrease in strain localization improves the resistance to fatigue-crack initiation. The convergence of the curves at high strain amplitudes results from homogenization of deformation by high strains.

Unfortunately, homogeneous deformation increases the rate of crack propagation because it allows single straight-running cracks during subcritical crack growth. The planar slip and inhomogeneous deformation of CP material enhance crack branching, increase the total crack path, and lower the effective stress intensity at the tip of the crack, all of which lower crack-growth rates (Ref 114). Figure 58(b) compares the fatigue crack propagation curves of the same material and shows the detrimental effect that a fine grain structure has on the fatigue crack propagation rate.

Combined effects of grain size, deformation mode, and environment on propagation behavior are shown in Fig. 59 (Ref 115) for ITMT-7475. Both aging treatment and grain size significantly affect the fatigue crack growth rates (FCGRs) measured in vacuum (Fig. 59a). Decreasing the grain size by ITMT and overaging, both of which homogenize deformation and decrease the reversibility of slip, increase FCGRs. Although the same trends are observed in air (Fig. 59b), the magnitude of the effect is considerably reduced due to environment-enhanced growth.

The results in Fig. 59 are consistent with other studies that show that slip character and grain size can have a pronounced effect on the fatigue crack growth behavior of age-hardenable aluminum alloys. When the strengthening precipitates are co-

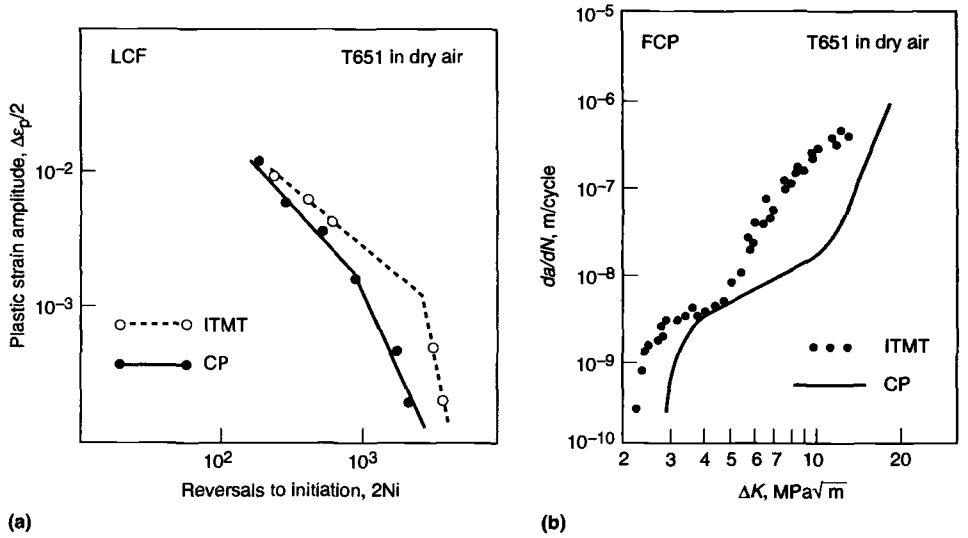

Fig. 58 Effects of intermediate thermomechanical treatments (ITMT) on (a) fatigue crack initiation and (b) fatigue crack propagation of 7XXX aluminum alloys. Source: Ref 113

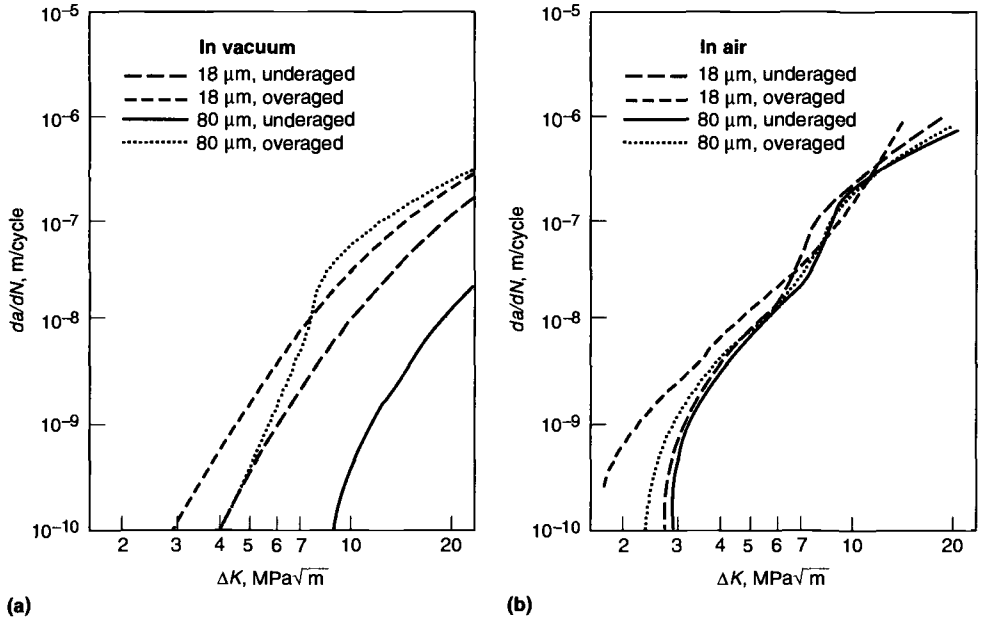

Fig. 59 Effects of grain size and aging treatment on the FCGR of intermediate thermomechanical treatment (ITMT) alloy 7045: (a) tests in vacuum, and (b) tests in laboratory air. Differences in a vacuum could not be accounted for by closure effects. Source: Ref 115

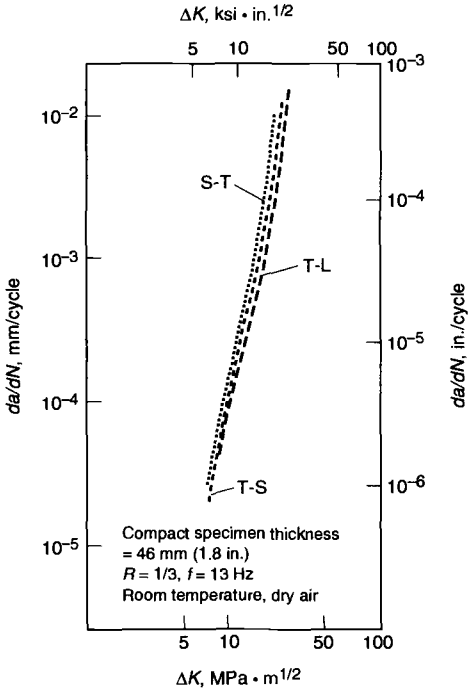

Fig. 60 Effect of orientation on fatigue crack growth rates in 180 and 196 mm (7.0 and 7.7 in.) 5083-O plate. Source: Ref 116

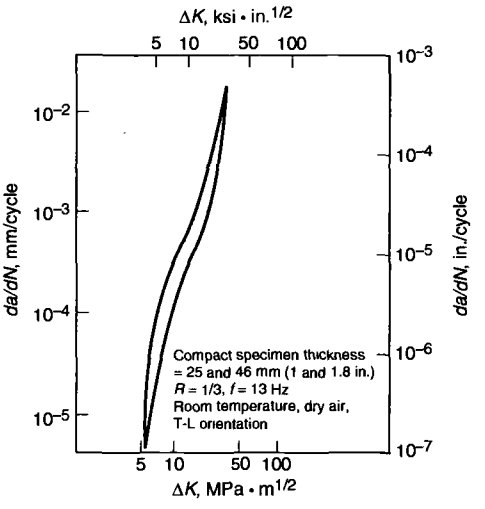

Fig. 61 Fatigue crack growth rates for 5083-O plate in thicknesses of 25, 70, and 178 mm (1, 1.8, and 7 in.). Source: Ref 116

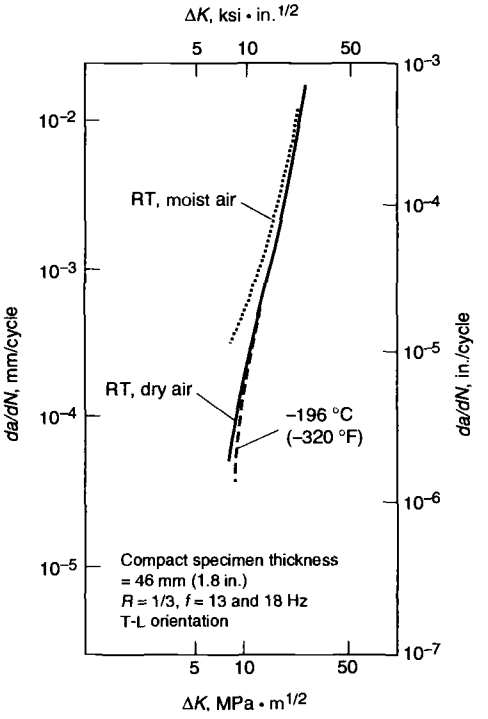

Fig. 62 Effect of temperature and humidity on fatigue crack growth in 180 mm (7.0 in.) 5083-O plate. Source: Ref 116

herent with the matrix (underaged condition) they are sheared by dislocations promoting coarse planar slip and inhomogeneous deformation. This favors fracture along slip planes and the occurrence of zigzag crack growth and crack branching. When the strengthening precipitates are incoherent with the matrix (overaged condition), they are looped and bypassed by dislocations promoting more homogeneous deformation and reducing crack tortuosity. A reduction in grain size (by enhancing multiple slip at low ΔK values) and an aggressive environment (by decreasing the plasticity needed for fracture) can also reduce crack tortuosity although the oxides formed in air can have an opposite effect on crack growth rates by increasing crack closure. The slower crack growth rates associated with planar slip and large grains have been attributed to:

(a) Slip being more reversible
(b) The tortuosity of the crack path
(c) The ΔK of zigzag and branched cracks being smaller than the ΔK calculated assuming a single crack normal to the stress axis
(d) Enhanced closure associated with increased surface roughness

A reduction in grain size and overaging reduce the reversibility of slip and crack tortuosity. Consequently, it is not surprising that the 18 μm grain size in Fig. 59(b), overaged material had the fastest crack growth of all the conditions studied. The different fatigue crack growth rates for the various materials may be related to the difference in the extent of crack closure that they exhibited in the air environment, as discussed in Ref 115. However, in a vacuum, differences in growth rates for the various materials could not be accounted for by closure effects. The influence of environment and in particular the improvement in fatigue crack growth resistance in vacuum is well known. The extent of the improvement depends on aging condition and grain size, with the most significant improvements derived for coarse-grained material in an underaged condition. One factor which may account for this is the marked extent of slip reversibility in the underaged material compared with the multiple slip situation in the overaged material.

Effects of Product Form and Orientation. The rate of fatigue crack propagation in aluminum alloys is relatively insensitive to product form and orientation. This is illustrated in Fig. 60 for thick 5083-O plate that was evaluated for use in

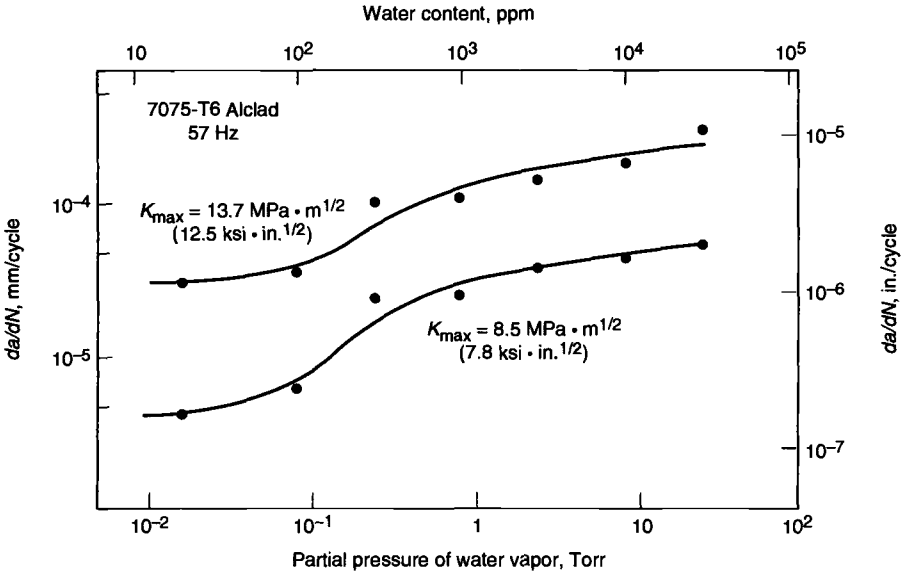

Fig. 63 Effects of moisture on fatigue crack growth rates in aluminum alloys. Source: Ref 101

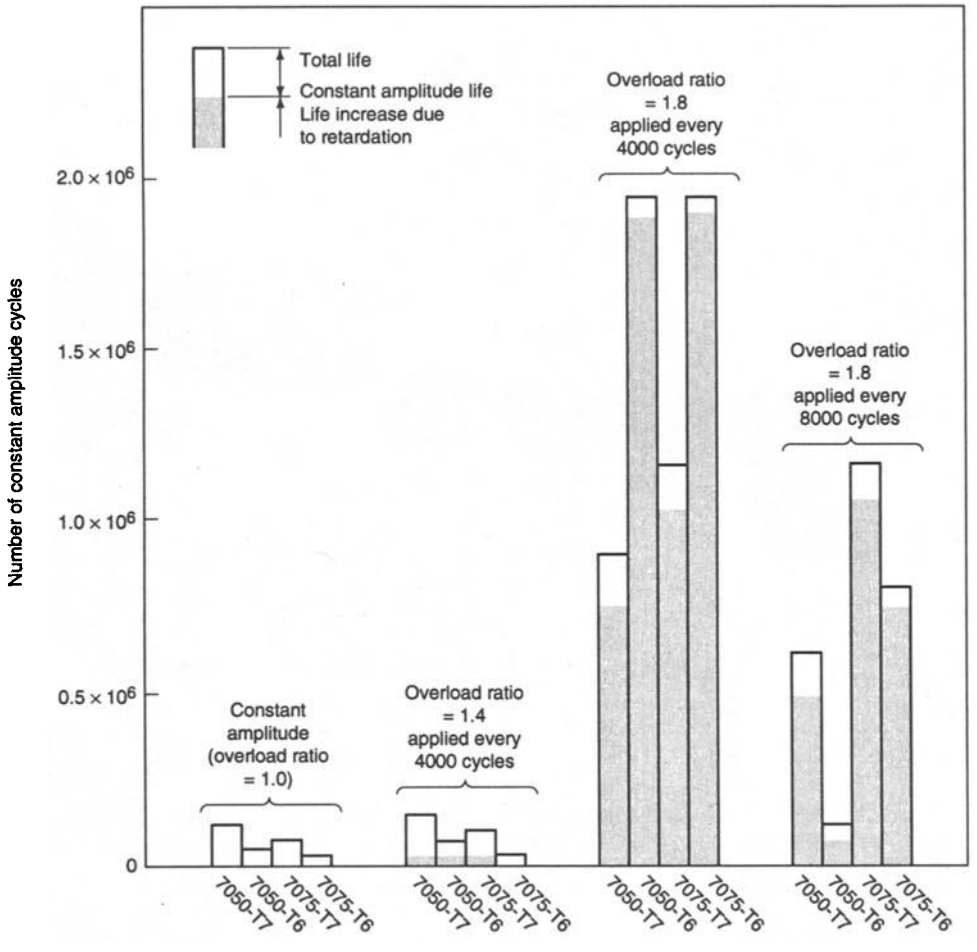

Fig. 64 Relative ranking of fatigue life of 7075 and 7050 aluminum alloys under constant amplitude and periodic single overload conditions. Source: Ref 119

tankage for liquefied natural gas; growth rates in specimens from four orientations were well within the range for replicate tests in any one orientation (Ref 116). It would be expected that in the high ΔK range, differences in growth rate would reflect differences in toughness, and therefore would indicate somewhat higher growth rates for stressing normal to the plane of the product—that is, in the S-L and S-T orientations. Product thickness also seems to have a small effect, as illustrated by the data for 5083-O in Fig. 61 (Ref 116).

Effects of Exposure Temperature. Although no significant amount of fatigue testing has been done at temperatures above room temperature, there has been a great amount of testing at subzero temperature, particularly at –196 °C (–320 °F). In general, fatigue crack growth rates below room temperature are about the same as, or lower than those, at room temperature (Fig. 62).

Effect of Humidity. The role of humidity and environment is a well-known factor affecting crack growth. As shown in Fig. 62, growth rates for alloy 5083-O are appreciably higher in moist air than in dry air (Ref 116). Growth rates in water solutions of sodium chloride are similar to those in moist air.

Data for Alclad 7075-T6 in Fig. 63 (Ref 117) illustrate that even relatively low levels of moisture can accelerate crack growth rates. Unless relative humidity is below 3 to 5%, it seems best to consider that accelerated fatigue crack growth rates are likely in service.

Effect of Load-Time History. Selection of the appropriate type of load cycle to be used in evaluating fatigue crack propagation rates of aluminum alloys has been found to be particularly critical. Staley (Ref 106) and Bucci et al. (Ref 118) noted that the variable amplitude crack propagation testing offers the following advantages: (a) increased sensitivity to microstructural effects; (b) relevancy to design through consideration of important effects of load history, especially overload/plastic zone interactions; (c) practical interpretation when results are expressed in terms of crack size versus fatigue life; and (d) suitability for automated testing and analysis. Bucci further indicated that there are important interactions between microstructure and crack growth under variable amplitude cyclic loading that are not accounted for in constant amplitude testing. Ratings of alloys based on constant amplitude testing are not very likely to provide realistic indications of fatigue performance under the usual service-type variable amplitude loading. The primary cause of this difference is that variable amplitude loading includes the effects of crack growth retardation on fatigue crack propagation—effects that cannot be demonstrated in constant amplitude testing. Crack growth retardation is caused by tension overloading and consequent plastic deformation. The variable amplitude test is believed to be more sensitive to alloy difference, and it clearly provides more useful information for alloy development investigations.

For example, as illustrated by the data for alloys 7075 and 7050 in Fig. 64 (Ref 119), quite different results are obtained in constant amplitude tests than in tests with single overloads every 4000 or 8000 cycles. Thus, information on the variation in load level during fatigue cycling is required for correct characterization of the fatigue behavior of aluminum alloys. More detailed information is provided in the article "Fatigue Crack Growth under Variable Amplitude Loading" in this Volume.

Effect of Load Ratio, *R*. The effect of stress or load ratio on fatigue crack growth rate (load ratio, *R*, is the ratio of minimum to maximum load in the fatigue cycle) is well known. This effect is shown for alloy 7075-T6 sheet about 2.5 mm (0.1 in.) in Fig. 65 (Ref 120). In general, and in all the data presented here, an increase in *R* at the same ΔK level causes an increase in growth rate. A modification of the Paris equation [$da/dN = C(\Delta K)^n$] that accounts for the effects of load ratio is the Forman equation, which is as follows:

$$\frac{da}{dN} = \frac{C(\Delta K)^n}{(1-R)K_c - \Delta K} \qquad \text{(Eq 7)}$$

For the data in Fig. 65, the Forman equation gives a good representation of the variation of *da/dN* with *R* for a wide range of crack growth rates.

Crack Growth in Alloy Selection and Design

Generally, fatigue crack growth resistance has only modest variations among present high-strength aluminum alloy mill products. Environmental factors, particularly moisture and chlorides, are more significant than material differences in affecting crack growth rates (Fig. 66). Separation of material differences in fatigue behavior is further confounded by the generally accepted practice of plotting results on log coordinates where relatively small shifts in a data trend could have a significant impact on the life of a part. For example, the width of the d*a*/d*N* band in Fig. 17 represents a factor of ten, affording considerable room for improvement if alloys can be selected or developed that confine their behavior to the crack growth rate lower bound. Moreover, many designers of high-performance structures will concede that a 50% life improvement or 10% weight reduction afforded by design to higher stress without reduction in fatigue strength is significant.

Although material differences generally have only a modest effect on fatigue crack growth rates, research work has established statistically significant effects of alloy microstructure and composition on fatigue crack growth resistance of high-strength aluminum alloys (Ref 43-46). These programs, which consisted of a set of highly controlled experiments on laboratory-fabricated 2XXX (Al-Cu-Mg-Mn) and 7XXX (Al-Zn-Mg-Cu) microstructures,* permitted the following conclusions on fatigue crack growth resistance under constant amplitude loading:

- High-purity and lower-copper versions of alloy 2024 (i.e., 2124 and 2048) provide improved resistance to regions 2 and 3 fatigue crack growth over their 2024 counterpart because of improved fracture toughness.
- Improved toughness through increased purity resulted in greatest improvements in 2XXX alloy fatigue crack propagation life in artificially aged T8-type tempers.
- Toughness and resistance to fatigue crack propagation increase as strength decreases in underaged and peak-aged tempers of Al-Cu-Mg-Mn alloys containing low levels of cold work. Overaged 2XXX tempers provide inferior combinations of strength, toughness, and resistance to fatigue crack growth.
- Compared to conventional 7XXX alloys, such as 7075, "improved" 7475 and 7050 alloys provide greater fatigue crack growth resis-

*Laboratory-fabricated microstructures were designed to simulate commercial material but were developed with greater controls of processing variables in order to systematically investigate their effect. Conclusions from these programs have been verified on commercial alloys.

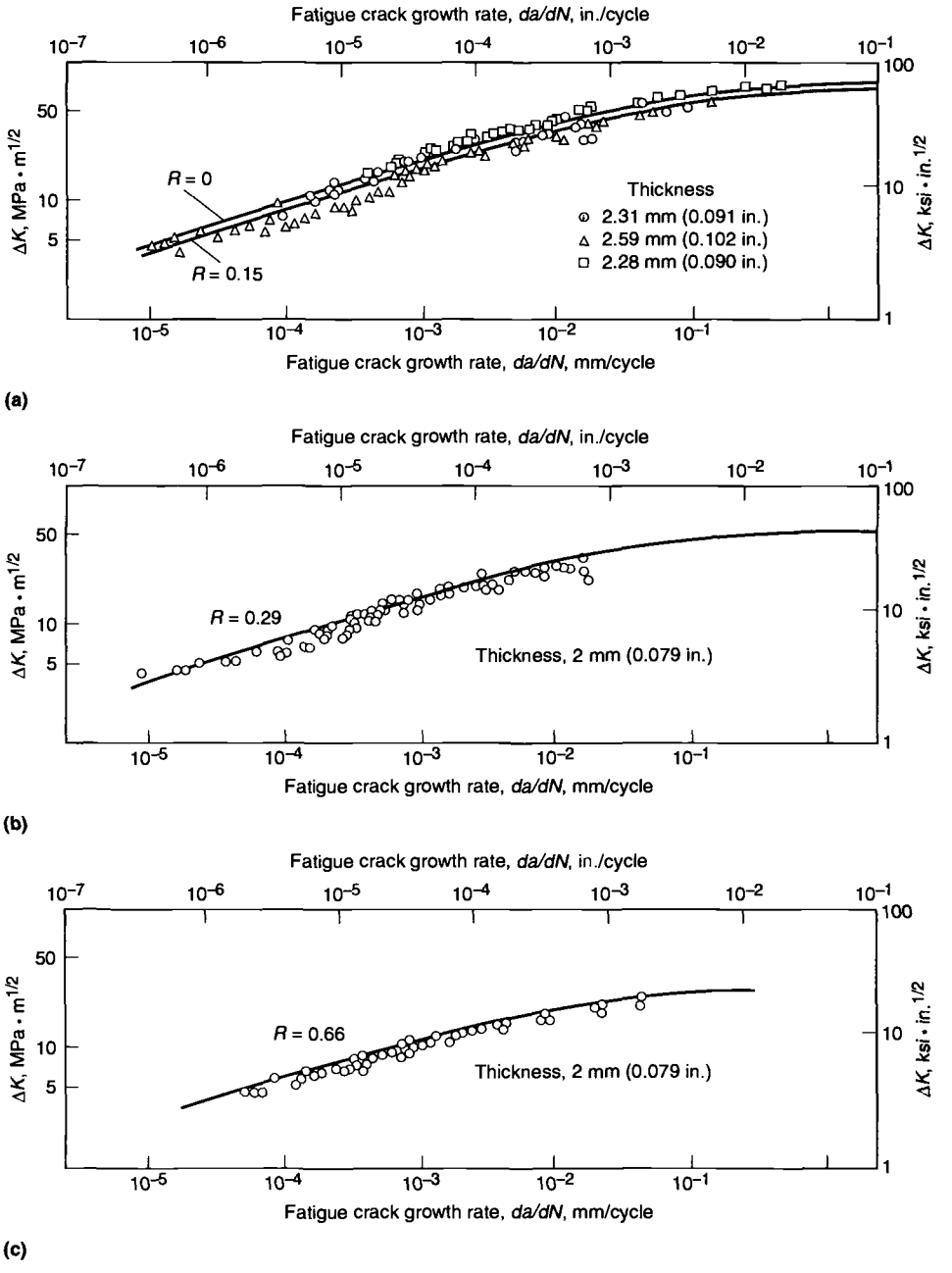

Fig. 65 Effect of load ratio, *R*, on fatigue crack growth rates in aluminum alloy 7075-T6. Source: Ref 120

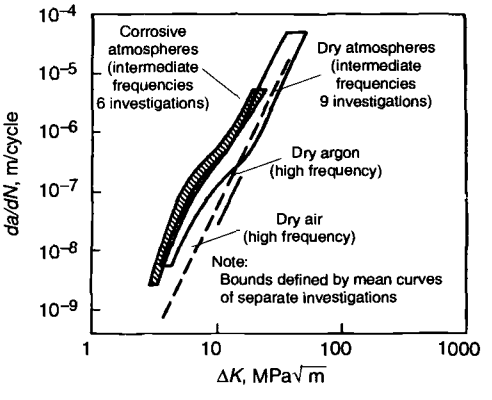

Fig. 66 Influence of environment and cycle frequency on fatigue crack growth ($R = 0$) of aluminum alloy 7075-T6. Source: Ref 121

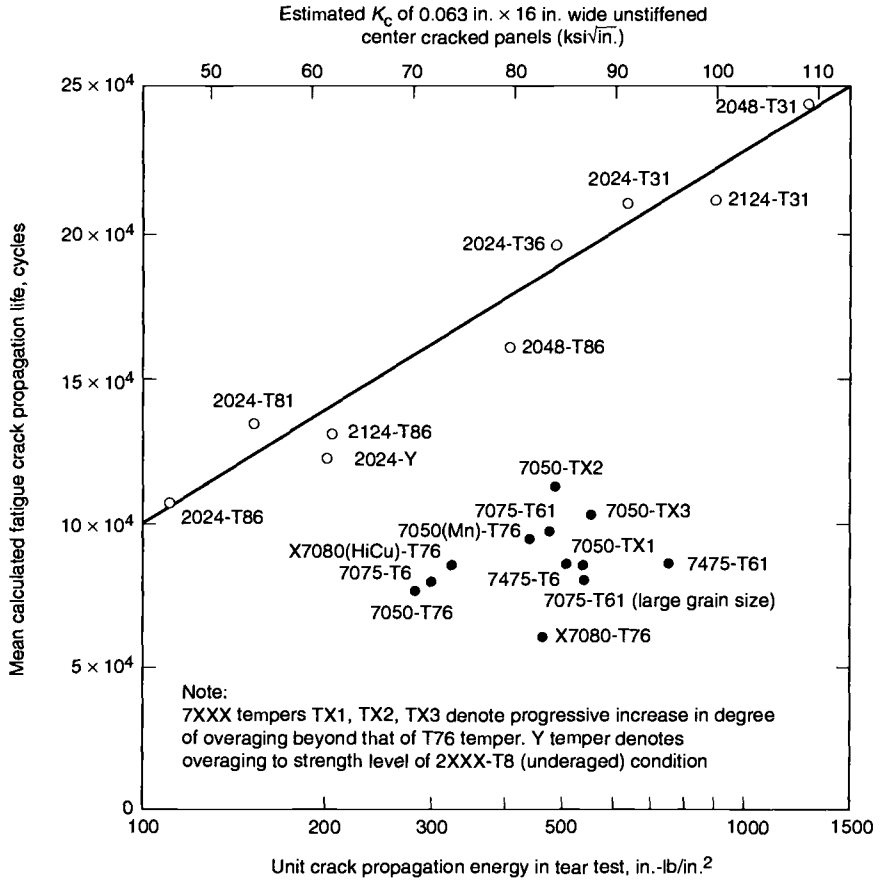

Fig. 67 Relationship between fatigue crack propagation performance and fracture toughness for laboratory-fabricated 2XXX and 7XXX aluminum alloy sheet. Mean crack growth life is that life averaged over four experimental conditions for each alloy. The four conditions were two frequencies, 2 and 20 Hz, and two environments, low (<5%) and high (>90%) relative humidity air. Life was determined from tests of 75 mm (3 in.) wide center crack tension panels where ΔK varied from 6.6 to 16.5 MPa $\sqrt{m}$ (6 to 15 ksi $\sqrt{in.}$) under a constant-stress amplitude of $\Delta\sigma$ = 36.5 MPa (5.3 ksi) and R = 0.33.

tance, in addition to better combinations of strength, toughness, and SCC resistance.

- Overaging 7XXX alloys to T7-type tempers and increasing the copper content to levels of alloy 7050 appears to increase resistance to fatigue crack growth by increasing resistance to corrosive attack by water vapor. (Note: The nominal copper contents are 1.6 and 2.3% for aluminum alloys 7075 and 7050, respectively.)

Fatigue resistance of 2XXX and 7XXX microstructures have been rated by constant-amplitude crack growth life in 76 mm (3 in.) wide center crack tension specimens (Ref 45). Life was then correlated with toughness (Fig. 67) and yield strength (Fig. 68). Good fatigue crack growth resistance of 2XXX alloys shows high correlation with increasing toughness and/or decreasing strength. Fatigue crack growth resistance of 7XXX alloys shows less correlation to toughness and/or strength. Instead, 7XXX alloy rating is better characterized by microstructure and resistance to environment.

Effects of Load History on Fatigue Resistance of Aluminum Alloys. Constant-amplitude fatigue data provide a basic reference and are a prerequisite for making and improving cumulative damage computations. However, an important factor to be considered in addressing fatigue performance of aluminum alloys is the interaction of in-service load history (generally variable amplitude rather than constant amplitude) with material and environmental parameters (Ref 40, 43, 44, 122, 123). It has been amply demonstrated under variable load history that high tensile overloads (at levels of stress intensity that do not promote significant tearing as K approaches K_c) produce significant delays in crack growth during subsequent fatigue cycles at lower amplitudes (see, for example, Fig. 69). The crack growth retardation is generally attributed to a reduction in crack tip stress intensity caused by residual plastic deformation or crack branching resulting from the overload. Compressive loads, hold times, or environmental effects are known to remove some of the benefits produced by the high overloads. However, fatigue crack propagation lives of components subjected to load histories with high tensile overloads are generally greater than linear damage life predictions assuming no load interaction effect (e.g., Fig. 70). Overload-delay phenomena have been well documented in the literature (Ref 124, 125).

Crack growth under variable amplitude loading sometimes shows alloy differences that are not readily apparent from constant-amplitude tests, the method most commonly used to rate alloy fatigue performance (Ref 123). Factors such as cyclic hardening, crack growth retardation characteristics, alloy strength-toughness combination (as varied by temper), and alloy-microstructure interaction with load history and environment all may have appreciable influence on spectrum fatigue life of a particular alloy. For example, Fig. 70 shows that ratings of fatigue crack growth resistance for several aluminum alloys tested under constant amplitude and flight simulation loading differ (Ref 126). Figure 71 shows that an approximate 12% strength reduction from T76 to T73 temper variation in alloy 7475 resulted in a life improvement which, in effect, made the difference between meeting and not meeting a two lifetime damage tolerant design requirement on a fracture-critical aircraft part (Ref 127). However, the magnitude of the improvement was not predictable from constant amplitude data.

Figure 72 is replotted data from Ref 128 that shows fatigue crack growth lives of aluminum alloy 7050 established from flight simulation testing of precracked center crack tension panels. Strength level was varied by heat treatment. Results show that up to a yield strength of about 500 MPa, monotonic decrease in life is associated with monotonic increase in strength. However, increases in 7050 strength beyond 500 MPa results in increased life until a strength level of about 580 MPa, where resistance to fatigue crack propagation diminishes again. The transition behavior indicated by results of Fig. 72 can be related to competing mechanisms that control the fatigue crack growth process. Related work (Ref 43, 44) showed that the dominant mechanism depends on the interaction of loading conditions, specimen configuration, and alloy microstructure.

The point to be emphasized by these illustrations is that complex competing alloy load-interaction mechanisms may be present in variable amplitude fatigue situations. Those mechanisms that dominate are, in part, application-dependent. Therefore, constant-amplitude loading may not always be sufficient or, for that matter, appropriate for rating alloys for optimum selection and/or design of fatigue-critical parts, and spectrum testing may be necessary. Though appreciable effort has been directed at establishing understanding and predictability of crack growth under variable load history, relatively little has been done to qualitatively rate crack growth retardation characteristics from one alloy to another. This work is confounded by the fact that alloy rating is somewhat spectrum- and environment-dependent. Use of appropriate standardized spectra for certain classes of applications (e.g., fighter, bomber, transport aircraft, automotive spectra) and standard test environments provides a database for basic alloy comparisons and improved understanding.

As illustrated by the preceding discussion, caution should be exercised in design use of K_{Ic} for anything other than calculating critical flaw size, since K_{Ic} may not necessarily be correlated with

da/dN, retardation characteristics, or alloy-crack growth interactions with environment.

REFERENCES

1. J.G. Kaufman and M. Holt, "Fracture Characteristics of Aluminum Alloys," Technical Paper 18, Alcoa Research Laboratories, 1965
2. J.G. Kaufman, "Aluminum Alloys for Arctic Applications," paper presented at the Conference on Materials Engineering in the Arctic (St. Jovite, Quebec), 1976
3. Aluminum Standards and Data, Aluminum Association, 1976
4. J.G. Kaufman, F.G. Nelson, and R.H. Wygonik, "Large Scale Fracture Toughness Tests of Thick 5083-O Plate and 5183 Welded Panels at Room Temperature, –260 and –320 °F," STP 556, ASTM, 1974
5. R.A. Kelsey, G.E. Nordmark, and J.W. Clark, "Fatigue Crack Growth in Aluminum Alloy 5083-O Thick Plate and Weld for Liquefied Natural Gas Tanks," STP 556, ASTM, 1974
6. "Aircraft Structural Integrity Program, Airplane Requirements," MIL-STD 1530, U.S. Air Force, 1972
7. H.P. Van Leeuwen and L. Schra, "Rate Effects on Residual Strength of Flawed Structures and Materials," NLR-TR76004U, National Aerospace Laboratory, NLR, The Netherlands, 1975
8. G.T. Hahn and A.R. Rosenfield, "Relations between Microstructure and the Fracture Toughness of Metals," Plenery Lecture III-211, Third International Conf. on Fracture (Munich), 1973
9. G.T. Hahn and A.R. Rosenfield, Metallurgical Factors Affecting Toughness of Aluminum Alloys, *Met. Trans.*, Vol 6A, 1975, p 653-668
10. J.T. Staley, "Microstructure and Toughness of Higher Strength Aluminum Alloys," STP 605, ASTM, 1976, p 71-103
11. M.V. Hyatt, New Aluminum Aircraft Alloys for the 1980s, *Met.*, Vol 46 (No. 2), 1977
12. J.T. Staley, "Update on Aluminum Alloy and Process Developments for the Aerospace Industry," paper presented at the Western Metal and Tool Exposition and Conference (WESTEC) (Los Angeles, CA), 1975
13. J.G. Kaufman, "Design of Aluminum Alloys for High Toughness and High Fatigue Strength," paper presented at the Conference on Alloy Design for Fatigue and Fracture Resistance (Brussels, Belgium), 1975
14. R.R. Senz and E.H. Spuhler, Fracture Mechanics Impact on Specifications and Supply, *Metals Progress*, 1975, p 64-66
15. D.O. Sprowls and E.H. Spahler, Avoiding SCC in High Strength Aluminum Alloys, Alcoa Green Letter GL188, Rev 1982-01
16. D.O. Sprowls, "Environmental Cracking—Does It Affect You?," ASTM Standardization News, Vol 24, No. 4, April 1996, p 2-7
17. M.O. Speidel, Hydrogen Embrittlement and Stress Corrosion Cracking of Aluminum Alloys, *Hydrogen Embrittlement and Stress Corrosion Cracking*, American Society for Metals, 1984, p 271-295
18. T.J. Summerson and D.O. Sprowls, "Corrosion Behavior of Aluminum Alloys," Plenary Paper during The International Conference in Celebration of the Centennial of the Hall-Heroult Process, University of Virginia, Charlottesville, VA, 15-20 June 1986, *Vol III of the Conference Proceedings*, Engineering Materials Advisory Services, Ltd., p 1576-1662
19. R.H. Jones and R.E. Ricker, "Mechanisms of Stress-Corrosion Cracking," in *Stress-Corro-*

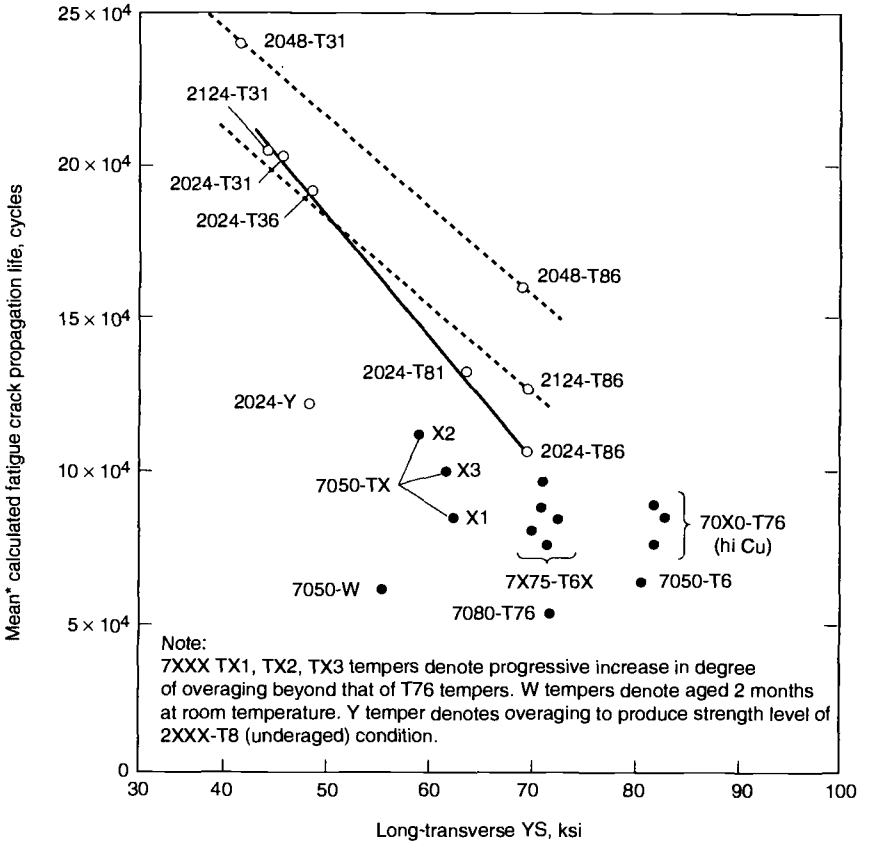

Fig. 68 Relationship between fatigue crack propagation performance and yield strength for laboratory-fabricated 2XXX and 7XXX aluminum alloy sheet. Mean crack growth life is that life averaged over four experimental conditions for each alloy. The four conditions were two frequencies, 2 and 20 Hz, and two environments, low (<5%) and high (>90%) relative humidity air. Life was determined from tests of 75 mm (3 in.) wide center crack tension panels where ΔK varied from 6.6 to 16.5 MPa $\sqrt{m}$ (6 to 15 ksi $\sqrt{in.}$) under a constant-stress amplitude of $\Delta\sigma$ = 36.5 MPa (5.3 ksi) and R = 0.33.

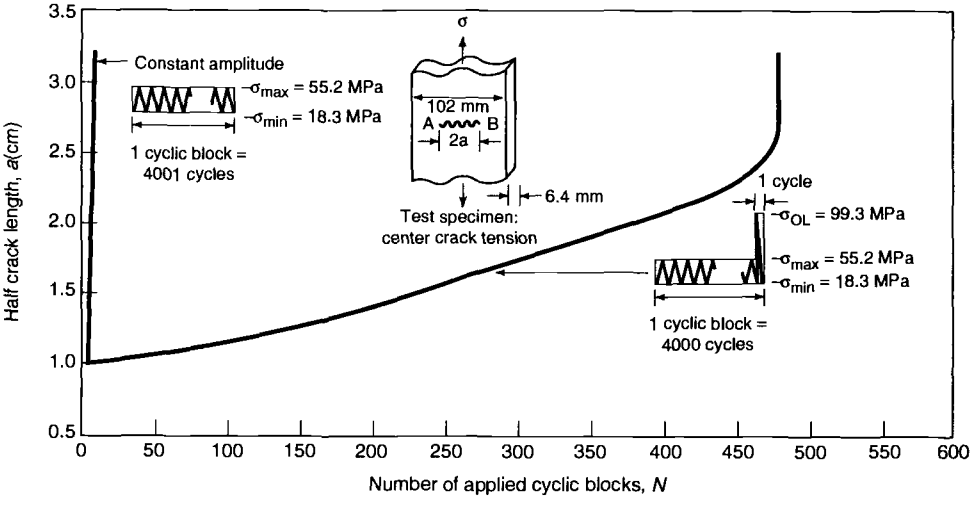

Fig. 69 Crack growth retardation produced by periodic single spike overload in aluminum alloy 7075-T6. Source: Ref 43

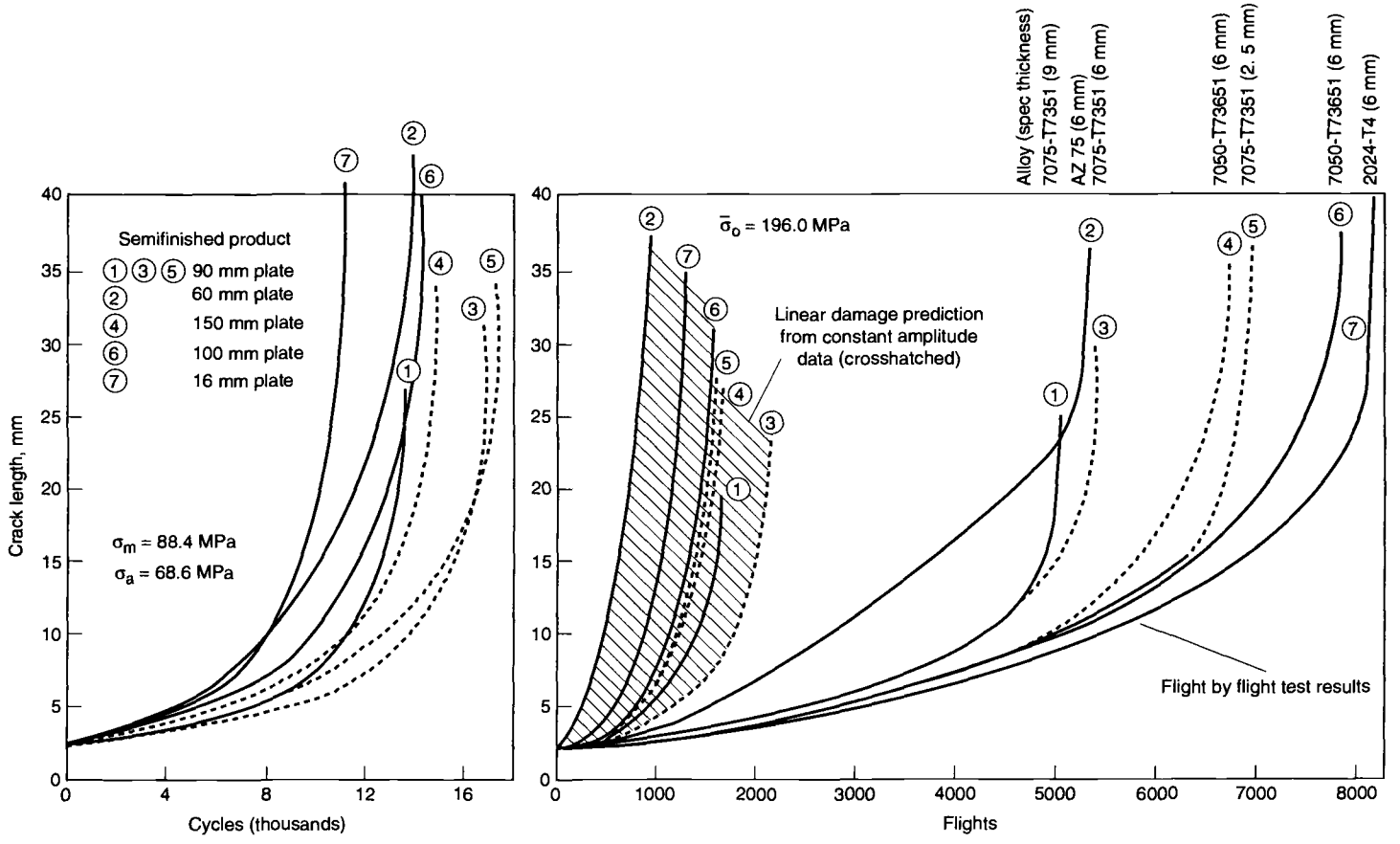

Fig. 70 Crack propagation tests under flight-by-flight and constant-amplitude loading for different aluminum alloys. Source: Ref 126

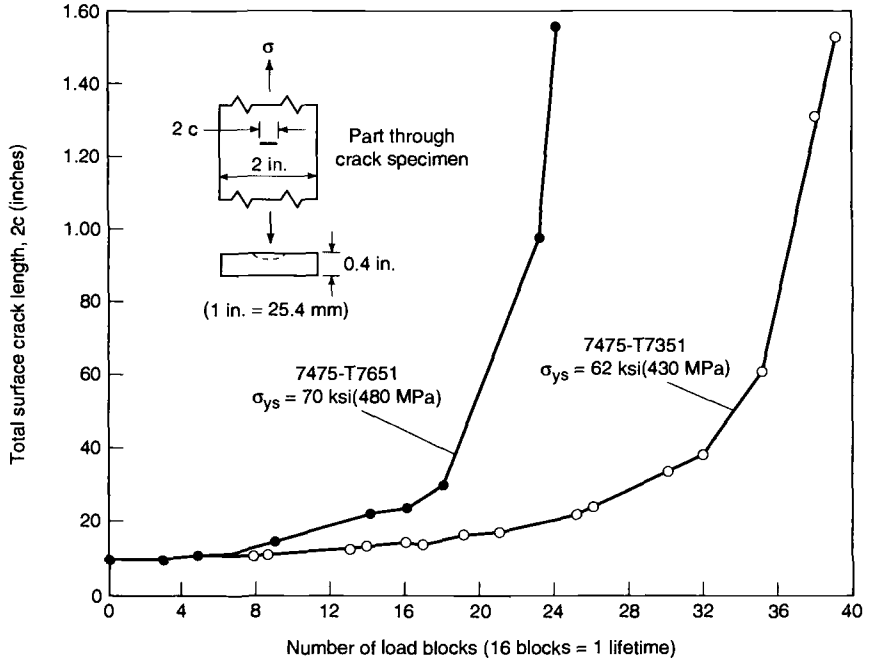

Fig. 71 Effect of overaging on part through crack growth of aluminum alloy 7475 subject to 500 h block flight-by-flight fighter spectrum loading in sump tank water. Source: Ref 127

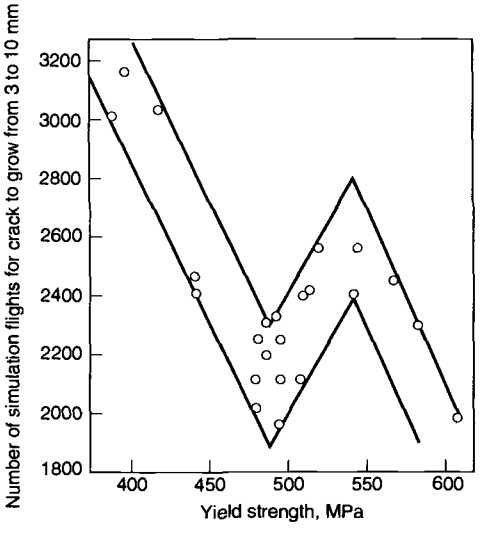

Fig. 72 Effect of yield strength on fatigue crack propagation life of alloy 7050 forging under flight simulation loading

sion Cracking—Materials Performance and Evaluation, Russell H. Jones, Ed., ASM International, 1992, p 23

20. R.N. Parkins, "Current Understanding of Stress-Corrosion Cracking," *Journal of Metals*, Dec 1992, p 12-19
21. B.W. Lifka, "Aluminum (and Alloys)," Chapter 46 of Section VI on Materials Testing in *Corrosion Tests and Standards: Application and Interpretation, ASTM Manual 20*, Robert Baborian, Ed., 1995, p 447-457
22. ISO 7539-1, International Standard on Corrosion of Metals—Stress Corrosion Testing—Part I: General Guidance on Testing Procedures, International Organization for

Standardization, Geneva, Switzerland, 1987
23. D.O. Sprowls, "Evaluation of Stress-Corrosion Cracking" in *Stress-Corrosion Cracking: Materials Performance and Evaluation*, Russell H. Jones, Ed., ASM International, 1992, p 316-405
24. W.B. Lisagor, "Environmental Cracking—Stress Corrosion," Chapter 25 of Section IV on Testing for Corrosion Types in *Corrosion Tests and Standards: Application and Interpretation, ASTM Manual 20*, Robert Baborian, Ed., 1995, p 240-252
25. ASTM G64, Standard Classification of Resistance to Stress-Corrosion Cracking of Heat-Treatable Aluminum Alloys, *Annual Book of ASTM Standards*, Section 3, Vol 03.02
26. ASTM G47, Standard Test Method for Determining Susceptibility to Stress-Corrosion Cracking of High Strength Aluminum Alloy Products, *Annual Book of ASTM Standards*, Section 3, Vol 03.02
27. D.O. Sprowls, "High Strength Aluminum Alloys with Improved Resistance to Corrosion and Stress-Corrosion Cracking," *Aluminum*, Vol 54 (No. 3), 1978, p 214-217
28. E.H. Hollingsworth and H.Y. Hunsicker, "Corrosion of Aluminum and Aluminum Alloys," in *Metals Handbook, 9th ed., Vol 13, Corrosion*, ASM International, 1987, p 583-609
29. M.O. Speidel, "Stress Corrosion Cracking of Aluminum Alloys," *Met. Trans. A*, Vol 6A, 1975, p 631-651
30. B.W. Lifka, "SCC Resistant Aluminum Alloy 7075-T73 Performance in Various Environments," *Aluminum*, Vol 53 (No. 12), 1977, p 750-752
31. M.V. Hyatt, "Use of Precracked Specimen in Stress Corrosion Testing of High Strength Aluminum Alloys," *Corrosion*, Vol 26 (No. 11), 1970, p 487-503
32. R.E. Davies, G.E. Nordmark, and J.D. Walsh, "Design Mechanical Properties, Fracture Toughness, Fatigue Properties, Exfoliation and Stress Corrosion Resistance of 7050 Sheet, Plate, Extrusions, Hand Forgings and Die Forgings," Final Report Naval Air Systems, Contract N00019-72-C-0512, July 1975
33. B. Sarker, M. Marek, and E.A. Stacke, Jr., *Met. Trans. A*, Vol 12A, 1981, p 1939
34. R.L. Templin, "Fatigue of Aluminum," H.W. Gillette Memorial Lecture, presented at the 57th Annual Meeting of ASTM, 1954
35. G.A. Butz and G.E. Nordmark, "Fatigue Resistance of Aluminum and Its Products," paper presented at the National Farm, Construction, and Industrial Machinery Meeting (Milwaukee, WI), Society of Automotive Engineers, 1964
36. T.W. Crooker, "Crack Propagation in Aluminum Alloys under High Amplitude Cyclic Load," Report 7286, Naval Research Laboratory, 1971
37. W.G. Clark, Jr., How Fatigue Crack Initiation and Growth Properties Affect Material Selection and Design Criteria, *Metals Eng. Quart.*, 1974, p 16-22
38. "Standard Recommended Practice for Constant Amplitude Axial Fatigue Tests of Metallic Materials," Designation E466-76, *Annual Book of ASTM Standards*, Part 10, 1976, p 502-506
39. C.M. Hudson and S.K. Seward, A Literature Review and Inventory of the Effects of Environment on the Fatigue Behavior of Metals, *Eng. Fracture Mech.*, Vol 8 (No. 2), 1976, p 315-329
40. "Corrosion Fatigue of Aircraft Materials," AGARD Report 659, North Atlantic Treaty Organization, 1977
41. C.Q. Bowles, "The Role of Environment, Frequency, and Wave Shape during Fatigue Crack Growth in Aluminum Alloys," Report LR-270, Delft University of Technology, The Netherlands, 1978
42. G.E. Nordmark, B.W. Lifka, M.S. Hunter, and J.G. Kaufman, "Stress Corrosion and Corrosion Fatigue Susceptibility of High Strength Alloys," Technical Report AFML-TR-70-259, Wright-Patterson Air Force Base, 1970
43. T.H. Sanders, R.R. Sawtell, J.T. Staley, R.J. Bucci, and A.B. Thakker, "Effect of Microstructure on Fatigue Crack Growth of 7XXX Aluminum Alloys under Constant Amplitude and Spectrum Loading," Final Report, Contract N00019-76-C-0482, Naval Air Systems Command, 1978
44. J.T. Staley, "How Microstructure Affects Fatigue and Fracture of Aluminum Alloys," paper presented at the International Symposium on Fracture Mechanics (Washington, DC), 1978
45. W.G. Truckner, J.T. Staley, R.J. Bucci, and A.B. Thakker, "Effects of Microstructure on Fatigue Crack Growth of High Strength Aluminum Alloys," Report AFML-TR-76-169, U.S. Air Force Materials Laboratory, 1976
46. J.T. Staley, W.G. Truckner, R.J. Bucci, and A.B. Thakker, Improving Fatigue Resistance of Aluminum Aircraft Alloys, *Aluminum*, Vol 53, 1977, p 667-669
47. M.V. Hyatt, "Program to Improve the Fracture Toughness and Fatigue Resistance of Aluminum Sheet and Plate for Airframe Applications," Technical Report AFML-TR-73-224, Wright-Patterson Air Force Base, 1973
48. C.R. Owen, R.J. Bucci, and R.J. Kegarise, Aluminum Quality Breakthrough for Aircraft Structural Reliability, *Journal of Aircraft*, Vol 26 (No. 2), Feb 1989, p 178-184
49. P.E. Magnusen, A.J. Hinkle, W.T. Kaiser, R.J. Bucci, and R.L. Rolf, Durability Assessment Based on Initial Material Quality, *Journal of Testing and Evaluation*, Vol 18 (No. 6), Nov 1990, p 439-445
50. A.J. Hinkle and M.R. Emptage, Analysis of Fatigue Life Data Using the Box-Cox Transformation, *Fatigue and Fracture of Engineering Materials and Structures*, Vol 14 (No. 5), 1991, p 591-600
51. N.E. Dowling, Fatigue Failure Predictions for Complicated Stress-Strain Histories, *J. Materials*, Vol 7, 1971, p 71
52. R.W. Landgraf and R.M. Wetzel, Cyclic Deformation and Fatigue Damage, *Proc. Int. Conf. Mechanical Behavior of Materials*, Vol 2, 1972
53. R.W. Landgraf, F.D. Richards, and N.R. LaPointe, "Fatigue Life Predictions for a Notched Member under Complex Load Histories," paper presented at the Automotive Engineering Congress (Detroit, MI), Society of Automotive Engineers, 1975
54. T.H. Sanders, J.T. Staley, and D.A. Mauney, "Strain Control Fatigue as a Tool to Interpret Fatigue Initiation of Aluminum Alloys," paper presented at the Tenth Annual International Symposium on Materials Science (Seattle, WA), 1975
55. R.W. Landgraf, The Resistance of Metals to Cyclic Deformation, *Achievement of High Fatigue Resistance in Metals and Alloys*, STP 467, ASTM, 1970, p 3-36
56. S.S. Manson and M. Hirschberg, *Fatigue—An Interdisciplinary Approach*, Syracuse University Press, 1964, p 133
57. R. Smith, M. Hirschberg, and S.S. Manson, "Fatigue Behavior of Materials under Strain Cycling in Low and Intermediate Life Range," Report NASA-TN-D-1574, National Aeronautics and Space Administration, April 1963
58. S.S. Manson, "Fatigue: A Complex Subject—Some Simple Approximations," The William M. Murray Lecture, presented at the Annual Meeting of the Society of Experimental Stress Analysis (Cleveland, OH), 1964
59. H.O. Fuchs and R.I. Stephens, *Metal Fatigue in Engineering*, John Wiley & Sons, 1980
60. Special Publication P-109, in *Proceedings of the SAE Fatigue Conference*, Society of Automotive Engineers, 1982
61. R.C. Rice, Ed., *Fatigue Design Handbook*, 2nd ed., Society of Automotive Engineers, 1988
62. J.B. Conway and L.H. Sjodahl, *Analysis and Representation of Fatigue Data*, ASM International, 1991
63. T.H. Sanders and E.A. Starke, *Metall. Trans. A*, Vol 7A, 1976, p 1407
64. F.S. Lin, Ph.D. thesis, Georgia Institute of Technology, 1978
65. Pelloux and R.E. Stoltz, *Proc. 4th International Conf. on Strength of Metals and Alloys*, 1976, p 1023
66. R. von Mises, *Z. Angew. Math. Mech.*, Vol 8, 1928, p 161
67. E.A. Calnan and C.J.B. Clews, *Philos. Mag.*, Vol 42, 1951, p 616
68. R.E. Sanders and E.A. Starke, *Mater. Sci Eng.*, Vol 28, 1977, p 53
69. G. Lutjering, T. Hamajima, and A. Gysler, *Proc. 4th Int. Conf. Fracture* (Waterloo, Canada), Vol 12, 1977, p 7
70. A.J. McEvily, J.B. Clark, and A.P. Bond, *Trans. ASM*, Vol 60, 1967, p 661
71. A.J. McEvily, R.L. Snyder, and J.B. Clark, *Trans. TMS-AIME*, Vol 227, 1963, p 452
72. F. Ostermann, *Metall. Trans.*, Vol 2, 1971, p 2897
73. W.H. Reimann and A.W. Brisbane, *Eng. Fract. Mech.*, Vol 5, 1973, p 67

74. D. Broek and C.Q. Bowles, *J. Inst. Met.*, Vol 99, 1971, p 255
75. E. DiRusso, M. Conserva, F. Gatto, and H. Markus, *Metall. Trans.*, Vol 4, 1973, p 1133
76. F. Mehrpay et al., *Metall. Trans.*, Vol 7A, 1976, p 761
77. W.G. Truckner, A.B. Thakker, and R.J. Bucci, "Research on the Investigation of Metallurgical Factors on the Crack Growth Rate of High Strength Aluminum Alloys," report to AFML, May 1975
78. R.A. Smith, *Fatigue Crack Growth—30 Years of Progress*, Pergamon Press, 1984, p 35
79. W.G. Truckner, J.T. Staley, R.J. Bucci, and A.B. Thakker, "Effects of microstructure on fatigue crack growth of high strength aluminum alloys," *U.S. Air Force Materials Laboratory Rep.*, AFML-TR-76-169, 1976
80. J.T. Staley, W.G. Truckner, R.J. Bucci, and A.B. Thakker, Improving fatigue resistance of aluminum aircraft alloys, *Aluminum*, Vol 54, 1977, p 667-669
81. M.V. Hyatt, "Program to improve the fracture toughness and fatigue resistance of aluminum sheet and plate for airframe applications," Wright-Patterson AFB, *Tech Rep.*, AFML-TR-73-224, 1973
82. R.J.H. Wanhill and G.F.J.A. Van Gestel, Fatigue fracture of aluminum alloy sheet materials at high growth rates, *Aluminum*, Vol 52, 1976, p 436-443
83. J.T. Staley, How microstructure affects fatigue and fracture of aluminum alloys, *Presented at Int. Symp. Fracture Mech.*, Washington, DC, 1978
84. D.L. Davidson and J. Lankford, Fatigue Crack Growth Mechanisms in Metals and Alloys: Mechanisms and Micromechanics, *International Materials Reviews*, Vol 37 (No. 2), 1992, p 45-76
85. C.M. Hudson and S. Seward, A Compendium of Sources of Fracture Toughness and Fatigue-Crack Growth for Metallic Alloys, Part I, *International Journal of Fracture*, Vol 14, 1978
86. C.M. Hudson and S. Seward, A Compendium of Sources of Fracture Toughness and Fatigue-Crack Growth for Metallic Alloys, Part II, *International Journal of Fracture*, Vol 20, 1982
87. C.M. Hudson and S. Seward, A Compendium of Sources of Fracture Toughness and Fatigue-Crack Growth for Metallic Alloys, Part III, *International Journal of Fracture*, Vol 39, 1989
88. C.M. Hudson and J. Ferrainolo, A Compendium of Sources of Fracture Toughness and Fatigue-Crack Growth for Metallic Alloys, Part IV, *International Journal of Fracture*, Vol 48, 1991
89. Damage Tolerant Design Handbook: A Compilation of Fracture and Crack-Growth Data for High-Strength Alloys, HB-01R, Volumes 1 through 4, MCIC, Dec 1983; with update and revision underway as of this printing
90. H. Boyer, *Atlas of Fatigue Curves*, ASM, 1986, p 322
91. C.T. Hahn and R. Simon, A Review of Fatigue Crack Growth in High Strength Aluminum Alloys and the Relevant Metallurgical Factors, *Engineering Fracture Mechanics*, Vol 5 (No. 3), Sept 1973, p 523-540
92. M.V. Hyatt, "Program to Improve the Fracture Toughness and Fatigue Resistance of Aluminum Sheet and Plate for Airframe Applications," Report AFML-TR-73-224, Wright-Patterson Air Force Base, 1973
93. L.H. Glassman and A.J. McEvily, Jr., "Effects of Constituent Particles on the Notch-Sensitivity and Fatigue Crack Propagation Characteristics of Aluminum-Zinc-Magnesium Alloys," NASA Technical Note, April 1962
94. D. Broek, The Effect of Intermetallic Particles on Fatigue Crack Propagation in Aluminum Alloys, *Fracture 1969*, Proceedings of the 2nd International Conference on Fracture, Chapman and Hall Ltd, 1969, p 754
95. E. DiRusso, M. Conserva, M. Buratti, and F. Gatto, A New Thermomechanical Procedure for Improving the Ductility and Toughness of Al-Zn-Mg-Cu Alloys in the Transverse Directions, *Materials Science and Engineering*, Vol 14 (No. 1), April 1974, p 23-26
96. J. Waldeman, H. Sulinski, and H. Markus, The Effect of Ingot Processing Treatments on the Grain Size and Properties of Aluminum Alloy 7075, *Metallurgical Transactions*, Vol 5, 1974, p 573-584
97. A.R. Rosenfeld and A.J. McEvily, "Some Recent Developments in Fatigue and Fracture," AGARD Report 610, Metallurgical Aspects of Fatigue and Fracture Toughness, NATO Advisory Group for Aerospace Research and Development, Dec 1973, p 23-55
98. C.E. Feltner and P. Beardmore, *Strengthening Mechanisms in Fatigue*, STP 476, American Society for Testing and Materials, 1969, p 77-112
99. J.C. Grosskreutz, Strengthening and Fracture in Fatigue (Approaches for Achieving High Fatigue Strength), *Metallurgical Transactions*, Vol 3 (No. 5), May 1972, p 1255-1262
100. B.K. Park, V. Greenhut, G. Lutjering, and S. Weissman, "Dependence of Fatigue Life and Flow Stress on the Microstructure of Precipitation-Hardened Al-Cu Alloys," Report AFML-TR-70-195, Wright-Patterson Air Force Base, Aug 1970
101. "Mechanism of Fatigue Enhancement in Selected High Strength Aluminum Alloys," Progress Report NADC-MA-7171, Naval Air Development Center, 10 Dec 1971
102. S.M. El-Sondoni and R.M. Peiloux, Influence of Inclusion Content on Fatigue Crack Propagation in Aluminum Alloys, *Metallurgical Transactions*, Vol 14 (No. 2), Feb 1973, p 519-531
103. G. Lutjering, H. Doker, and D. Munz, Microstructure and Fatigue Behavior of Al-Alloys, *The Microstructure and Design of Alloys*, Proceedings of the 3rd International Conference on Strength of Metals and Alloys (Cambridge, England), Vol 1, Aug 1973, p 427-431
104. L.P. Karjalainen, The Effect of Grain Size on the Fatigue of an Al-Mg Alloy, *Scripta Metallurgica*, Vol 7 (No. 1), Jan 1973, p 43-48
105. D. Broek and C.Q. Bowles, The Effect of Precipitate Size on Crack Propagation and Fracture of an Al-Cu-Mg Alloy, *Journal of the Institute for Metals*, Vol 99, Aug 1971, p 255-257
106. J.T. Staley, How Microstructure Affects Fatigue and Fracture of Aluminum Alloys, *Fracture Mechanics*, N. Perrone et al., Ed., University Press of Virginia, 1978, p 671
107. M.V. Hyatt and W.E. Quist, AFML Tech. Rept. TR-67-329, 1967
108. J.T. Staley, Tech. Rept. Naval Air Systems Command Contract M00019-71-C-0131, May 1972
109. J.G. Kaufman, *Design of Aluminum Alloys for High Toughness and High Fatigue Strength*, Presented at 40th Meeting of the Structures and Materials Panel, NATO, Brussells, Belgium, April 1975
110. J.T. Staley, *Microstructure and Toughness of High-Strength Aluminum Alloys*, presented at ASTM Symposium on Properties Related to Toughness, Montreal, Canada, June 1975
111. J.S. Santner, AFML Tech. Rept. TR-76-200, March 1977
112. R.E. Sanders, Jr. and E.A. Starke, Jr., *Met. Trans.*, Vol 9A, 1978, p 1087
113. J.C. Williams and E.A. Starke, Jr., The Role of Thermomechanical Processing in Tailoring the Properties of Aluminum and Titanium Alloys, in *Deformation, Processing, and Structure*, G. Krauss, Ed., ASM, 1984
114. Fu-Shiong Lin and E.A. Starke, Jr., *Mater. Sci. Eng.*, Vol 43, 1980, p 65
115. R.D. Carter, E.W. Lee, E.A. Starke, Jr., and C.J. Beevers, "An Experimental Investigation of the Effects of Microstructure and Environment on Fatigue Crack Closure of 7575," *Met. Trans.*, Vol 15A, 1984, p 558
116. J.G. Kaufman and R.A. Kelsey, Fracture Toughness and Fatigue Properties of 5083-O Plate and 5183 Welds for Liquefied Natural Gas Application, STP 579, American Society for Testing and Materials, 1975, p 138-158
117. R.P. Wei, Some Aspects of Environmentally Enhanced Fatigue Crack Growth, *Engineering Fracture Mechanics*, Vol 1 (No. 4), April 1970, p 633-651
118. R.J. Bucci, A.B. Thakker, T.H. Sanders, R.R. Sawtell, and J.T. Staley, Ranking 7XXX Aluminum Alloy Fatigue Crack Growth Resistance Under Constant Amplitude and Spectrum Loading, STP 714, American Society for Testing and Materials, Oct 1980, p 41-78
119. T.H. Sanders, R.R. Sawtell, J.T. Staley, R.J. Bucci, and A.B. Thakker, "Effect of Microstructure on Fatigue Crack Growth of 7XXX Aluminum Alloys Under Constant Strain and Spectrum Loading," Final Report, Contract N00019-76-C-0482, Naval Air Systems Command, 1978
120. R.G. Forman, R.E. Kearney, and R.M. Engle, Numerical Analysis of Crack Propagation in Cyclic Loaded Structures, *Transactions of ASME, Journal of Basic Engineering*, Vol 89 (No. 3), Sept 1967, p 459-464

121. C.T. Hahn and R. Simon, A Review of Crack Growth in High Strength Aluminum Alloys, *Eng. Fracture Mech.*, Vol 5 (No. 3), 1973, p 523-540
122. J. Schijve, The Accumulation of Fatigue Damage in Aircraft Materials and Structures, *AGARDograph*, No. 157, 1972
123. R.J. Bucci, "Spectrum Loading—A Useful Tool to Screen the Role of Microstructure on Fatigue Crack Growth Resistance of Metal Alloys," STP 631, ASTM, 1977, p 388-401
124. H.A. Wood, The Use of Fracture Mechanics Principles in the Design and Analysis of Damage Tolerant Aircraft Structures, *AGARDograph*, No. 176, 1973
125. Fatigue Crack Growth under Spectrum Loads: Proceedings of Symposium presented at the 78th Annual Meeting of the American Society for Testing and Materials, STP 595, ASTM, 1976
126. K.O. Sippel and D. Weisgerber, "Crack Propagation in Flight by Flight Tests on Different Materials," paper presented at the ICAF Colloquium, 1975
127. W.S. Johnson and J.W. Hagemeyer, Yield Strength Considerations for Selecting Material Subjected to Spectrum Loads, *Int. J. Fracture Mech.*, 1977
128. L. Schra and H.P. Van Leeuwen, "Heat Treatment Studies of Aluminum Alloy Type 7075 Forgings," Interim Report 2, NLR-TR-76008C, National Aerospace Laboratory, NLR, The Netherlands, 1976